1-1-2014

Models for a Carbon Constrained, Reliable Biofuel Supply Chain Network Design and Management

Mohammad Marufuzzaman

Models for a carbon constrained, reliable biofuel supply chain network design and management

By

Mohammad Marufuzzaman

A Thesis
Submitted to the Faculty of
Mississippi State University
in Partial Fulfillment of the Requirements
for the Degree of Doctor of Philosophy
in Industrial and Systems Engineering
in the Department of Industrial and Systems Engineering

Mississippi State, Mississippi

August 2014

Models for a carbon constrained, reliable biofuel supply chain network design and management

By

Mohammad Marufuzzaman

Approved:

Sandra D. Eksioglu
(Major Professor)

Burak Eksioglu
(Committee Member)

Hugh R. Medal
(Committee Member)

Xiaopeng Li
(Committee Member)

Kari Babski-Reeves
(Graduate Coordinator)

Jason M. Keith
Interim Dean
Bagley College of Engineering

Name: Mohammad Marufuzzaman

Date of Degree: August 15, 2014

Institution: Mississippi State University

Major Field: Industrial and Systems Engineering

Major Professor: Dr. Sandra D. Eksioglu

Title of Study: Models for a carbon constrained, reliable biofuel supply chain network design and management

Pages of Study: 170

Candidate for Degree of Doctor of Philosophy

This dissertation studies two important problems in the field of biomass supply chain network. In the first part of the dissertation, we study the impact of different carbon regulatory policies such as carbon cap, carbon tax, carbon cap-and-trade and carbon offset-mechanism on the design and management of a biofuel supply chain network under both deterministic and stochastic settings. These mathematical models identify locations and production capacities for biocrude production plants by exploring the trade-offs that exist between transportations costs, facility investment costs and emissions. The model is solved using a modified L-shaped algorithm. We used the state of Mississippi as a testing ground for our model. A number of observations are made about the impact of each policy on the biofuel supply chain network.

In the second part of the dissertation, we study the impact of intermodal hub disruption on a biofuel supply chain network. We present mathematical model that designs multi-modal transportation network for a biofuel supply chain system, where intermodal hubs

are subject to site-dependent probabilistic disruptions. The disruption probabilities of intermodal hubs are estimated by using a probabilistic model which is developed using real world data. We further extend this model to develop a mixed integer nonlinear program that allocates intermodal hub dynamically to cope with biomass supply fluctuations and to hedge against natural disasters. We developed a rolling horizon based Benders decomposition algorithm to solve this challenging NP-hard problem. Numerical experiments show that this proposed algorithm can solve large scale problem instances to a near optimal solution in a reasonable time. We applied the models to a case study using data from the southeast region of U.S. Finally, a number of managerial insights are drawn into the impact of intermodal-related risk on the supply chain performance.

Keywords: Biofuel supply chain, carbon emission, carbon regulatory policies, intermodal hub disruption, Benders decomposition

DEDICATION

To my parents and my wife Rantu.

ACKNOWLEDGEMENTS

I am deeply indebted to my advisor and role model Dr. Sandra D. Eksioglu for her constant support, guidance and inspiration throughout my doctoral studies at Mississippi State University. Without her guidance and assistance, this dissertation would never have been accomplished. She taught me how to conduct independent research, deliver effective presentation and provide suffice motivation that will definitely continue to benefit me in the near future.

I would like to thank other members of my dissertation committee: Dr. Burak Eksioglu, Dr. Hugh Medal and Dr. Xiaopeng Li for their time, effort and feedback that was invaluable to me. I also express my sincere gratitude to Dr. Rafael Hernandez from University of Louisiana at Lafayette, Dr. Yongxi (Eric) Huang from Clemson University, Dr. Andro Mondala from Western Michigan University and Dr. Xiaopeng Li from Mississippi State University for co-authoring a number of articles with me.

I acknowledge financial support from the National Science Foundation (grant CMMI 1052671), Mississippi Department of Transportation (grant SPR-1(66)/106461-179000), Sustainable Energy Research Center (SERC) through project USDOE DEFG3606GO86025 and National Center for Intermodal Transportation and Economic Competitiveness (NCITEC) through project USDOT 009067-019 for conducting my research in the last three and half years at Mississippi State University.

I have been very fortunate to have great lab-mates. Special thanks to Dr. Gokce Palak, Dr. Md. Roni, Dr. Abdullah Al Khaled, Dr. Huseyin Tunc, Satish Vadlamani, Apurba Kumar Nandi, Daniela Gonzales, Eghbal Rashidi, Hadi Karimi, Zahra Azadi, Adindu Emelogu, Yang Chen and Sushil Poudel for their true companionship.

Finally, my eternal thanks to my parents for their love, affection and support. My last word is for my wife Rantu, who was always with me in all my joys and sorrows. Words are never enough to express my love for her.

TABLE OF CONTENTS

LIST OF TABLES

LIST OF FIGURES

CHAPTER 1

INTRODUCTION

1.1 Introduction

There is growing concern worldwide about the impact of greenhouse gases (GHG) on the environment. A number of studies indicate that global warming is mainly due to the increase in GHG emissions, such as, carbon dioxide, methane and nitrous oxide [106]. Freight transportation and other supply chain-related activities are major contributors to GHG emissions. International Energy Agency (IEA) [65] states that 19% of the energy consumption, and almost a quarter of the energy-related carbon dioxide emissions worldwide are due to transportation. In the USA, transportation contributes 28% of the total energy consumption [34].

Companies such as Walmart, Tesco, and Hewlett Packard [61] are responding to these concerns by taking steps toward reorganizing their supply chain, using fuel efficient vehicles, or modifying their operations. These companies have come to realize that reductions in GHG emissions help to strengthen their brand image and to develop competitive advantage. The expectation is that other companies will join this trend, and work to update their supply chain design and management strategies in order to reduce the final products carbon footprint. In this research we present mathematical models which minimize transportation costs, and at the same time, account for carbon emissions due to supply chain

related activities. Through these models we provide insights on the impacts that potential carbon regulatory policies, such as carbon cap, carbon tax, carbon cap-and-trade and carbon offset, will have on transportation mode selection decisions. The mathematical models we propose helped us make some interesting observations with respect to the tradeoffs that exist between costs and emissions.

In the last few years there has been an increasing interest in the production of second generation biofuels. The sources of biomass feedstock used for production of second generation biofuels are agricultural residues, forest residues, energy crops, industrial waste, etc. The reason for such an interest is twofold. First, these types of biomass are secured at low or no cost. Second, the production of this biomass does not interfere with the production of food. However, a big challenge with the production of second generation biofuels is the high production costs, and biomass transportation costs. Biomass transportation costs are high due to the fact that these products are bulky in nature, and have a low ratio of energy per unit of mass. These challenges have been a great motivation for researchers to identify novel methods of producing second generations biofuels. Also, there is a number of articles which address biomass transportation, and other biomass supply chain and logistics related issues. Following this stream of research, we use a case study to demonstrate the role that the mathematical models we propose will have on reducing transportation costs, and transportation-related carbon emissions in this new and promising industry.

In Chapter 2, we present a two-stage stochastic programming model used to design and manage biodiesel supply chains. This is a mixed-integer linear program and an extension of the classical two-stage stochastic location-transportation model. The proposed model

optimizes not only costs but also emissions in the supply chain. The model captures: the impact of biomass supply and technology uncertainty on supply chain-related decisions; the tradeoffs that exist between location and transportation decisions; and the tradeoffs between costs and emissions in the supply chain. The objective function and model constraints reflect the impact of different carbon regulatory policies, such as carbon cap, carbon tax, carbon cap-and-trade, and carbon offset mechanisms on supply chain decisions. We solve this problem using algorithms that combine Lagrangian relaxation and L-shaped solution methods, and we develop a case study using data from the state of Mississippi. The results from the computational analysis point to important observations about the impacts of carbon regulatory mechanisms as well as the uncertainties on the performance of biocrude supply chains.

Transportation infrastructures, particularly those bearing intermodal traffic, may be vulnerable to various disruption risks, such as natural disasters ([93], [144] e.g., 2005 Hurricane Katrina, 2008 China and 2009 Haiti Earthquakes) and human-caused disasters ([97], [102] e.g., 2003 U.S. Northeast blackout, 2010 Gulf of Mexico Oil Spill). Hence, proper redundancy needs to be deployed among the biofuel supply chain to enhance the system reliability against infrastructure disruptions. This indicates that thee is a need to develop a modeling framework for reliable design of a biofuel supply chain network. Such a design shall not only efficiently transport biomass under the normal scenario (when every intermodal hub is functioning normally), but also hedge against possible losses due to unexpected infrastructure disruptions. To address this need Chapter 3 presents a mathematical model that designs a reliable multi-modal transportation network for a biofuel supply chain

system, where intermodal hubs are subject to site-dependent probabilistic disruptions. The disruption probabilities of intermodal hubs are estimated by using a probabilistic model which is developed using real world data. We developed an accelerated Benders decomposition algorithm to solve this challenging $\mathcal{NP}$-hard problem. Numerical analysis show that the model selects to use intermodal hubs located in areas with low disruption probabilities. In case of a disaster, the reliable solution results in 6.21% savings over the minimum cost solution.

In Chapter 4, we further extend the model presented in Chapter 3 to a mixed integer nonlinear programming model that allocates intermodal hub dynamically to cope with biomass supply fluctuations and to hedge against natural disasters. Biomass supply is highly seasonal, but the high production seasons for biomass in the Southeast USA often coincide with or are followed by hurricanes, and drought seasons, both of which impact transportation. The dynamic intermodal hub location model this chapter presents enables this supply chain to cope with biomass supply fluctuations and to hedge against natural disasters. The mixed integer nonlinear programming model proposed is an $\mathcal{NP}$-hard problem, and we develop an accelerated Benders decomposition algorithm and a hybrid rolling horizon algorithm to solve this problem. We tested the performance of the algorithm on a case study using data from the Southeast USA. The numerical experiments show that this proposed algorithm can solve large scale problem instances to a near optimal solution in a reasonable time. Numerical analyses indicate that, under normal conditions, the minimum cost model outperforms the reliable models. However, under disaster scenarios, the minimum cost model is 2.65% to 9.20% more expensive than the reliable and static model;

and 6.28% to 17.73% more expensive than the reliable and dynamic model. Thus, the reliable and dynamic intermodal hub-and-spoke supply chain for biomass can aid supply chain management decisions, especially when considering the potential impacts of natural disasters.

In summary, our study provides models and algorithms for reliable and environmentally friendly biofuel supply chain network. We have conducted a number of real life experiments that will help the investors to make location and routing decisions to ensure long-term success in terms of cost, reliability and emission perspectives.

CHAPTER 2

A TWO-STAGE STOCHASTIC PROGRAMMING MODEL FOR DESIGNING A CARBON CONSTRAINED BIOFUEL SUPPLY CHAIN NETWORK UNDER UNCERTAINTY

2.1 Introduction

In the past few years there has been a growing interest in the production of second-generation biofuels. The raw materials for these biofuels include agricultural residues, forest residues, energy crops, industrial waste, etc. The reasons why second-generation biofuels are gaining traction over first-generation biofuels are manifold. The foremost reason is that they do not interfere with the production of food. Other benefits of using second generation biofuels include their availability at low or almost no cost and their contribution to reducing transportation-related Green House Gas (GHG) emissions [5]. However, a big challenge with second-generation biofuels is the high cost of production and transportation. Biomass transportation costs are high because these products are bulky in nature and have a low ratio of energy per unit of mass [88]. This also suggest that the carbon footprint of biofuels is high. These challenges motivate researchers to identify cost-efficient biofuel supply chain designs with a small carbon footprint for second-generation biofuels.

There is a growing concern in our society about the increased levels of GHG emissions. Many governments across the world are taking actions in response to these concerns, including the Kyoto Protocol [134], the European Union Emission Trading System (EU ETS) [44], among others. For example, the EU ETS limits the amount of carbon allowances a company can use to perform day-to-day activities. Based on this system, a company can sell unconsumed allowances on the market and make a profit. When in need, the company can purchase additional allowances at a cost. These legislations force companies to change the way they make their decisions and manage their supply chains. For example, companies may invest in energy efficient equipments, facilities, and vehicles. This chapter shows that great reductions in GHG emissions come at a small cost when companies modify their business rules and operations [61].

This chapter focuses on the supply chain of biodiesel when produced by treating wastewater (see Figure 2.1). The raw material for production of biodiesel is biocrude which is produced via wastewater sludge generated from wastewater treatment (WWT) plants, pulp and paper mills, poultry slaughtering and processing plants, fresh and frozen fish processing plants, fats and oils from animal and marine plants and meat packing plants. Some WWT facilities apply microbiological processes to treat domestic and/or industrial wastewater and generate a semi-solid, nutrient and organic rich by-product commonly known as sludge. Municipal and industrial wastewater sludge is considered an attractive option to produce biocrude for a number of reasons. Firstly, significant amounts of wastewater sludge are available in the U.S. For example, municipal WWT facilities in the U.S. produce approximately 6.2 million dry metric tons of sludge annually. This amount is

expected to increase in the near future due to expected growth in urbanization and industrialization [148]. Secondly, municipal sewage sludge contains high concentration of lipids [69] which fall in the range between C_{10} to C_{18}. These fatty acids are considered necessary for the production of biodiesel. Finally, using municipal sewage sludge has the potential to solve some environmental issues associated with sludge treatment and disposal. For example, the EPA estimates that the cost of disposing sludge in the U.S. is roughly $2 billion/year. Therefore, making use of the wastewater sludge to produce biodiesel reduces environmental impacts and costs associated with sludge treatment and disposal.

Biocrude production is subject to biomass and technology development uncertainties. For example, the amount of sludge generated in Mississippi has fluctuated from 2006-2010 (see Table 2.1). These fluctuations were due to a number of unpredictable events. For example, the 2010 Gulf of Mexico oil spill damaged the marine and wildlife habitants over 491 miles of coastline in Louisiana, Mississippi, Alabama and Florida. This disaster negatively impacted the Gulf's fishing and tourism industries [102]. Consequently, the amount of sludge generated from fish processing plants and animal and marine plants decreased. Another important factor which impacts the yield of sludge supply is population growth. Due to Mississippi's population growth, the amount of wastewater, and eventually the amount of sludge generated, is projected to increase in the near future [132]. However, the distribution of population and the expected growth rate is uncertain.

The second-generation biofuel industry is new, and therefore, the existing technologies are still in the development phases. Changes and improvements in these technologies will impact conversion rates of biomass to biofuel, and consequently will impact total system

Table 2.1

Input Data: Sludge Supply in Mississippi

Sludge suppliers	No. of suppliers	Amount generated (tons/year)				
		2006	2007	2008	2009	2010
WWT plants	64	859,598	1,064,146	835,571	1,031,986	980,385
Pulp & paper mills	8	100,011	85,934	90,345	103,332	98,165
Poultry slaughtering & processing plants	11	150,415	133,042	148,322	161,487	153,410
Fresh and frozen fish processing plants	9	9,379	9,722	9,040	10,524	9,996
Fat & oil from animal and marine plants	1	678	790	869	875	831
Meat packing plants	1	254	416	376	392	372
Total	94	1,120,335	1,294,050	1,084,523	1,308,596	1,243,159

costs and biofuel production. For example, the technology that we rely on in this study converts wastewater sludge to biodiesel. The existing conversion rate of sludge to biocrude has proven valid in laboratory settings [37, 88]. However, that rate may vary in a large-scale production plant. In 2012 a pilot plant was built in order to test this technology on a larger scale [125, 126].

This chapter proposes mathematical formulations to design and manage the supply chain of biodiesel when produced through wastewater treatment. These models capture the stochastic nature of biomass supply and technology development. These models are extensions of the classical two-stage stochastic location-transportation model [13]. These models integrate location, transportation and production-related decisions in the supply chain. The models capture the tradeoffs that exists between costs and emissions in the supply chain. More specifically, the models proposed minimize transportation and production costs, and at the same time, minimize the carbon emissions due to supply chain related activities. We use these models to understand the impacts that potential carbon regulatory policies such as carbon cap, carbon tax, carbon cap-and-trade, and carbon offset mecha-

nism, will have on supply chain designs and operation decisions. We note that currently, there is no federal regulation in the U.S. that restricts carbon emissions resulting from transportation, except for electrically powered transport [59]. However, in the near future, companies will probably be faced with regulations which restricting emissions originating from transportation and other supply chain-related activities. Some regulations have already been enacted. For example, policies articulated by executive order in California set statewide GHG emission-reduction targets for 2010, 2020, and 2050. The policy makers also set goals for in-state biofuel production and electricity generation from biomass, and they established a goal to reduce the carbon intensity of transportation fuels, which include development of a low carbon fuel standard (LCFS) [151]. These regulations force companies to seek additional opportunities to select less environmentally impactful modes of transportation or increase fuel efficiency of existing vehicles. This chapter's numerical analysis provides interesting observations with respect to the tradeoffs that exist between costs and emissions under different regulatory mechanisms.

In summary, this chapter's main contribution is proposing two-stage, location transportation stochastic programming models for biofuels which account for costs and emissions in the supply chain. These models address several issues which are not well-discussed in biofuel supply chain literature (see Section 2.2). In addition to the modeling approach, another contribution of this chapter is it's solution algorithms developed to solve the two-stage stochastic programming models. Last but not least, this study develops a case study using real-life data from the state of Mississippi. The numerical analysis provides several managerial insights to aid companies in making sustainable supply chain-related decisions.

2.2 Literature Review

In the last few years researchers have developed a growing interest in biofuels supply chain and logistics management. This section presents a review of the literature which is most relevant to the problem addressed in this work.

2.2.1 Biofuel Supply Chains Under Uncertainty

There are a few papers in the literature on deterministic models which take an integrated view of plant location, production, and transportation decision of biofuel supply chains [38, 63, 156, 3]. The main drawback of the models listed above is that they assume the problem parameters are known in advance. However, biofuel supply chains are subject to a number of uncertainties related to supply, demand, price, and technology development, so building models which account for these uncertainties results in meaningful solutions. Awudu and Zhang [5] provide an extensive review of papers incorporating uncertainty and sustainability issues in models for biofuel supply chains. The authors point out that there are a limited number of research papers that consider uncertainty and sustainability in the design and management of biofuel supply chains. Other related papers considering biofuel supply chain uncertainties include research by Cundiff et al. [31], Kim et al. [71], Chen and Fan [22], and Gebreslassie et al. [47].

The work conducted by Cundiff et al. [31] is one of the first that discusses the impact of supply uncertainties in the biofuel supply chain, such as, the impact of weather conditions on biomass yields. The modeling effort is devoted to the design of an efficient biomass delivery system. Chen and Fan [22] introduce a two-stage stochastic programming model

that identifies refinery and terminal sizes and locations, a feedstock resource allocation strategy, an ethanol production and transportation plan under feedstock biomass supply and biofuel demand uncertainties. Gebreslassie et al. [47] propose a bi-criterion, multi-period, stochastic mixed integer linear programming model to address the optimal design of hydrocarbon biorefinery supply chains under supply and demand uncertainties. The aim of this study is to reduce expected annualized total system costs and financial risks simultaneously. Kim et al. [71] propose a mixed integer linear program to determine the processing locations, volumes, supply networks, and the logistics of transporting forest waste to conversion facilities, and from conversion to the market. Their model captures the impact of system uncertainties on profits to maximize the overall expected profit.

In addition to stochastic programming and related optimization models, simulation models have also been used to model biofuel supply chains under uncertainty ([40], [75], [42]).

2.2.2 Carbon Emissions in the Supply Chain

Most of the work on GHG emissions focuses on analyzing pricing mechanisms, or market design implications for different carbon regulatory policies [124, 53, 17, 149]. Bonney and Jeber [14] examine the environmental consequences of common operational activities in the supply chain, and they suggest that all functions within the product life cycle, including inventory planning and control, should be looked at from an environmental point of view. The study conducted by Benjaafar et al. [10] is one of the first papers that proposes including carbon emissions-related costs and constraints in some of the traditional inven-

tory management models, such as, the Economic Lot-Size and Economic Order Quantity models. The authors examine the impact of different carbon regulatory policies on operational decisions in the supply chain. Hua et al. [62] also investigate the impact of carbon emissions trading mechanisms on inventory management and consequently on the final product's carbon footprint. Cholette and Venkat [23] calculate the energy consumed and carbon emitted during transportation and inventory holding in the wine industry. The authors show that energy consumption and carbon emissions are influenced by the structure of the supply chain.

Freight transport is a major contributor to GHG emissions. Bouer et al. [8] address the issue of incorporating environmentally related costs into freight transportation planning. They propose an integer linear programming formulation that minimizes GHG emissions due to transportation activities. Hoen et al. [60] investigate the impact of two carbon regulatory policies on transportation mode selection decisions. Recent studies by [56, 101] use multi-criteria optimization models to address the relationship that exists between cost and environmental variables. The authors use environmental criteria to identify biorefinery locations. Zamboni et al. [155] propose a multi-objective optimization model to address the impacts of GHG emissions on a corn-based bioethanol supply chain. The authors adopted a well-to-tank (WTT) approach to evaluate the impacts of supply chain operations on global warming during the entire product life cycle. Giarola et al. [51] extend this model by considering second-generation bioethanol production technologies.

2.2.3 Solution Algorithms

Efficient solution approaches have been developed for solving two-stage stochastic mixed integer programming problems. Some of the approaches use variations of branch-and-bound algorithm to solve the problem, or, when appropriate, use extensions of Benders decomposition algorithm. Escudero et al. [43] provide an efficient branch-and-fix coordination method for solving large-scale, two-stage stochastic problems with mixed 0-1 first stage variables. Ahmed et al. [2] developed a branch-and-bound algorithm for solving two-stage stochastic integer programs with mixed-integer first-stage variables, and pure-integer second-stage variables. Sherali and Fraticelli [119], Sen and Higle [115] and Ntaimo and Sen [95] propose branch-and-cut algorithms for solving two-stage stochastic programs having first stage pure 0-1 variables and 0-1 mixed-integer recourse variables.

Caroe and Tind [21] propose a generalized Benders decomposition algorithm to solve two-stage stochastic programming problems that contain 0-1 mixed-integer recourse variables, which are either pure continuous or pure first stage 0-1 variables. Sen and Sherali [116] and Sherali and Zhu [118] propose a modified Benders decomposition algorithm where the integer sub-problems are solved using a branch-and-cut decomposition algorithm. Caroe and Schultz [20] and Hemmecke and Schultz [57] present a branch-and-bound algorithm for solving stochastic programming problems with mixed-integer variables in both stages. Instead of finding an optimal solution, the authors focused on obtaining high quality feasible solutions using a Lagrangian relaxation approach. Takriti and Birge [127] extended these works by developing a Lagrangian relaxation solution method.

This method incorporates a Progressive Hedging algorithm [105] which updates the Lagrange multipliers.

Most recently, Rawls and Turnquist [103] propose a Lagrangian based L-shaped algorithm that can solve large scale problem instances in a reasonable amount of time. The general idea behind this extension is to develop an algorithm for finding feasible solutions for the integer variables of the master problem. This is important when the master problem is considered difficult to solve. The Lagrangian based L-shaped algorithm proposed in this paper is an extension of the algorithm proposed in [103]. We have improved the performance of the algorithm by adding valid cuts into the master problem. The computational experience with the biocrude supply chain network model indicates that the algorithm provides high quality solutions.

2.2.4 Our Contribution to the Existing Literature

Our work, although related, is different from the papers discussed above. The main contribution of our work is investigating the biodiesel supply chain under biomass supply and technology development uncertainties. These models identify supply chain designs that minimize the delivery cost of biodiesel and its carbon footprint. The paper analyzes the impact of four carbon regulatory mechanisms on production planning, inventory control, transportation mode selection and facility location decisions.

Another important contribution to the literature is developing the L-shaped based algorithm to solve model proposed. The development of this algorithm was inspired and reflects characteristics of the problem on-hand. Within the L-shaped algorithm we incorporates a

Lagrangean-relaxation model to solve the master problem. We develop valid inequities to improve the performance of the Lagrangean-relaxation algorithm. Numerical experiments show that the algorithm provides high quality solutions in a reasonable amount of time.

2.3 Problem Description and Model Formulation

The main objective of this chapter is to build models that aid the design and management of biodiesel supply chains while taking uncertainties into account. We propose an extension of the two-stage location-transportation stochastic programming model in order to capture the tradeoffs that exist between location and transportation costs; the tradeoffs that exist between cost and emission in this supply chain; and the uncertain nature of sludge supply and technology development. The model we propose identifies locations for biocrude plants, selects one or a combination of transportation modes for delivering sludge, and finally identifies transportation quantities between different stages of the supply chain. Figure 2.1 presents the structure of the biodiesel supply chain consisting of three sludge suppliers, two potential locations for biocrude plants, two diesel production plants, and three customers.

The Biodiesel Supply Chain Network (BSCN) for production of biodiesel consists of a set of nodes $\mathcal{N}$ and a set of arcs $\mathcal{A}$. The set of nodes consists of subset $\mathcal{K}$ representing sludge supply nodes, subset $\mathcal{J}$ representing potential biocrude plant locations, subset $\mathcal{I}$ representing diesel plants, and subset $\mathcal{G}$ representing customer locations. In this network, nodes in $\mathcal{K}$ have a sludge supply which could be used to produce biocrude and eventually biodiesel. Existing diesel plants process biocrude into biodiesel. The demand in each node

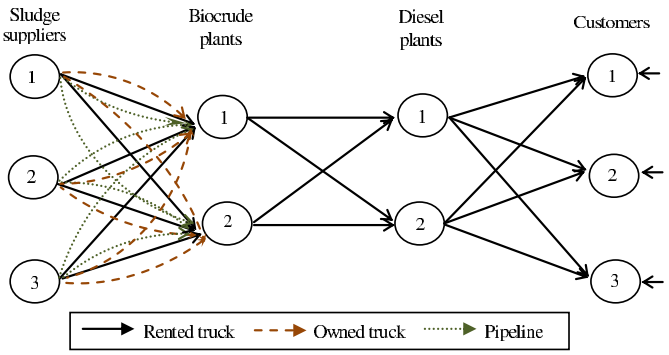

Figure 2.1

Network representation of Biodiesel Supply Chain (BSCN)

of $\mathcal{G}$ represents a customer's demand for biodiesel. Nodes in $\mathcal{J}$ and $\mathcal{I}$ are transshipment nodes.

Three different products flow along the arcs of this network: sludge flows from supply to biocrude plant nodes; biocrude flows from biocrude plants to diesel plant nodes; and biodiesel flows from diesel plants to customer nodes. There are three arcs between each supply and biocrude plant nodes. We use these arcs to represent the fact that three different modes of transportation could be used to ship sludge: pipeline, facility owned truck, and rented truck. A single transportation arc exists between each biocrude plant and diesel plant node and between diesel plant and customer node, which represent the use of rented trucks for shipment of biodiesel and diesel. We consider additional transportation modes are used for shipping sludge when the transportation volume is high.

The transportation cost function for facility owned trucks and pipelines consists of a fixed and a variable component. The fixed cost component for facility owned trucks consists of the annual sales tax, insurance cost, management cost, and overhead cost. These

costs are not a function of the distance traveled or quantity shipped, and this is why we consider them to be fixed. The variable costs include the fuel, labor, tire, maintenance and repair costs. The fixed costs for pipeline transportation represent the cost of establishing a pipeline of a particular capacity, and the variable cost represents the cost of operating the pipeline. Transportation costs for rented trucks have only a variable component (given in $/(mile*ton)) which represents a fixed $ amount typically charged by third-party service providers per mile and per ton shipped [22, 85].

Let ν_m^p be the fixed transportation cost ($ per full-truck load) for product p ($p \in \mathcal{P}$) when using transportation mode m (m = Facility owned truck, Rented truck). Let, β_m^p be the variable transportation cost ($/mile per full-truck load) for product p when using transportation mode m, and ξ_m^p transportation capacity of mode m to ship product p. Let α_f be the variable unit cost for operating a pipeline of capacity f, d_{ij} distance from node i to node j.

Equation (2.1) presents the unit cost ($/ton) for transporting sludge from a supply node $k \in \mathcal{K}$ to a biocrude plant $j \in \mathcal{J}$.

$$c_{kjm}^1 = \begin{cases} \frac{\beta_1^1 * d_{kj}}{\xi_1^1} & \text{for } m = \text{Rented truck}, \\ \frac{\nu_2^1 + \beta_2^1 * d_{kj}}{\xi_2^1} & \text{for } m = \text{Facility-owned truck}, \\ \alpha_f * d_{kj} & \text{for } m = \text{Pipeline}; f = 1, \ldots, \mathcal{F}. \end{cases} \tag{2.1}$$

Equations (2.2) and (2.3) present unit transportation costs ($/gallon) for a rented truck when used for biocrude and biodiesel shipments.

$$c^2_{ji} = \frac{\nu^2_2 + \beta^2_2 * d_{ji}}{\xi^2_2} \qquad \text{for } j \in \mathcal{J}, i \in \mathcal{I}. \tag{2.2}$$

$$c^3_{ig} = \frac{\nu^3_2 + \beta^3_2 * d_{ig}}{\xi^3_2} \qquad \text{for } i \in \mathcal{I}, g \in \mathcal{G}. \tag{2.3}$$

With each arc of the network we associate not only transportation costs but also transportation related emissions. Let e^1_{kjm} denote emissions (kg of CO_2) due to shipping 1 ton of sludge from location $k \in \mathcal{K}$ to $j \in \mathcal{J}$ using transportation mode m. Let, e^2_{ji} denote emissions due to shipping 1 gallon of biocrude from $j \in \mathcal{J}$ to $i \in \mathcal{I}$ using trucks, and let e^3_{ig} denote emissions due to shipping 1 gallon of biodiesel from $i \in \mathcal{I}$ to $g \in \mathcal{G}$ using trucks. Equations (2.4) to (2.7) are used to calculate emissions along the transportation arcs. These equations were developed in a recent work by [82]. Appendix A presents the formulas we use to calculate emissions for each mode of transportation.

$$\begin{aligned} e^1_{kjm} &= \zeta^1_m + \tau^1_m * d_{kj} \\ &\quad \text{for } \ m = \text{Facility owned, Rented truck} \end{aligned} \tag{2.4}$$

$$\begin{aligned} e^1_{kjm} &= (0.746 * P_p * \pi_h * E^e * n_{kj})/\Upsilon_p * C_p \\ &\quad \text{for } \ m = \text{Pipeline} \end{aligned} \tag{2.5}$$

$$e^2_{ji} = \zeta^2_2 + \tau^2_2 * d_{ji} \tag{2.6}$$

$$e^3_{ig} = \zeta^3_2 + \tau^3_2 * d_{ig} \tag{2.7}$$

In these equations, ζ^p_m and τ^p_m denote the fixed (kg/ton) and variable (kg/(ton*mile)) emissions. Fixed emissions are a function of the power requirements and the efficiency of

the pump used during loading and unloading of a truck or a pipeline. For truck transportation, variable emissions depend on the distance traveled and the type of truck used. The definition of variable emissions for pipeline transportation is somewhat different because emissions are a function of capacity and length of the pipeline. For pipeline transportation, variable emissions depend on the power of the pump used P_p (hp), pump efficiency Υ_p, number of operating hours per year π_h (hr/year), number of booster pumps required from origin k to destination j, n_{kj}, pipeline capacity C_p (tons/year), and the amount of CO_2 emitted per kWh of electricity generated E^e (kg/kWh).

2.3.1 Formulation of the Two-Stage Stochastic Programming Model without Carbon Emissions Considerations

The two-stage stochastic programming model we present below allows us to capture the impact of the stochastic nature of sludge supply on location and transportation decisions in the supply chain; it also allows us to capture the timing of decisions in the supply chain. Facility location decisions, pipeline establishment decisions, and decisions about the number of trucks to purchase are long-term decisions made prior to observing the realization of biomass supply. These are the first-stage decisions in our model, which define the structure of the supply chain. Once these decisions are made, then, based on the availability of biomass supply -the realization of supply - the operational decisions related to biocrude and biodiesel production and transportation are made. For simplicity, the formulation below only captures sludge supply uncertainties.

The first-stage decision variables for our model are X_{lj} which is a binary variable that takes the value 1 if a biocrude plant of capacity $l \in \mathcal{L}$ is located at site $j \in \mathcal{J}$, and 0

otherwise; Z_{fkj} which is a binary variable that takes the value 1 if a pipeline of capacity $f \in \mathcal{F}$ is installed between supplier $k \in \mathcal{K}$ and biocrude plant $j \in \mathcal{J}$, and 0 otherwise; V_j which is the total number of trucks purchased for shipping sludge to biocrude plant $j \in \mathcal{J}$. Due to the physical characteristics of sludge and biocrude, the same trucks cannot be used to ship both products.

The investment cost for a biocrude plant of capacity $l \in \mathcal{L}$ is denoted by ψ_l. The investment costs for establishing a pipeline of capacity $f \in \mathcal{F}$ are denoted by ϑ_f. The purchase cost of a truck is denoted by v_1^1. Let $s_k(\omega)$ denote the amount of sludge available at site $k \in \mathcal{K}$ under scenario $\omega \in \Omega$. The model considers a fixed number of scenarios ($|\Omega|$), each of which represents a particular realization of biomass supply in each supply node. There is a positive probability ($prob(\omega)$) associated with each scenario.

Here are the second stage decision variables. The amount of sludge available for production of biodiesel at node $k \in \mathcal{K}$ under each scenario ω affects the amount of sludge transported to biocrude plant $j \in \mathcal{J}$. This amount in our model is represented by the decision variable $Y_{kjm}^1(\omega)$. Sludge availability under a particular scenario ω also impacts the values of the following decision variables: $W_{lj}(\omega)$ which is the amount of biocrude produced at plant $j \in \mathcal{J}$ of capacity $l \in \mathcal{L}$; $Y_{ji}^2(\omega)$ which is the amount of biocrude shipped from plant $j \in \mathcal{J}$ to diesel refinery $i \in \mathcal{I}$; $Y_{ig}^3(\omega)$ which is the amount of biodiesel shipped from diesel refinery $i \in \mathcal{I}$ to customer $g \in \mathcal{G}$; and $U_g(\omega)$ which is the amount of biodiesel shortage at customer g. The decision variables introduced in this paragraph are scenario-specific and are known as the second-stage or recourse variables. We assume that there are substitute products (such as, soybean-, canola-, sunflower-, palm- or coconut oil-based

biodiesels) which can be used to satisfy customers' demand for biodiesel. The best market price for a substitute product is denoted by ρ. This price, which is exogenously determined, equivalently represents the penalty paid for not satisfying customers' demand. The value of this penalty serves as a threshold level for the unit cost of delivering biodiesel to the market since there is no point in producing a product at a cost higher than the existing market price.

Other parameters that we use in the model formulation are ϕ which is the conversion rate (tons/gallon) of sludge to biocrude; γ which is the conversion rate (gallon/gallon) of biocrude to biodiesel; p_l^1 which is the unit production cost at a biocrude plant of capacity $l \in \mathcal{L}$; p_i^2 which is the unit production cost of biodiesel at diesel refinery $i \in \mathcal{I}$; b_g which is the demand for biodiesel at customer $g \in \mathcal{G}$; and q_i which is production capacity of biodiesel plant $i \in \mathcal{I}$.

The objective function of the biocrude supply chain network (BSCN) design model we propose minimizes the expected annual costs of the supply chain. This objective totals the first-stage costs and the expected second-stage costs. The first-stage costs comprise the annual equivalent investment costs to locate biocrude plants, to install pipelines, and to purchase trucks at biocrude plants. The second stage costs comprise the expected production, transportation, and penalty costs. The following is our model formulation.

(BSCN): Minimize z= $\sum_{j\in\mathcal{J}}\sum_{l\in\mathcal{L}} \psi_l X_{lj} + \sum_{f\in\mathcal{F}}\sum_{k\in\mathcal{K}}\sum_{j\in\mathcal{J}} \vartheta_f Z_{fkj} + \sum_{j\in\mathcal{J}} v_1^1 V_j + E_\omega\{\sum_{k\in\mathcal{K}}\sum_{j\in\mathcal{J}}\sum_{m\in\mathcal{M}}$

$c_{kjm}^1 Y_{kjm}^1(\omega) + \sum_{j\in\mathcal{J}}\sum_{i\in\mathcal{I}} c_{ji}^2 Y_{ji}^2(\omega) + \sum_{i\in\mathcal{I}}\sum_{g\in\mathcal{G}} (c_{ig}^3 + p_i^2) Y_{ig}^3(\omega) + \sum_{l\in\mathcal{L}}\sum_{j\in\mathcal{J}} p_l^1 W_{lj}(\omega) + \sum_{g\in\mathcal{G}} \rho U_g(\omega)\}$

Subject to

$$\sum_{l\in\mathcal{L}} X_{lj} \leq 1 \qquad \forall j \in \mathcal{J} \tag{2.8}$$

$$\sum_{j\in\mathcal{J}}\sum_{m\in\mathcal{M}} Y^1_{kjm}(\omega) \leq s_k(\omega) \quad \forall k \in \mathcal{K}, \omega \in \Omega \tag{2.9}$$

$$Y^1_{kjm}(\omega) - \xi^1_1 t_{kj} V_j \leq 0 \quad \forall k \in \mathcal{K}, j \in \mathcal{J}, \omega \in \Omega, m = \text{Fcl. own. truck} \tag{2.10}$$

$$Y^1_{kjm}(\omega) - \sum_{f\in\mathcal{F}} f * Z_{fkj} \leq 0 \quad \forall k \in \mathcal{K}, j \in \mathcal{J}, \omega \in \Omega, m = \text{Pipeline} \tag{2.11}$$

$$W_{lj}(\omega) \leq l * X_{lj} \quad \forall l \in \mathcal{L}, j \in \mathcal{J}, \omega \in \Omega \tag{2.12}$$

$$\sum_{k\in\mathcal{K}}\sum_{m\in\mathcal{M}} \phi Y^1_{kjm}(\omega) = \sum_{l\in\mathcal{L}} W_{lj}(\omega) \quad \forall j \in \mathcal{J}, \omega \in \Omega \tag{2.13}$$

$$\sum_{i\in\mathcal{I}} Y^2_{ji}(\omega) = \sum_{l\in\mathcal{L}} W_{lj}(\omega) \quad \forall j \in \mathcal{J}, \omega \in \Omega \tag{2.14}$$

$$\sum_{j\in\mathcal{J}} \gamma Y^2_{ji}(\omega) = \sum_{g\in\mathcal{G}} Y^3_{ig}(\omega) \quad \forall i \in \mathcal{I}, \omega \in \Omega \tag{2.15}$$

$$\sum_{g\in\mathcal{G}} Y^3_{ig}(\omega) \leq q_i \qquad \forall i \in \mathcal{I}, \omega \in \Omega \tag{2.16}$$

$$\sum_{i\in\mathcal{I}} Y^3_{ig}(\omega) + U_g(\omega) = b_g \qquad \forall g \in \mathcal{G}, \omega \in \Omega \tag{2.17}$$

$$X_{lj} \in \{0,1\} \quad \forall l \in \mathcal{L}, j \in \mathcal{J} \tag{2.18}$$

$$Z_{fkj} \in \{0,1\} \quad \forall f \in \mathcal{F}, k \in \mathcal{K}, j \in \mathcal{J} \tag{2.19}$$

$$V_j \in Z^+ \qquad \forall j \in \mathcal{J} \tag{2.20}$$

$$Y^1_{kjm}(\omega) \geq 0 \quad \forall k \in \mathcal{K}, j \in \mathcal{J}, m \in \mathcal{M}, \omega \in \Omega \tag{2.21}$$

$$Y^2_{ji}(\omega) \geq 0 \quad \forall j \in \mathcal{J}, i \in \mathcal{I}, \omega \in \Omega \tag{2.22}$$

$$Y^3_{ig}(\omega) \geq 0 \quad \forall i \in \mathcal{I}, g \in \mathcal{G}, \omega \in \Omega \tag{2.23}$$

$$W_{lj}(\omega) \geq 0 \quad \forall l \in \mathcal{L}, j \in \mathcal{J}, \omega \in \Omega \tag{2.24}$$

$$U_g(\omega) \geq 0 \quad \forall g \in \mathcal{G}, \omega \in \Omega \tag{2.25}$$

Constraints (4.3) ensure that at most one biocrude plant of capacity $l \in \mathcal{L}$ is operating at a particular location $j \in \mathcal{J}$. Constraints (4.5) ensure that the amount of sludge shipped from supplier $k \in \mathcal{K}$ is less than or equal to the amount of sludge available under scenario ω. Constraints (4.6) limit the amount of sludge transported by facility owned trucks at plant $j \in \mathcal{J}$. This amount depends on the number of trucks purchased, truck capacity, and the number of trips between supplier k and plant j (denoted by parameter t_{jk}). Constraints (4.7) show that the maximum amount of sludge transported by pipeline is limited by pipeline capacity. Note that in our model we assumed that the number of available rented trucks is not limited; therefore, we did not impose any capacity constraints for the rented trucks. Constraints (4.8) connect the binary biocrude facility location variables with the continuous biocrude production variables. These constraints also show that the total amount of biocrude produced is limited by production capacity of the plant. Constraints (4.9) calculate the total amount of biocrude produced from sludge at plant $j \in \mathcal{J}$ under scenario ω. Constraints (4.10) are the flow balance constraints at biocrude plant $j \in \mathcal{J}$. Constraints (4.12) are the flow balance constraints at diesel refinery $i \in \mathcal{I}$. Constraints (4.13) show that the total amount of biodiesel shipped from a diesel refinery is limited by its production capacity. Constraints(4.14) are the flow conservation constraints at customer $g \in \mathcal{G}$. These constraints indicate that customers' demand for biodiesel will be fulfilled either by using biocrude or other substitute products. Constraints (4.15) and (4.16) are binary constraints, and constraints (4.17) are the integrity constraints. Finally, (4.18) to (4.22) are the nonnegativity constraints.

2.4 Model Extension with Carbon Emission Considerations

This section presents four extensions of the (BSCN) model formulation to capture the impact that different carbon regulatory policies have on the supply chain design and management decisions. These policies include carbon cap, carbon tax, carbon cap-and-trade, and carbon offset. These extensions were inspired by recent work from Benjaafar et al. [10] who explores the impact of those carbon-regulatory policies on supply chain operations. The authors also provide similar extensions for the classical economic lot-sizing problem.

In this chapter we focus only on CO_2 emissions due to production and transportation in the supply chain since they contribute more than 95% of the total GHG emissions. The goal is to show later on in the computational results that certain modifications to production and transportation-related decisions (such as transportation mode selection, production schedule, and shipment schedule) can significantly reduce system-wide emissions at minimum cost.

2.4.1 Model Formulation of Carbon Cap Policy

Under a carbon cap policy, a company has a limited amount of carbon allowances to use, which is referred to as the *carbon cap* and denoted by c^{cap}. The World Resources Institute (WRI) has developed tools which support consistent and transparent public reporting of corporate value chain emissions [152]. Based on these standards, companies should account for emissions within their facility as well as emissions due to related upstream and downstream activities. That means, a biocrude plant should also be counting

emissions due to in-bound and out-bound supply chain activities. In order to present this limitation posed on the supply chain operations due to the carbon cap policy, we add the following constraints to (BSCN) model formulation. We refer to this new formulation as (BSCN-Cap) model.

$$\sum_{k\in\mathcal{K}}\sum_{j\in\mathcal{J}}\sum_{m\in\mathcal{M}} e^1_{kjm}Y^1_{kjm}(\omega) + \sum_{l\in\mathcal{L}}\sum_{j\in\mathcal{J}} e^4_{lj}W_{lj}(\omega) + \sum_{j\in\mathcal{J}}\sum_{i\in\mathcal{I}} e^2_{ji}Y^2_{ji}(\omega)$$
$$+\sum_{i\in\mathcal{I}}\sum_{g\in\mathcal{G}}(e^3_{ig}+e^5_{ig})Y^3_{ig}(\omega) \le c^{cap} \qquad \forall\omega\in\Omega \tag{2.26}$$

Here, e^4_{lj} denotes emissions per gallon of biocrude produced at a facility of capacity $l \in \mathcal{L}$, and e^5_{ig} denotes emissions due to biodiesel production at a diesel refinery.

2.4.2 Model Formulation of Carbon Tax Policy

A carbon tax policy imposes a financial penalty per unit of CO_2 emitted. Such a mechanism sets no limit on CO_2 emissions in the supply chain. This formulation assumes a linear relationship between emissions and carbon taxes. Let c^{tx} be the amount of tax paid per unit of CO_2 emitted. The objective function of the (BSCN) model is updated as follows to account for these taxes. We refer to this new formulation as (BSCN-Tax) model.

$$\text{Minimize z=}\sum_{j\in\mathcal{J}}\sum_{l\in\mathcal{L}}\psi_l X_{lj}+\sum_{f\in\mathcal{F}}\sum_{k\in\mathcal{K}}\sum_{j\in\mathcal{J}}\vartheta_f Z_{fkj}+\sum_{j\in\mathcal{J}}v^1_1V_j+E_\omega\{\sum_{k\in\mathcal{K}}\sum_{j\in\mathcal{J}}\sum_{m\in\mathcal{M}}(c^1_{kjm}+$$
$$c^{tx}e^1_{kjm})Y^1_{kjm}(\omega)+\sum_{j\in\mathcal{J}}\sum_{i\in\mathcal{I}}(c^2_{ji}+c^{tx}e^2_{ji})Y^2_{ji}(\omega)+\sum_{i\in\mathcal{I}}\sum_{g\in\mathcal{G}}(c^3_{ig}+p^2_i+c^{tx}(e^3_{ig}+e^5_{ig}))Y^3_{ig}(\omega)+$$
$$\sum_{l\in\mathcal{L}}\sum_{j\in\mathcal{J}}(p^1_l+c^{tx}e^4_{lj})W_{lj}(\omega)+\sum_{g\in\mathcal{G}}\rho U_g(\omega)\}$$

2.4.3 Model Formulation of Carbon Cap-and-Trade Policy

A carbon cap-and-trade policy imposes a carbon cap on supply chain operations. However, a carbon market exists where companies can trade their carbon allowances. A company can sell unused carbon allowances, or it can purchase additional carbon allowances to maintain supply chain operations. We make the following reasonable assumptions to reformulate the (BSCN) model under a carbon cap-and-trade policy: (a) carbon selling and purchasing prices are equal; (b) there is no limit on the amount of carbon allowances sold/purchased, and carbon trading decisions of this supply chain do not impact the market price; (c) the total cost/benfit function due to purchasing/selling carbon allowances is linear.

Let, c^p denote the market price per unit (kg) of carbon traded, and $c^{t+}(\omega)$ and $c^{t-}(\omega)$ denote the amount of carbon allowance purchased and sold under scenario ω. We propose the following formulation for this problem which we refer to as the (BSCN-CAT) model.

$$\text{Minimize z=} \sum_{j\in\mathcal{J}}\sum_{l\in\mathcal{L}} \psi_l X_{lj} + \sum_{f\in\mathcal{F}}\sum_{k\in\mathcal{K}}\sum_{j\in\mathcal{J}} \vartheta_f Z_{fkj} + \sum_{j\in\mathcal{J}} v_1^1 V_j + E_\omega\{\sum_{k\in\mathcal{K}}\sum_{j\in\mathcal{J}}\sum_{m\in\mathcal{M}} c_{kjm}^1 Y_{kjm}^1(\omega)$$
$$+ \sum_{j\in\mathcal{J}}\sum_{i\in\mathcal{I}} c_{ji}^2 Y_{ji}^2(\omega) + \sum_{i\in\mathcal{I}}\sum_{g\in\mathcal{G}} (c_{ig}^3 + p_i^2) Y_{ig}^3(\omega) + \sum_{l\in\mathcal{L}}\sum_{j\in\mathcal{J}} p_l^1 W_{lj}(\omega) + \sum_{g\in\mathcal{G}} \rho U_g(\omega)$$
$$+ c^p(c^{t+}(\omega) - c^{t-}(\omega))\}$$

subject to: (4.3)-(4.22)

$$\sum_{k\in\mathcal{K}}\sum_{j\in\mathcal{J}}\sum_{m\in\mathcal{M}} e_{kjm}^1 Y_{kjm}^1(\omega) + \sum_{l\in\mathcal{L}}\sum_{j\in\mathcal{J}} e_{lj}^4 W_{lj}(\omega) + \sum_{j\in\mathcal{J}}\sum_{i\in\mathcal{I}} e_{ji}^2 Y_{ji}^2(\omega) +$$
$$\sum_{i\in\mathcal{I}}\sum_{g\in\mathcal{G}} (e_{ig}^3 + e_{ig}^5) Y_{ig}^3(\omega) + c^{t-}(\omega) \le c^{cap} + c^{t+}(\omega) \quad \forall\omega\in\Omega \qquad (2.27)$$

$$c^{t+}(\omega), c^{t-}(\omega) \ge 0 \quad \forall\omega\in\Omega \qquad (2.28)$$

2.4.4 Model Formulation of Carbon Offset Policy

A carbon offset policy works like a carbon cap-and-trade policy. This policy imposes a carbon cap. A carbon market exists where additional carbon allowances can be purchased, if necessary, to maintain operations. However, unused carbon allowances cannot be sold. This implies that the supply chain of a product does not benefit from emitting less carbon than the corresponding cap.

Let, c^o be the unit price of carbon offset and $c^{t+}(\omega)$ denote the amount of carbon allowance purchased under scenario ω. We propose the following formulation for this problem which we refer to as (BSCN-CO) model.

$$\text{Min. z=} \sum_{j\in\mathcal{J}}\sum_{l\in\mathcal{L}} \psi_l X_{lj} + \sum_{f\in\mathcal{F}}\sum_{k\in\mathcal{K}}\sum_{j\in\mathcal{J}} \vartheta_f Z_{fkj} + \sum_{j\in\mathcal{J}} v_1^1 V_j + E_\omega\{\sum_{k\in\mathcal{K}}\sum_{j\in\mathcal{J}}\sum_{m\in\mathcal{M}} c_{kjm}^1 Y_{kjm}^1(\omega)$$

$$+ \sum_{j\in\mathcal{J}}\sum_{i\in\mathcal{I}} c_{ji}^2 Y_{ji}^2(\omega) + \sum_{i\in\mathcal{I}}\sum_{g\in\mathcal{G}} (c_{ig}^3 + p_i^2) Y_{ig}^3(\omega) + \sum_{l\in\mathcal{L}}\sum_{j\in\mathcal{J}} p_l^1 W_{lj}(\omega) + \sum_{g\in\mathcal{G}} \rho U_g(\omega) + c^o c^{t+}(\omega)\}$$

subject to: (4.3)-(4.22)

$$\sum_{k\in\mathcal{K}}\sum_{j\in\mathcal{J}}\sum_{m\in\mathcal{M}} e_{kjm}^1 Y_{kjm}^1(\omega) + \sum_{l\in\mathcal{L}}\sum_{j\in\mathcal{J}} e_{lj}^4 W_{lj}(\omega) + \sum_{j\in\mathcal{J}}\sum_{i\in\mathcal{I}} e_{ji}^2 Y_{ji}^2(\omega) + \sum_{i\in\mathcal{I}}\sum_{g\in\mathcal{G}} (e_{ig}^3 + e_{ig}^5) Y_{ig}^3(\omega) \le c^{cap} + c^{t+}(\omega) \quad \forall\omega\in\Omega \tag{2.29}$$

$$c^{t+}(\omega) \ge 0 \quad \forall\omega\in\Omega \tag{2.30}$$

2.5 Algorithmic Approaches

The computational challenges faced when solving the models presented above motivated the development of a number of solution approaches discussed in this section. These

computational challenges were inevitable since they represent a special case of the deterministic uncapacitated facility location problem, which has been shown to be NP-hard [28].

In this two-stage stochastic programming model, the first-stage decision variables are integer, but the second-stage decision variables are continuous. Laporte and Louveaux [74] present an algorithm to solve problems which include integer variables in the first-stage. The solutions algorithms we develop rely on and are extensions of the L-shaped method developed by Laporte and Louveaux.

2.5.1 L-Shaped Algorithm

Let $\Theta(X, Z, V)$ denote the expected value of the second-stage sub-problem of (BSCN) for the given values in the first-stage variables. The following is the deterministic equivalent formulation of (BSCN), referred to as (D-BSCN).

(D-BSCN) Minimize z= $\sum_{j\in\mathcal{J}}\sum_{l\in\mathcal{L}}\psi_l X_{lj}+\sum_{f\in\mathcal{F}}\sum_{k\in\mathcal{K}}\sum_{j\in\mathcal{J}}\vartheta_f Z_{fkj}+\sum_{j\in\mathcal{J}} v_1^1 V_j+\Theta(X,Z,V)$

subject to:

$$\sum_{l\in\mathcal{L}} X_{lj} \leq 1 \qquad \forall j \in \mathcal{J} \tag{2.31}$$

$$X_{lj} \in \{0,1\} \quad \forall l \in \mathcal{L}, j \in \mathcal{J} \tag{2.32}$$

$$Z_{fkj} \in \{0,1\} \quad \forall f \in \mathcal{F}, k \in \mathcal{K}, j \in \mathcal{J} \tag{2.33}$$

$$V_j \in Z^+ \qquad \forall j \in \mathcal{J} \tag{2.34}$$

The L-shaped algorithm is an iterative method. In each iteration, the problem solved is a relaxation of (D-BSCN), which instead of minimizing $\Theta(X, Z, V)$, minimizes an outer

approximation of $\Theta(X, Z, V)$. Birge and Louveaux [13] show that $\Theta(X, Z, V)$ is a piece-wise linear convex function when the number of scenarios considered $|\Omega|$ is finite. Thus, the linear functions generated by the algorithm lie on or below $\Theta(X, Z, V)$. Iteratively, the algorithm improves this approximation till an optimal solution is found. Laport and Louveaux [74] show that the L-shaped method converges to an optimal solution in a finite number of steps when the optimality and feasibility cuts added are valid; and when for a given set of first stage variables, the value of $\Theta(X, Z, V)$ can be computed.

The performance of the L-shaped algorithm relies on its ability to approximate $\Theta(X, Z, V)$. The following formulation (M-BSCN) is an approximation of model (D-BSCN). This formulation is solved iteratively, and Φ^n is the objective function value obtained at iteration n.

$$\text{(M-BSCN) } \Phi^n := \text{ Minimize } \sum_{j\in\mathcal{J}}\sum_{l\in\mathcal{L}} \psi_l X_{lj} + \sum_{f\in\mathcal{F}}\sum_{k\in\mathcal{K}}\sum_{j\in\mathcal{J}} \vartheta_f Z_{fkj} + \sum_{j\in\mathcal{J}} v_1^1 V_j + \theta$$

subject to: (2.31)-(2.34)

$$V_j \leq \sum_{l\in\mathcal{L}} N_l^T X_{lj} \qquad \forall j \in \mathcal{J} \tag{2.35}$$

$$\sum_{k\in\mathcal{K}}\sum_{f\in\mathcal{F}} Z_{fkj} \leq \sum_{l\in\mathcal{L}} X_{lj} \qquad \forall j \in \mathcal{J} \tag{2.36}$$

$$\theta \geq \theta^n + \sum_{j\in\mathcal{J}}\{\sum_{l\in\mathcal{L}} \lambda_{lj}^n (X_{lj} - X_{lj}^n) + \sum_{f\in\mathcal{F}}\sum_{k\in\mathcal{K}} \delta_{fkj}^n (Z_{fkj} - Z_{fkj}^n) + \Upsilon_j^n (V_j^n - V_j)\} \qquad \forall n = 1, \ldots, N \tag{2.37}$$

Constraints (2.35) and (4.34) are valid inequalities for problem (BSCN). Constraints (2.35) set an upper bound on the number of trucks (denoted N_l^T) that can be purchased by

a facility of capacity $l \in \mathcal{L}$. These two sets of constraints allow investments on purchasing trucks and building pipelines to those locations where facilities are located. Computational performance indicates that adding these constraints improves the running time of the algorithm.

Let N represents the number of iterations the algorithm has performed so far. In each iteration, (M-BSCN) is solved and the values for (X, Z, V) are obtained. These values become an input for the scenario-based problems (S-BSCN(ω)). The solutions obtained from solving these problems are used to calculate the value for $\Theta(X, Z, V)$. Each scenario-based problem is a linear, capacitated minimum cost network flow problem. The following is the formulation for the scenario-based problem ω during the $n-th$ iteration of the L-shaped algorithm.

(S-BSCN(ω)) $\theta^n(X_{lj}, Z_{fkj}, V_j, \omega) :=$ Minimize$\{\sum_{k\in\mathcal{K}}\sum_{j\in\mathcal{J}}\sum_{m\in\mathcal{M}} c^1_{kjm}Y^1_{kjm}(\omega)+$

$$\sum_{j\in\mathcal{J}}\sum_{i\in\mathcal{I}} c^2_{ji}Y^2_{ji}(\omega) + \sum_{i\in\mathcal{I}}\sum_{g\in\mathcal{G}}(c^3_{ig}+p^2_i)Y^3_{ig}(\omega) + \sum_{l\in\mathcal{L}}\sum_{j\in\mathcal{J}} p^1_l W_{lj}(\omega) + \sum_{g\in\mathcal{G}}\rho U_g(\omega)\}$$

subject to: (4.5)-(4.14) and (4.18)-(4.22)

$$X_{lj} = X^n_{lj} \quad : \Lambda^n_{lj}(\omega) \qquad \forall l \in \mathcal{L}, j \in \mathcal{J} \tag{2.38}$$

$$Z_{fkj} = Z^n_{fkj} \quad : \Delta^n_{fkj}(\omega) \qquad \forall f \in \mathcal{F}, k \in \mathcal{K}, j \in \mathcal{J} \tag{2.39}$$

$$V_j = V^n_j \quad : \Upsilon^n_j(\omega) \qquad \forall j \in \mathcal{J} \tag{2.40}$$

The linear equations (2.37) are constructed for specific sets of values for (X, Z, V). The generation of the $n-th$ linear equation is based on the value of partial derivatives

of $\Theta(X, Z, V)$ for changes in X, Z, and V. These values are in fact the dual variables from constraints (4.36), (4.37) and (4.38). Let $\Lambda^n_{lj}(\omega)$, $\Delta^n_{fkj}(\omega)$ and $\Upsilon^n_j(\omega)$ denote the dual variables for the ω scenario-based problem during the $n-th$ iteration of the L-shape algorithm, then the slope coefficients used in the linear equation (2.37) are computed as:

$$\Lambda^n_{lj} = \sum_{\omega \in \Omega} prob(\omega) \Lambda^n_{lj}(\omega) \tag{2.41}$$

$$\Delta^n_{fkj} = \sum_{\omega \in \Omega} prob(\omega) \Delta^n_{fkj}(\omega) \tag{2.42}$$

$$\Upsilon^n_j = \sum_{\omega \in \Omega} prob(\omega) \Upsilon^n_j(\omega) \tag{2.43}$$

The intercept term is:

$$\theta^n = \sum_{\omega \in \Omega} prob(\omega) \theta^n(\omega). \tag{2.44}$$

For any given set of values in first-stage decision variables, problems (S-BSCN(ω)) are always feasible. The feasibility of these problems is always maintained because of constraints (4.14). These constraints enforce customer demand to be satisfied either through production, or through substitute products available in the market. Thus, even in the case when the value of all the first-stage variables is zero, customer demand is still satisfied.

The objective function value of problem (M-BSCN) is a lower bound for (D-BSCN) [13]. This is because (M-BSCN) minimizes instead an outer approximation of the convex function $\Theta(X, Z, V)$. For a given set of first stage variables, the scenario based problems are used to calculate the actual value of $\Theta(X, Z, V)$. At each iteration, a solution of the master problem and its subproblem provides an upper bound for the original prob-

lem (BSCN). The L-shaped algorithm terminates when the relative error gap between the generated lower and upper bounds is less than ϵ.

Table 2.2 describes the L-shaped algorithm. We use CPLEX to solve (M-BSCN) and (S-BSCN(ω)) for all $\omega \in \Omega$. The computational efficiency of this algorithm depends mainly on the computational efforts required to solve (M-BSCN). The algorithms discussed next aim to reduce the running time of this algorithm.

2.5.2 Multi-cut L-Shaped Algorithm

The L-shaped algorithm adds a single optimality cut in each iteration of the master problem (M-BSCN). This cut aims to approximate the solution space of the scenario-based subproblems (S-BSCN(ω)). Instead, in every iteration of the multi-cut L-shaped algorithm, $|\Omega|$ linear equations are added to the first stage problem. These additional constraints are generated by disaggregating the single cut (2.37) used in the L-shaped algorithm. The following (MC-BSCN) is the first stage problem solved when using this algorithm.

$$\text{(MC-BSCN)}\ \Phi^n := \text{Min.} \sum_{j\in\mathcal{J}}\sum_{l\in\mathcal{L}} \psi_l X_{lj} + \sum_{f\in\mathcal{F}}\sum_{k\in\mathcal{K}}\sum_{j\in\mathcal{J}} \vartheta_f Z_{fkj} + \sum_{j\in\mathcal{J}} v_1^1 V_j + \sum_{\omega\in\Omega} prob(\omega)\theta_\omega$$

Subject to: (2.31)-(2.34)

$$\begin{aligned}\theta_\omega \;\geq\; & \theta_\omega^n + \sum_{l\in\mathcal{L}}\sum_{j\in\mathcal{J}} \Lambda_{lj\omega}^n (X_{lj} - X_{lj}^n) + \sum_{f\in\mathcal{F}}\sum_{k\in\mathcal{K}}\sum_{j\in\mathcal{J}} \Delta_{fkj\omega}^n (Z_{fkj} - Z_{fkj}^n) \\ & + \sum_{j\in\mathcal{J}} \Upsilon_{j\omega}^n (V_j^n - V_j) \quad \forall n = 1,\ldots,N, \omega\in\Omega \end{aligned} \tag{2.45}$$

To solve this problem we slightly adjust the algorithm presented in Table 2.2. These modifications are: STEP 3 is not executed, and STEP 4 solves (MC-BSCN) instead.

The multi-cut L-shaped algorithm was introduced by Birge and Louveaux [12] to enhance the convergence of the L-shaped algorithm. The algorithm is expected to take fewer number of iterations to reach optimality. However, each iteration is likely to take longer due to the larger set of constraints in (MC-BSCN). This is particularly true when the restricted master problem is a mixed integer program.

2.5.3 Lagrangian Relaxation with L-Shaped Algorithm

We developed a problem-specific, Lagrangian relaxation-based algorithm to solve (M-BSCN) problem within the L-shaped algorithm. We relax constraints (2.31) and obtain the following Lagrangian relaxation problem. (LR-BSCN) $L(\Xi) =$

$$\min \sum_{j\in\mathcal{J}}\sum_{l\in\mathcal{L}} \psi_l X_{lj} + \sum_{f\in\mathcal{F}}\sum_{k\in\mathcal{K}}\sum_{j\in\mathcal{J}} \vartheta_f Z_{fkj} + \sum_{j\in\mathcal{J}} v_1^1 V_j + \theta + \sum_{j\in\mathcal{J}} \Xi_j \left(\sum_{l\in\mathcal{L}} X_{lj} - 1\right)$$

subject to: (2.32)-(2.37).

Ξ_j are the Lagrangian multipliers where $\Xi_j \geq 0; \forall j \in \mathcal{J}$. We use a subgradient method [94] to solve the Lagrangian dual problem. Table 2.3 provides the details of the Lagrangian relaxation algorithm. Within the L-shaped algorithm presented in Table 2.2, this algorithm is used instead of STEP 1.

The algorithm starts by initializing the decision variables, iteration number (r), and a threshold value of the error gap (ε_{LR}). The purpose of initializing the decision variables is to start the algorithm with an upper bound value which is better than some arbitrarily high value. We use a simple procedure that opens the minimum number of facilities to ensure that the expected customer demand is satisfied. Next, the algorithm calculates a minimum number of trucks to purchase to ensure the delivery of biomass supply to each facility.

Formulation (LR-BSCN) is then solved using CPLEX. The solution to this relaxation is a lower bound for (M-BSCN). Thus, it is also a lower bound for model (BSCN). When the relative gap between the lower and the upper bounds generated is smaller than the threshold value ε_{LR}, the algorithm stops. Otherwise, the values of Lagrangian multipliers are updated, and problem (LR-BSCN) is resolved.We refer the readers to a recent study by Rawls and Turnquist [103] for details about the convergence and computation performance of this heuristic approach.

2.5.4 Lagrangian Relaxation with Multi-cut L-Shaped Algorithm

The Lagrangian relaxation algorithm is also used with the Multi-cut L-shaped algorithm to solve the first-stage problem. The following is the corresponding Lagrangian relaxation problem obtained by relaxing constraints (2.31).

(LR-M-BSCN) $L(\Xi) =$

$$\min \sum_{j\in\mathcal{J}}\sum_{l\in\mathcal{L}} \psi_l X_{lj} + \sum_{f\in\mathcal{F}}\sum_{k\in\mathcal{K}}\sum_{j\in\mathcal{J}} \vartheta_f Z_{fkj} + \sum_{j\in\mathcal{J}} v_1^1 V_j + \sum_{\omega\in\Omega} prob(\omega)\theta_\omega + \sum_{j\in\mathcal{J}} \Xi_j(\sum_{l\in\mathcal{L}} X_{lj} - 1)$$

subject to: (2.32)-(4.34), and (4.39)

$$\Xi_j \geq 0 \qquad\qquad \forall j \in \mathcal{J}.$$

Similar to the Lagrangian-relaxation algorithm in Table 2.3, the algorithm developed to solve $L(\Xi)$ relies on using the subgradient algorithm to determine the value of the Lagrange multipliers. We follow the same steps as explained in Algorithms 1 and 2. Algorithm 2 finds lower bounds to (BSCN) by solving the (LR-M-BSCN) formulation using the Lagrangian relaxation algorithm.

2.6 Computational Study and Managerial Insights

This section presents the results of our computational study and provides some managerial insights suggested by solving (BSCN). We use the state of Mississippi as the testing grounds for our models. The following subsections describe the data used, present the results from the experimental study, and compare the performances of the L-shaped algorithms developed.

2.6.1 Data Description

The major suppliers of sludge are municipal WWT facilities. Other suppliers are industrial facilities such as pulp and paper plants, poultry slaughtering and processing plants, fresh and frozen fish processing plants, etc. This study considers a total of 94 WWT facilities and industrial plants located in Mississippi. Figure **??** presents the distribution of these plants, which is highly correlated with the distribution of population. The largest plants are located in highly populated areas, such as, the capital of the state (in the center) and the Gulf Coast (in the South).

2.6.1.1 Biodiesel Demand

Our study assumes that the biodiesel produced will be used to satisfy fuel needs in Mississippi. The population distribution is a good indicator of the demand distribution for biodiesel. Therefore, we used the relative size of a county's population- as compared to the whole state - to identify what percent of biodiesel produced would be delivered there. Of the total 82 counties, we selected 52 as customer locations. The criterion used to select

these counties is their population size. We use the centroid of the county as the point to which biodiesel is to be delivered.

We set the overall demand for biocrude to the constant value of 96 million gallons a year (MGY). This value corresponds to the total amount of biocrude that could be produced using the amount of sludge available in the state. The total fuel consumption in Mississippi in 2005 was 1,700 MGY [87]. Note that, if 10% of this fuel is substituted by biofuels, then, a total of 170 MGY of biofuel would be consumed annually in Mississippi. The U.S. Energy Information Administration reports that, each year, Mississippi produces around 54.0 MGY [133] of ethanol but consumes around 94.94 MGY [96] of ethanol. Therefore, a need clearly exists to explore additional renewable energy sources to meet the in-state demand for ethanol.

2.6.1.2 Investment Costs

The cost of transporting sludge is relatively high due to its high water content and low yield. Therefore, it makes sense to co-locate biocrude plants with large capacity WWT facilities and industrial plants. We use a threshold value of 1,000 tons of sludge generated per year to identify facilities which could potentially co-locate with a biocrude plant. Additionally, we eliminated from our list a few small size facilities which were located in remote areas and far from other WWT facilities. This procedure identified a set of 26 facilities considered to be potential locations for biocrude plants.

The data about investment and operating costs of a biocrude plant came from a research paper by Mondala et al. [88]. We consider three potential biocrude plant sizes: 5 MGY, 10

MGY, and 20 MGY. The estimated investment costs are $9.45M, $17.84M and $31.6M, respectively.

Our study assumes that biocrude would be shipped for further processing to one of the 10 diesel refineries located in Mississippi and its neighboring states. It is expected that biocrude will displace the use of fossil fuels for diesel production, and therefore, no additional investments in capacity are required at these plants.

Based on the availability of sludge in Mississippi, the maximum capacity of a pipeline is expected to be 150 tons per day (TPD). Other potential capacities considered are 90 TPD and 120 TPD. Investment costs for building pipelines with capacities 90 TPD, 120 TPD and 150 TPD are estimated to be $65,398, $77,480 and $88,569 correspondingly. We refer the readers to a recent work by Marufuzzaman et al. [85] for details about pipeline installation and operating costs.

2.6.1.3 Transportation Costs

We consider that three different modes of transportation are available for shipping sludge: facility-owned trucks, rented trucks, and pipelines. The associated transportation costs are shown in Table 2.4. Truck transportation costs are calculated for a single trailer truck with a load capacity of 30 tons and average traveling speed of 40 miles per hour. Pipeline transportation costs are estimated for one-way PVC plastic pipeline. The solid content of sludge is 5%. Table 2.5 summarizes the key financial and operational parameters used to estimate pipeline transportation costs. Details about pipeline transportation costs and design considerations can be found at [85].

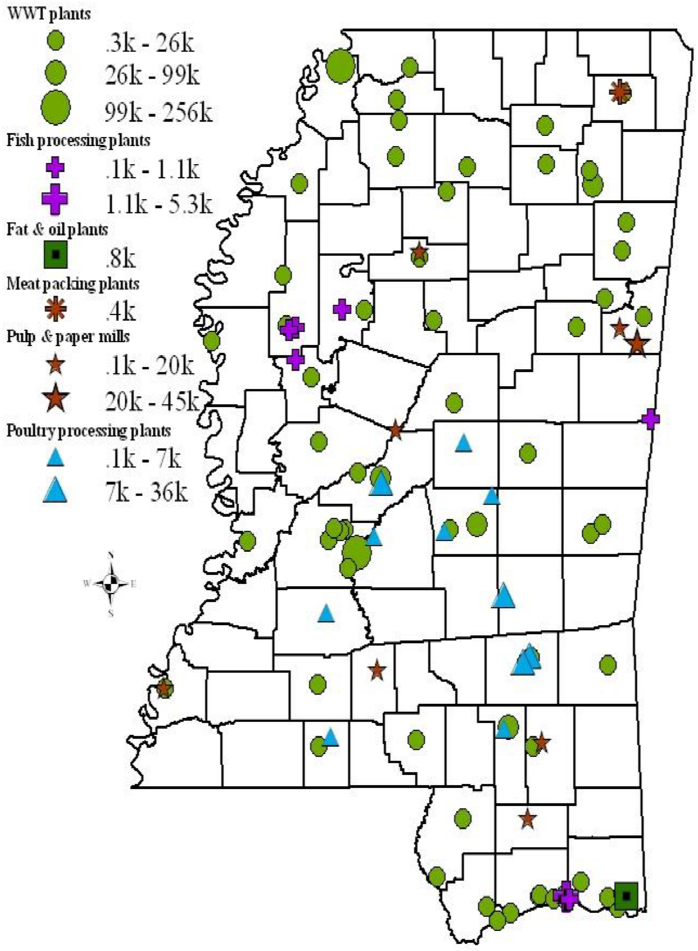

Figure 2.2

Locations and yields of sludge generating facilities

We consider that trucks with a load capacity of 8,000 gallons are used to transport biocrude and biodiesel. The corresponding cost components are listed in Table 2.4. We assume that a shipment is moved from its origin to its destination using the corresponding shortest path. We used Arc GIS Desktop 10 to create a transportation network, and used this network to identify the shortest paths. The network includes local, rural, and urban roads, along with the major highways in Mississippi.

2.6.1.4 Scenario Definitions and Probability of Occurrence

We generate a total of 10 scenarios to capture fluctuations in sludge supply at different locations. Five of these scenarios are based on historical data from 2006 to 2010 (Table 2.1). We assign a probability of 15% to each of these five scenarios. Table 2.6 provides descriptions about the remaining scenarios and the corresponding probabilities. Scenarios 9 and 10 consider an increase/decrease of activities in the two industries that contribute the most to generating sludge in Mississippi. The assignment of these probabilities for each scenario was determined from discussions with experts.

In addition to investigating the impact of biomass supply fluctuations on biodiesel production and costs, we also investigate the impact of the technology used to generate biocrude on production and costs. A prior study by Eksioglu et al. [40] used a conversion rate of 0.26. This rate means 0.26 tons of biocrude are produced from one ton of sludge. This value came from studies conducted in small scale at a laboratory. The chances are that the conversion rates to be observed in a large production plant will probably be different. Another related study by Marufuzzaman et al. [82] notes that fluctuations of the

conversion rate have a great impact on costs and production quantity. These observations are a motivation for creating a total of five different scenarios. The highest probability is assigned to the conversion rate, which has been identified from laboratory studies. Table 2.7 summarizes the scenario definitions with the associated probabilities. Note that, the two scenario sets are used independently in order to capture the feedstock supply and technology uncertainties.

2.6.2 Experimental Results

This section discusses the results of our computational study. All the algorithms are coded in GAMS 24.2.1 [48] on a desktop with Intel Pentium Centrino Dual computer with 2.80 GHz processor and 1.0 GB RAM. The optimization solver used is ILOG CPLEX 12.6.

Computational analysis of (BSCN-Cap) : Figure 2.3 shows the impact of varying emissions caps on total system costs and biodiesel production. Each graph has two lines, one that presents the results from the stochastic solution for model (BSCN-Cap) and the other that presents the results of the corresponding expected value solution. In order to generate these results, we consider only supply uncertainties. Figure 2.3 presents the relationship between the carbon cap and total system costs. Comparing the stochastic and expected value lines shows that the stochastic solution outperforms the expected value solutions. The stochastic models identify solutions which result in, on average, savings of $2.99 million per year and an average increase of production by 3.08 MGY.

The results indicate that biodiesel production decreases and total system costs increase as the carbon cap gets tighter. However, note the stepwise shape of the graphs as the carbon

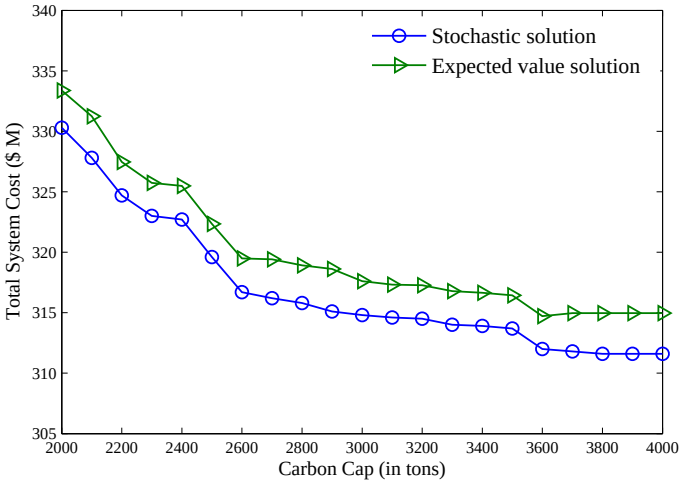

Figure 2.3

Carbon cap vs. costs under supply uncertainty

cap decreases. This shape indicates that the decrease in production and increase in costs is not smooth with the decrease of the carbon cap. A carbon cap is a hard constraint for the system and directly impacts its emissions. As the cap gets tighter, the system design and management is adjusted to meet emissions requirements at a slight increase in costs. For example, reducing the carbon cap from 3,200 tons/year to 2,900 tons/year does not impact biocrude production, but it does impact costs. Total systems cost increases from $314 million to $317 million. The 9.7% reduction in emissions, due to the change on the carbon cap, results in a 0.96% increase in the total system costs. This indicates the potential to reduce carbon emissions in the supply chain through changes in supply chain operations at minimum cost.

Note that, we assume the fuel efficiency of trucks remains unchanged despite the decrease in the carbon cap or increase in the carbon tax and carbon market price. A related

study [81] depicts the positive impact on improvements in truck's fuel efficiency that is reducing supply chain-related emissions.

Computational analysis of (BSCN-Tax): Figure 2.4 presents the impact of the carbon tax on biodiesel production and total unit costs. Figure 2.4 indicates that increasing the carbon tax directly (linearly) increases total unit costs. However, biodiesel production is not impacted when the tax rate is less than \$3/kg (or equivalently \$3,000/ton) of CO_2 because the unit delivery cost of biodiesel is less than \$3/gallon. The increase in tax beyond \$3/kg of CO_2 increases the unit cost of biodiesel beyond \$3/gallon, and therefore, other substitute products are used instead. The graphs also indicate that the stochastic model outperforms the expected value solution. The average cost savings from the stochastic solutions are \$3.16 million/year and the average production increase is 3.05 MGY.

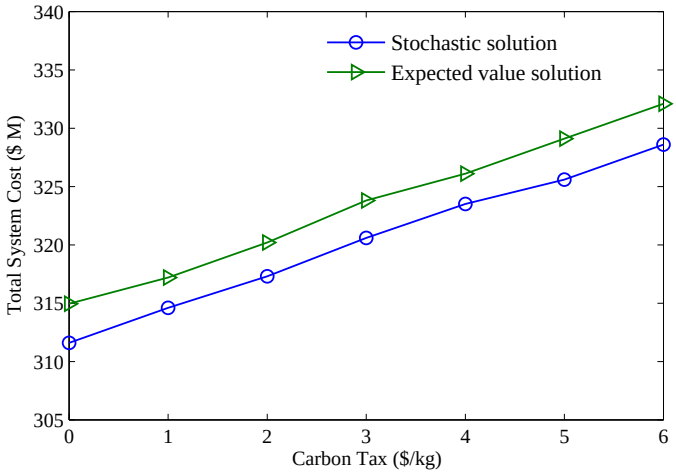

Figure 2.4

Carbon tax vs. costs under supply uncertainty

A recent survey conducted by the Intergovernmental Panel on Climate Change (IPCC) found that an optimal carbon tax rate would be between $3 and $95 per metric ton. 100 related studies were used to estimate a range for the optimal tax rate [86]. The values of tax rates we use in our analysis are very high. We used such values in order to identify the level of tax rate which impacts decisions about supply chain design and management.

Computational analysis of (BSCN-CAT):

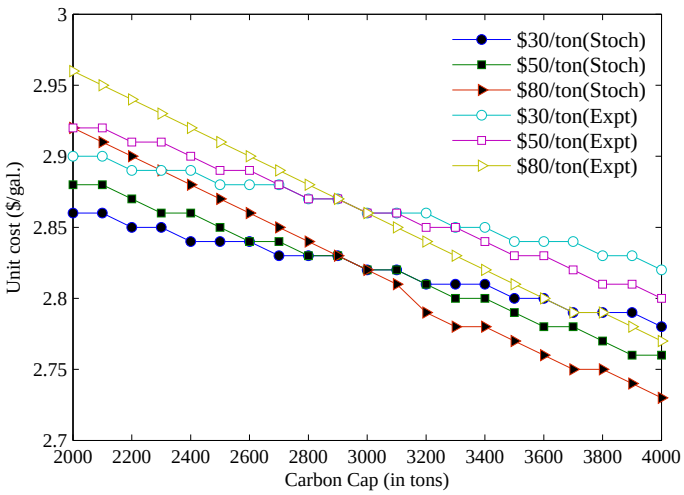

Figure 2.5

Carbon price versus costs under a carbon cap-and-trade policy

Figure 2.5 represents the relationship between carbon cap, and unit cost at different carbon market prices. The figure indicates that an increase in the carbon market price would result in lower supply chain costs when the cap is loose and higher costs when the cap is tight. This is because at low cap and at high carbon price, there is an incentive for companies to sell carbon credits which are considered an additional source of income.

However, as the cap becomes tighter, it costs more to buy additional credits and results in higher supply chain costs. In all the experiments we performed, biodiesel production was maintained because the unit cost of biodiesel is less than the $3/gallon, which is assumed to be the market price for substitute products.

Computational analysis of (BSCN-CO): Figure 2.6 shows the effect of a carbon offset mechanism on total system cost and on the amount of carbon credits purchased. We consider three different carbon offset prices c^o ($/ton) $\in \{5, 10, 20\}$. The motivation for selecting these values was the observation that in the last few years the carbon offset price has varied from $2.75/ton-$12/ton (Chicago Climate Exchange). Decreasing the carbon cap implies that the amount of carbon credits available to maintain supply chain activities is decreasing. Thus, in order to maintain its operations, this supply chain is faced with these decisions: (a) reduce production; (b) purchase additional carbon credits in the market; or (c) modify supply chain operations.

The focus of regulatory mechanisms such as the ones discusses here is to curb the total carbon emissions in the supply chain of a particular region, or a county, or the whole world. The parameters used in the calculations will differ, but, the mathematical models we propose and the methods we use to calculate emissions can easily adopted to other regions.

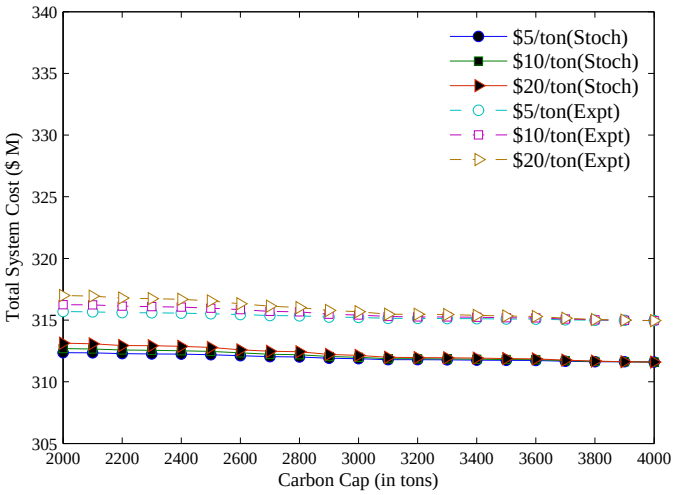

Figure 2.6

Carbon price vs. costs under carbon offset policy

2.6.3 Analyzing the Performance of Solution Algorithms

This section describes our computational experiences related to the algorithms proposed in Section 2.5 when solving the biodiesel supply chain problem. The dimensions of the deterministic equivalent problem are presented in Table 2.8.

Table 2.9 summarizes the results of the algorithms proposed. We use the following terminating criteria for these algorithms: (a) $\varepsilon = 0.01$ (b) $time_{max} = 36,000$ seconds and, (c) $iter_{max} = 1,000$. The first column of Table 2.9 presents the number of scenarios studied, followed by the solution method used, the corresponding objective function value found, error gap, number of iterations, and running time. The error gap is calculated as follows: Error (in %) = $100 * (UB - LB)/UB$.

Our computational experience in solving the problem using (BSCN-ML) and (BSCN-LR-ML) algorithms has been very good. The algorithm finds high quality feasible solu-

tions for the master problem in all problem instances. This impacts the quality of solution of the subproblem, and consequently the quality of the overall solution. Algorithms (BSCN-ML) and (BSCN-LR-ML) outperform (BSCN-L) and (BSCN-LR-L) since the multiple optimality cuts added in each iteration do a better job in approximating $\Theta(X, Z, V)$. Both (BSCN-ML) and (BSCN-LR-ML) algorithms provide solutions within 1% error gap in a reasonable amount of time. The other algorithms stop because of the time limit or iteration limit.

We observed that during the initial iterations of the algorithm, the master problem did not receive enough information from the subproblem and therefore, the quality of solutions was poor. We were able to find feasible solutions to the master problem as the number of the optimality cuts increased. Thus, in order to reduce the running time of the Lagrangean-relaxation during the initial iterations of the L-shaped algorithm, we set the error gap for the Lagrangian relaxation algorithm (ε_{LR}) to 0.05. This error gap is dynamically adjusted to 0.01 as the algorithm progresses and the gap between upper and lower bound of the L-shaped algorithm improves. Often, during the initial iterations of the L-shaped algorithm, the Lagrangian-relaxation algorithm did not converge to the pre-specified error gap. This is why we terminate the Lagrangian-relaxation algorithm when one of the following criteria is met: (i) the improvement on the lower bound after r consecutive iterations is below a threshold value; or (ii) the maximum number of iterations is reached. We proceed solving the subproblem by using the best known feasible solution of the master problem obtained so far.

When solving problems of large size, the chances are that the optimality gap of Lagrangian-relaxation algorithm may still be greater than zero. In this case the readers are encouraged to apply well-known techniques, such as, branch and bound [24], variable fixing [121] and reduction tests [24] to reduce this optimality gap.

Note that, CPLEX also emerges as a good tool to solve the problem within 1% error gap for all the instances studied. However, the running time of CPLEX is, on average, 3.3 and 25.7 times higher as compared to (BSCN-ML) and (BSCN-LR-ML).

2.6.4 Performance evaluation of stochastic solutions

This section evaluates the performance of the stochastic programming models developed to capture supply and technology development uncertainties. For this purpose, we calculate the expected value of perfect information ($EVPI$) and the value of stochastic solution (VSS). $EVPI$ measures the value of knowing the future with certainty [13]. Thus, $EVPI$ represents the difference between the wait and see solution (WSS) and the objective function value from solving (BSCN). VSS measures the value of stochastic solution and it is calculated as the difference between the objective function value of (BSCN) and the expected value solution (EEV). A summary of these results is reported in Tables 2.10 and 2.11.

$EVPI$ is calculated using the results listed in Table 2.10. The WSS for each scenario are calculated by solving (BSCN) assuming in the future we face this single scenario only. Then, we use these results to calculate $WSS = (\$316.77M + \$287.10M + \$319.67M + \$284.02M + \$298.66M) * 0.15 + (\$269.15M + \$338.22M + \$276.45M + \$304.57M +$

$\$287.69M) * 0.05 = \$299.73M$. Therefore, $EVPI = \$310.9M - \$299.73M = \$11.17M$. This means, if it were possible to know perfectly the future of annual sludge supply, then the total system costs would only be \$299.73M. However, since no one can predict the future, by solving the stochastic programming model, we identify a supply chain with total costs of \$310.9M. The value of $EVPI$ - $\$11.17M$ - indicates how much is worth knowing the future with certainty.

In order to calculate VSS we first need to calculate EEV. Calculating EEV requires two simple steps. We first solve the deterministic version of (BSCN) by using expected values of biomass supply instead. Next, we use this solution to set the values of the first-stage variables in formulation (BSCN) and then resolve. The corresponding objective function value is EEV. Then, VSS = EEV - \$310.90M = \$314.15M - \$310.90M = \$3.25M. Therefore, \$3.25M represents the savings realized by solving the stochastic model formulation (BSCN) rather than solving the corresponding deterministic formulation of our problem.

Similarly, we use the data in Table 2.11 to calculate $EVPI$ and VSS for the case when we solve (BSCN) under technology development uncertainty. In this case, $WSS = \$303.32M$, and the corresponding $EVPI = \$3.70M$. This means, the value of knowing perfectly the future of technological innovations is \$3.70M. The value of $EEV = \$309.25M$, and $VSS = \$2.23M$. Thus, \$2.23M are the total savings which can result from modeling and solving this supply chain problem as a two-stage stochastic program, rather than solving the corresponding deterministic model.

Tables 2.10 and 2.11 also present the amount of biodiesel produced under each scenario. The results of Table 2.11 indicate that, as the conversion rate increases, the amount of biodiesel produced increases.

In summary, the performance of supply chain is impacted by uncertainties in sludge supply and technology development. Therefore, it is worthwhile to adopt stochastic programming modeling to design and manage biodiesel supply chains. Experimental results indicate that total cost savings result when a stochastic approach is used to solve the problem as opposed to an expected value approach.

2.7 Conclusion

This chapter discusses a two-stage stochastic programming model to design and manage a biodiesel supply chain under feedstock and technology development uncertainties. The technology we rely on in this study uses wastewater sludge to produce biocrude, which is further processed into biodiesel. The main sources of wastewater sludge are WWT plants, pulp and paper mills, poultry slaughtering and processing plants, fresh and frozen fish processing plants, fat and oil from animal and marine plants, and meat packing plants. Based on the models proposed, the expected delivery cost of biodiesel is \$2.72/gallon. We have extended our model in order to account for CO_2 emissions due to supply chain activities. We model the impact of different carbon regulatory mechanisms, such as carbon cap, carbon tax, carbon cap and trade, and carbon offset on the design and management of supply chains for biofuels.

We propose four solution algorithms to solve the two-stage stochastic programming model. These algorithms are the L-shaped algorithm (BSCN-L); the Multi-cut L-shaped algorithm (BSCN-ML); the Lagrangian relaxation with L-shaped algorithm (BSCN-LR-L); and the Lagrangian relaxation with Multi-cut L-shaped algorithm (BSCN-LR-ML). Computational results showed that all four algorithms performed well for moderately sized problems. However, as the problem size increases, we observe that the multi-cut L-shaped algorithms (BSCN-ML) and (BSCN-LR-ML) outperform the rest.

The computational analyses provide some insightful results about the impact of carbon regulatory mechanisms on supply chain costs and emissions. Based on the results, the carbon cap mechanism imposes a hard constraint on the amount of CO_2 emitted in the supply chain. Thus, emissions are the lowest under this mechanism. The other mechanisms provide more flexibility. Results indicate that a carbon cap-and-trade mechanism is more efficient than a carbon offset mechanism since a carbon cap-and-trade motivates companies to emit less CO_2 even when the carbon cap is loose and not restrictive. This is due to the existence of a market where unused carbon credits can be sold for a profit.

We compare the stochastic and expected value solutions in several scenarios. The stochastic solutions are consistently better in respect to costs and emissions. This justifies the use of stochastic programming approach to solve this supply chain problem.

Table 2.2

Algorithm 1: L-shaped algorithm for BSCN problem (BSCN-L)

STEP 0:
Initialize, ε. Set, $n \leftarrow 1$, $LB \leftarrow -\infty, UB \leftarrow +\infty$
STEP 1:
Solve (M-BSCN) to obtain Φ^n, X_{lj}^n, Z_{fkj}^n, V_j^n
If $(\Phi^n > LB)$ **Then**
$LB \leftarrow \Phi^n$
End If
STEP 2:
For all $\omega \in \Omega$ **Do**
Solve (S-BSCN(ω)) to obtain $\theta_\omega^n, \Lambda_{lj}^n(\omega), \Delta_{fkj}^n(\omega), \Upsilon_j^n(\omega)$
End for
Calculate θ^n using (2.44)
$\varrho^n \leftarrow \theta^n + \sum_{j\in\mathcal{J}} \sum_{l\in\mathcal{L}} \psi_l X_{lj} + \sum_{f\in\mathcal{F}} \sum_{k\in\mathcal{K}} \sum_{j\in\mathcal{J}}$
$\vartheta_f Z_{fkj} + \sum_{j\in\mathcal{J}} v_1^1 V_j$
If $(\varrho^n < UB)$ **Then**
$UB \leftarrow \varrho^n$
End If
STEP 3:
Calculate $\Lambda_{lj}^n, \Delta_{fkj}^n, \Upsilon_j^n$ using (2.41), (2.42), (2.43)
STEP 4:
If $((UB - LB)/UB < \varepsilon)$ **Then STOP**
Else
Add to (M-BSCN):
$\theta \geq \theta^n + \sum_{l\in\mathcal{L}} \sum_{j\in\mathcal{J}} \Lambda_{lj}^n (X_{lj} - X_{lj}^n) + \sum_{f\in\mathcal{F}} \sum_{k\in\mathcal{K}}$
$\sum_{j\in\mathcal{J}} \Delta_{fkj}^n (Z_{fkj} - Z_{fkj}^n) + \sum_{j\in\mathcal{J}} \Upsilon_j^n (V_j^n - V_j)$
$n \leftarrow n + 1$; **GoTo STEP 1**
End If

Table 2.3

Algorithm 2: Lagrangian relaxation algorithm

STEP 1

Initialize, ε_{LR}, $\overline{X}_{lj}$, $\overline{Z}_{fkj}$, $\overline{V}_j$.

Set, $r \leftarrow 1$, stop $\leftarrow$ **False**, $\Xi_j^r \geq 0$, $no_{impr} \leftarrow 0$, $\eta^r \leftarrow 2$, $s_s \leftarrow 0$

While (stop = **False**) **Do**

Solve (LR-BSCN) to obtain $L(\Xi)^r$, X_{lj}^r, Z_{fkj}^r, V_j^r

If $(L(\Xi)^r > LB)$ **Then**

$LB \leftarrow L(\Xi)^r$

$no_{impr} \leftarrow 0$

Else

$no_{impr} \leftarrow no_{impr} + 1$

If$(no_{impr} > 5)$ **Then**

$\eta^{r+1} \leftarrow \eta^r/2$

$no_{impr} \leftarrow 0$

End If

End If

$\overline{UB} = min\{UB, \sum_{j\in\mathcal{J}} \sum_{l\in\mathcal{L}} \Psi_l \overline{X}_{lj} + \sum_{f\in\mathcal{F}} \sum_{k\in\mathcal{K}} \sum_{j\in\mathcal{J}} \vartheta_f \overline{Z}_{fkj} + \sum_{j\in\mathcal{J}} \nu_1^1 \overline{V}_j\}$

If $((\overline{UB} - LB)/\overline{UB} \leq \varepsilon_{LR})$ **Then**

stop $\leftarrow$ **True**

Else

$s_s \leftarrow \eta^r \frac{\overline{UB} - LB}{\sum_{j\in\mathcal{J}} (\sum_{l\in\mathcal{L}} X_{lj} - 1)^2}$

$\Xi_j^{r+1} = \max\{0, \Xi_j^r + s_s(\sum_{l\in\mathcal{L}} X_{lj} - 1)\}$

End If

$r \leftarrow r + 1$

End While

Table 2.4

Unit transportation cost for truck and pipeline

Costs	Parameters	Value	Unit
Sludge transportation:			
Fixed cost-rented truck	ν_2^1	4.56	\$/ton
Variable cost-rented truck	β_2^1	0.072	\$/ton/mile
Variable cost-owned truck	β_1^1	0.058	\$/ton/mile
Variable cost-pipeline@150tons/day	α_f	0.186	\$/ton/mile
Biocrude & Biodiesel transportation:			
Loading/unloading	ν_2^2, ν_2^3	0.02	\$/gallon
Time dependent	β_2^2, β_2^3	32.0	\$/hr/trucload
Distance dependent	β_2^2, β_2^3	1.30	\$/mile/trucload

Table 2.5

Parameters required to calculate pipeline transportation costs

Parameter	Value	Unit
Pipeline operating life	30	Years
Pipeline operating days	350	Days
Slurry design velocity	2.7	ms^{-1}
Pump efficiency	80	%
Discount rate	10	%
Labor cost	29.20	h^{-1}
Labor hour requirement	8,400	$hyear^{-1}$
Electricity cost	60.0	\$ MWh^{-1}
Pipeline maintenance cost	0.5	% of its capital cost
Pump station maintenance cost	3.0	% of its capital cost
Contingency	10	% of its capital cost

Table 2.6

Scenario definitions under feedstock supply uncertainty

Scenario	Explanation	Probability
1-5	Historical data collected from previous five years	0.75
6	Sludge supply of every facility is increased by 20%	0.05
7	Sludge supply of every facility is decreased by 20%	0.05
8	The change of sludge supply at a WWT plant is equal to the average change of population in Mississippi in the last 10 years	0.05
9	Sludge supply from pulp & paper decreased by 20%	0.05
10	Sludge supply from poultry production increased by 20%.	0.05

Table 2.7

Scenario definitions under technology uncertainty

Scenario	Explanation	Probability
1	1 ton of sludge generates 0.20 tons of biocrude	0.05
2	1 ton of sludge generates 0.24 tons of biocrude	0.10
3	1 ton of sludge generates 0.26 tons of biocrude	0.70
4	1 ton of sludge generates 0.28 tons of biocrude	0.10
5	1 ton of sludge generates 0.32 tons of biocrude	0.05

Table 2.8

Problem size of the deterministic equivalent of the model

$\lvert\mathcal{K}\rvert$	$\lvert\mathcal{J}\rvert$	$\lvert\mathcal{I}\rvert$	$\lvert\mathcal{G}\rvert$	$\lvert\mathcal{M}\rvert$	$\lvert\mathcal{L}\rvert$	$\lvert\mathcal{F}\rvert$	No. of binary variables	No. of integer variables	No. of continuous variables	No. of constraints
94	26	10	52	3	3	3	104	7,332	8,243	7,732

Table 2.9

Comparison of solution quality

$\|\Omega\|$	Solution Method	Obj. Val. ($ M)	Error (%)	No. of iter.	CPU time (sec)
5	CPLEX	311.5	0.91	N/A	3,487.1
	BSCN-L	312.4	3.09	1,000	3,541.8
	BSCN-ML	312.3	0.90	97	974.7
	BSCN-LR-L	313.3	3.46	1,000	2,812.3
	BSCN-LR-ML	312.4	0.97	43	192.4
6	CPLEX	309.9	0.97	N/A	4,712.4
	BSCN-L	311.9	3.42	1,000	8,816.8
	BSCN-ML	311.4	0.94	194	1,214.9
	BSCN-LR-L	312.8	3.48	1,000	4,221.7
	BSCN-LR-ML	311.5	0.90	47	201.9
7	CPLEX	312.9	0.94	N/A	5,489.7
	BSCN-L	316.8	3.95	1,000	9,845.7
	BSCN-ML	314.5	0.92	210	1,411.1
	BSCN-LR-L	317.6	4.18	1,000	4,301.4
	BSCN-LR-ML	315.0	0.95	56	248.6
8	CPLEX	310.4	0.93	N/A	6,626.5
	BSCN-L	313.9	3.66	1,000	11,341.2
	BSCN-ML	313.4	0.86	256	2,089.1
	BSCN-LR-L	316.8	4.13	1,000	6,097.6
	BSCN-LR-ML	313.8	0.96	68	281.8
9	CPLEX	311.4	0.87	N/A	8,478.9
	BSCN-L	315.6	2.76	1,000	14,749.1
	BSCN-ML	313.2	0.89	281	3,161.2
	BSCN-LR-L	316.9	5.05	1,000	6,229.4
	BSCN-LR-ML	313.4	0.96	82	303.9
10	CPLEX	310.6	0.98	N/A	13,247.4
	BSCN-L	315.2	4.27	1,000	21,779.1
	BSCN-ML	312.4	0.92	344	3,881.5
	BSCN-LR-L	315.9	4.44	1,000	7,582.8
	BSCN-LR-ML	313.0	0.93	126	409.3

Table 2.10

Stochastic vs. deterministic solutions under feedstock supply uncertainty

Strategies	Value ($M)	Biodiesel Production (MGY)
Stochastic programming	310.9	75.83
Wait and see solutions		
Scenario-1	316.77	69.98
Scenario-2	287.10	80.34
Scenario-3	319.67	67.74
Scenario-4	284.02	81.62
Scenario-5	298.66	77.56
Scenario-6	269.15	90.71
Scenario-7	338.22	60.48
Scenario-8	276.45	83.96
Scenario-9	304.57	74.40
Scenario-10	287.69	80.25
Expected value solution	314.15	72.71

Table 2.11

Stochastic vs. deterministic solutions under technology uncertainty

Strategies	Value ($M)	Biodiesel Production (MGY)
Stochastic programming	307.02	74.62
Wait and see solutions		
Scenario 1	344.45	57.62
Scenario 2	317.51	69.14
Scenario 3	303.16	74.70
Scenario 4	288.10	79.68
Scenario 5	266.42	91.30
Expected value solution	309.25	73.34

CHAPTER 3

ANALYZING THE IMPACT OF INTERMODAL-RELATED RISK TO THE DESIGN AND MANAGEMENT OF BIOFUEL SUPPLY CHAIN

3.1 Introduction

The U.S. biofuel industry is expanding at a fast rate. The production of bio-ethanol in the U.S. has dramatically increased from 1.15 billion gallons in 2000 to 10.01 billion gallons in 2011 [142], and is projected to reach 11.67 billion gallons in 2020 [142]. Such an increase in bioethanol production mandates substantial expansion of existing biofuel supply chain infrastructure. The efficiency and reliability of a biofuel supply chain will be determined by the performance of an integrated biofuel production and transportation system that not only operates well under normal condition but also hedge against risk when a disruption occurs.

Biomass needs to be transported from a field to a biorefinery at a minimal cost. This requires a lean logistics network that efficiently connects origin fields and destination refineries with proper transportation modes. The biomass feedstock used for production of the first generation biofuels (corn- and soybean-based) is bulky, non-flowable and as a consequence difficult to load on a truck. This yields very high costs of loading, transporting and unloading biomass, which consequentially limits its economic transportation distance[1].

[1]Economic transportation distance is the distance below which truck is considered as an economic mode of transportation.

Brower [16] pointed out that moving biomass more than 50 miles to a conversion facility severely impacts profits. Due to this limited coverage radius, production capacities of the biorefineries are usually low. This restrains the biorefineries benefiting from economies of scale, and the unit cost of biomass keeps high. In order to alleviate this problem Idaho National Laboratory proposed a biomass delivery system [58]. This system relies on pre-processing biomass prior to transporting. Densified biomass has physical characteristics which are similar to corn, soybean and other grains; therefore, it is easy to load/unload and transport. Handling and transportation costs for densified biomass are smaller than those for unprocessed biomass; thus, long hauls become an option. Hess et al. [58] reported that depending on the amount and distance traveled, rail or truck can be used to deliver densified biomass to a biorefinery. As a result, large-capacity biorefineries can get shipments not only from local suppliers, but from suppliers located further away.

Large-capacity biorefineries require to develop a robust and integrated logistics system where the densified biomass is shipped via different modes of transportation such as truck, rail and barge. In case of unprocessed biomass, truck is considered as the only mode of transportation to ship biomass to biorefineries. Using rail or barge instead, not only reduces cost, but also alleviates congestion in the highways and as a result improves safety. Therefore, there is a need to establish intermodal hubs in a biofuel supply chain network where two or more transportation modes meet, such as rail ramps, in-land ports, sea ports, etc. Locating an intermodal hub close to the biorefinery allows it to use an economical transportation mode to replenish inventories. For example, the only biorefinery in Mississippi is the Bunge-Ergon which is located in Vicksburg, right on the Mississippi River at

the port of Vicksburg, MS. KiOR Inc., a company of next-generation renewable fuel builds its first plant near the Port of Columbus, MS. KiOR already announced to invest in building more biorefineries in Mississippi in the coming years.

Transportation infrastructures, particularly those bearing intermodal traffic, may be vulnerable to various disruption risks, such as natural disasters ([93], [144] e.g., 2005 Hurricane Katrina, 2008 China and 2009 Haiti Earthquakes) and human-caused disasters ([97], [102] e.g., 2003 U.S. Northeast blackout, 2010 Gulf of Mexico Oil Spill). Furthermore, some areas are recognized as disaster prone areas. For instance, Figure 3.1 shows that in total 39 different storms affected North Carolina between 2000-2008 [122]. Hurricanes in North Carolina history are responsible for over $11 billion damage loss and almost 1,000 total fatalities. Similarly, the Mississippi river and its tributaries have flooded on numerous occasions in the past [131]. Hence, proper redundancy needs to be deployed among the biofuel supply chain to enhance the system reliability against infrastructure disruptions. This indicates that there is a need to develop a modeling framework for reliable design of a biofuel supply chain network. Such a design shall not only efficiently transport biomass under the normal scenario (when every intermodal hub is functioning normally), but also hedge against possible losses due to unexpected infrastructure disruptions.

To address this need, this chapter proposes a model for the design of reliable multi-modal logistics network for a biofuel supply chain system and analyzes the impact of intermodal hub related risk to this system. We extend the traditional hub location model to one that considers risks associated with intermodal hubs, including flooding, hurricane and drought. The output of our model provides location of intermodal hubs, number of

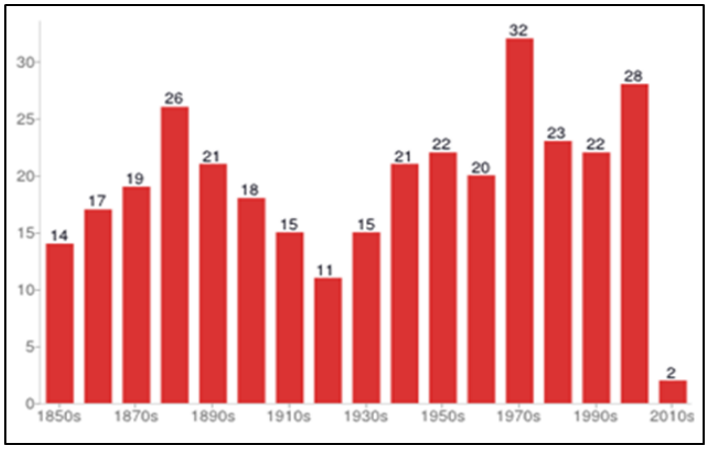

Figure 3.1

Storms affecting NC (1851-2012) [122]

containers transported between the intermodal hubs, amount of densified biomass transported via trucks and the number of intermodal hubs used under both normal and disrupted scenarios. Additionally, we propose a probabilistic model to estimate disruption probabilities for the intermodal hubs. We identified that our proposed model is an extension of the fixed charge, uncapacitated network design problem and is known to be an $\mathcal{NP}$-hard problem [79]. Therefore, solving the model in general is a very challenging task. This motivates us to develop a highly customized solution approach based on the traditional Benders decomposition algorithm. To enhance our algorithm, we create several stronger cuts, including pareto-optimal cuts, trust region and knapsack inequality. Furthermore, we integrate the ϵ-Benders decomposition algorithm [49] into our framework, which yields even stronger cuts. From multiple numerical experiments, we show that the ϵ-Benders decomposition algorithm is capable of producing a near-optimum solution in a reasonable amount of time.

In addition to proposing the general model, another important contribution of this chapter is applying this model to a real-world case study. We use the southeast region of U.S. as a testing ground in our case study. This region possesses a number of favorable factors (e.g., abundant biomass, low wages and non-unionized labor) that are likely to attract intensive biofuel infrastructure investment in the future. The outcome of this study provides a number of managerial insights such as optimal deployment of intermodal hubs and biorefineries, amount of densified biomass transported via different modes of transportation under both normal and disrupted scenarios, which can effectively aid decision makers to design a robust biofuel supply chain network. Finally, we showed how the total supply chain performance and intermodal hub deployment are affected by parameters such as intermodal hub disruption probabilities, irregularity in biomass supply and the penalty coefficient chosen by the decision maker.

3.2 Literature Review

A major stream of research within the biofuel supply chain literature is to identify the best modes of transportation so as to minimize the transportation cost. To achieve this goal, a number of studies (e.g., [73], [80], [114]) analyzed the cost effectiveness of different modes of transportation to deliver biomass to biorefineries. Early studies mainly focus on supply chain decisions at operation level. Later studies further integrated both strategic planning and tactical decisions into the design of biomass supply chain networks in order to deliver biomass at a more competitive price to the end users. Work by [156], [38], [39], [63], [3], [7], [147] and [108] analyze plant location and transportation issues

in biofuel supply chain networks under a deterministic setting. These papers consider perfectly reliable facilities and known demand. Chen and Fan [22], Kim et al., [71] and Marufuzzaman et al., [83] extended those formulations by providing stochastic models that can be used to generate reliable solutions for the design and management of a biofuel supply chain network. Additionally, Gebreslassie et al. [47] incorporated financial risk in a hydrocarbon biorefinery supply chain system. All these models assume that supply chain infrastructure is always functioning perfectly and thus they fail to address unexpected transportation hub disruptions observed in reality [29], [102].

In the context of general network design, researchers have become increasingly interested in the effect of facility disruptions. Daskin [32, 33] was the first to consider facility unavailability in a maximal covering location problem. Drezner [36] has extended this work to reliable location design in a p-median problem. Snyder and Daskin [121] proposed an integer programming model for the stochastic fixed charge p-median location problem where the authors assumed that the facility disruptions occur independently and with an identical probability. Cui et al. [30] further extended this work to cases with site-dependent disruption probabilities by creating both discrete and continuous models. The continuous model has been generalized by Li and Ouyang [77] to incorporate spatially correlated disruption patters. Shen et al. [117] proposed a two-stage stochastic program and a nonlinear integer program for problems where the open facilities fail at a certain probability. The authors proposed a 4-approximation algorithm and several heuristic approaches to produce near-optimal solutions in a reasonable amount of time. Most recently, Li et al. [76] provided nonlinear integer programming models for a reliable p-median problem and

a reliable uncapacitated fixed-charge location problem under disruption correlations. By using the rate of return on fortification investment, the authors also provided an alternative to assess the effectiveness of the design solutions.

Similar to the literature on facility locations discussed above, biofuel supply infrastructure is also impacted by various adversary incidents, such as water scarcity, flooding, routine maintenance, or adverse weather condition [113]. However, there are very few studies that addressed the impact of biorefinery disruptions in a biofuel supply chain network. Li et al. [78] developed a discrete and a continuous location model for a reliable bio-ethanol supply chain network. The authors showed the impact of disruption probabilities on optimal refinery deployment decisions. Wang and Ouyang [146] proposed a game-theoretical based continuous approximation model to locate biorefineries under spatial competition and facility disruption risks. However, these studies only considered failure risks at biorefineries, and little has been done on disruptions at intermediate transportation hubs that can significantly impact this supply chain system.

The biofuel supply chain system from biomass production to biorefineries can be viewed as a hub-and-spoke transportation network. Other industries, such as, package delivery [120], telecommunication [70], and airline transportation [6], [18], [26] also used hub-and-spoke to design their distribution networks. A brief overview of the hub location problems and solution methodologies can be found from a recent study of SteadieSeifi et al. [123]. All these studies assume that transportation hubs are always functioning and never fail, which however cannot adequately describe real-world systems that involve various uncertainties from the supply side. A few studies focused on managing and rescheduling rail

and port operations during different disrupted scenarios such as equipment and operational failure and physical damage to the terminal berths [66], [112]. An et al. [4] proposed a reliable single and multiple allocation hub-and-spoke network design problems where disruptions at hubs and the resulting hub unavailability can be mitigated by backup hubs and alternative routes. Different from the literature, the model presents in this paper considers the impact of intermodal hub failures on supply chain design context and provided a real life example for the densified biomass supply chain network. Furthermore, we estimate the disruption probability of intermodal hubs using a probabilistic model. We observed that previous studies assume a given disruption probability for each facility and seldom validate this value with real-world disaster mechanisms [121], [30], [77], [78]. Most recently, Huang and Pang [64] developed a mechanism to calculate disruption probability of a biorefinery which is prone to seismic hazard. In this study, we extend this concept and propose a methodology to calculate the disruption probabilities (caused by natural disasters) based on the real world data. The aim is to better estimate the disruption probabilities for the intermodal hubs.

3.3 Problem Description and Model Formulation

The main objective of this chapter is to build a reliable model that aids the design and management of a biofuel supply chain network while taking intermodal hub disruptions into account. The network design problem consists of locating a set of intermodal hubs and biorefineries among candidate locations and determining the routes of biomass flows from its origin (harvesting sites) to destination (biorefineries). The design shall minimize

the total set-up cost and the expected long run transportation cost across all hub disruption scenarios. We assume that the intermodal hubs are subject to site-dependent probabilistic disruptions. Figure **??** presents the structure of the biofuel logistic network consisting of biomass suppliers, potential locations for intermodal hubs (rail ramps or ports) and biorefineries.

We now present two model formulations for the biofuel logistics network design problem, i.e., a basic hub-and-spoke model **[HUB-B]** that assumes that every hub is always functioning perfectly and a reliable hub-and-spoke model **[HUB-R]** that considers possible hub disruptions instead. The notation is summarized in Table 3.1. We will first introduce the basic model **[HUB-B]**.

Consider a logistic network $\mathcal{G} = (\mathcal{N}, \mathcal{A})$, where $\mathcal{N}$ is the set of nodes and $\mathcal{A}$ is the set of arcs (shown in Figure 3.2). Set $\mathcal{N}$ consists of the set of harvesting sites $\mathcal{I}$, the set of candidate intermodal hub locations $\mathcal{J}$ and the set of candidate biorefinery locations $\mathcal{K}$ (Let, $\mathcal{H} = \mathcal{J} \bigcup \mathcal{K}$). Each site $i \in \mathcal{I}$ produces s_i unit of densified biomass (we assume that biomass is densified right at the harvesting sites), and the total biofuel production in this system is set to be no less than d. Locating an intermodal hub of capacity level $l \in \mathcal{L}$ at each location $j \in \mathcal{J}$ costs a fixed set-up cost Ψ_{lj}. Similarly, locating a biorefinery of capacity $l \in \mathcal{L}$ at each location $k \in \mathcal{K}$ costs a fixed set-up cost Ψ_{lk}. Each shipments from harvesting sites are consolidated at an intermodal hub in $\mathcal{J}$ before being delivered to a biorefinery in $\mathcal{K}$. We assume that every biorefinery in $\mathcal{K}$ is co-located with an intermodal hub with a sufficiently large capacity, and the transportation expense between the refinery and its co-located intermodal hub is negligible. The set of arcs $\mathcal{A}$ is partitioned into three disjoint

subsets, i.e., $\mathcal{A} = \mathcal{A}_1 \cup \mathcal{A}_2 \cup \mathcal{A}_3$, where $\mathcal{A}_1$ represents the set of arcs joining harvesting sites $\mathcal{I}$ with intermodal hubs $\mathcal{J}$, $\mathcal{A}_2$ represents the set of arcs between intermodal hubs $\mathcal{J}$ and biorefinery $\mathcal{K}$, and finally $\mathcal{A}_3$ represents the set of arcs that directly connect from harvesting sites $\mathcal{I}$ to biorefinery $\mathcal{K}$. Each arc $(i, j) \in \mathcal{A}_1$ carries local collection low-volume traffic between a harvesting site and an intermodal hub that are usually spaced by a small distance (e.g., on the order of 10-20 miles). Therefore, trucks are preferable on $(i, j) \in \mathcal{A}_1$ and its unit-volume traffic cost is specified as the link length of c_{ij}. An inter-hub arc $(j, k) \in \mathcal{A}_2$ usually carries large-volume long-haul traffic and uses either rail or barge as their major transportation mode. We represent c_{jk} as a unit transportation cost along arc $(j, k) \in \mathcal{A}_2$. Therefore, a unit flow along an origin-destination route $\{(i, j), (j, k)\}$ costs $c_{ijk} = c_{ij} + c_{jk}$. Furthermore, we allow biomass to be shipped by trucks along a direct arc $(i, k) \in \mathcal{A}_3$ from harvesting site $i \in \mathcal{I}$ to biorefinery $k \in \mathcal{K}$, which incurs a unit transportation cost c_{ik}. Since trucking usually has a higher unit cost than larger-volume rail and waterway modes, cost c_{ik} is likely to be much higher than regular cost c_{ijk}, and thus the long-haul trucking mode is mostly used only in emergency. Since densified biomass is usually transported in cargo containers between intermodal hubs, in addition to unit transportation cost we consider that along each inter-hub arc $(j, k) \in \mathcal{A}_2$, sending each container with a capacity of v_{jk}^{cap} incurs a fixed cost ξ_{jk}. This fixed cost represents the costs associated with loading and unloading a single railcar. We introduce the following location and allocation decision variables in our model.

The primary decision variables $\mathbb{Y} := \{Y_{lj}\}_{l \in \mathcal{L}, j \in \mathcal{J} \bigcup \mathcal{K}}$ determine the size and location to open intermodal hubs and biorefineries, i.e.,

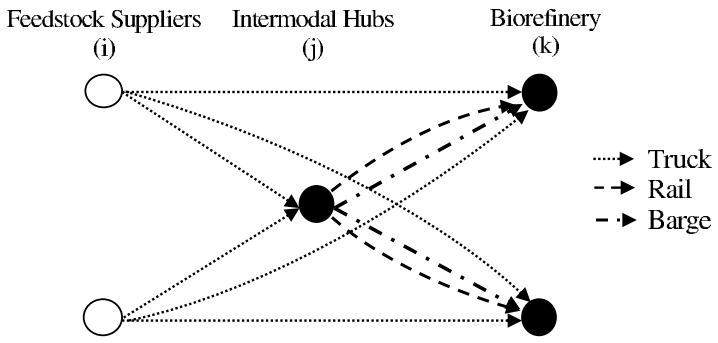

Figure 3.2

An example of intermodal supply chain network

$$Y_{lj} = \begin{cases} 1 & \text{if an intermodal hub of size } l \text{ is opened at location } j \\ 0 & \text{otherwise;} \end{cases}$$

$$Y_{lk} = \begin{cases} 1 & \text{if a biorefinery of size } l \text{ is opened at location } k \\ 0 & \text{otherwise;} \end{cases}$$

The second set of decision variables $\mathbb{Z} := \{Z_{jk}\}_{j\in\mathcal{J},k\in\mathcal{K}}$ decides the number of container flow between each pair of hubs. The remaining decisions are how to route the biomass flows from its origin to destination. Let $\mathbb{X} := \{X_{lk}\}_{(l,k)\in\mathcal{A}}$ denote the flow of biomass along each link $(l.k) \in \mathcal{A}$ in this network. With this, we can formulate the basic model **[HUB-B]** as follows,

$$\textbf{[HUB-B]} \text{ Minimize } \sum_{(lk)\in\mathcal{A}} c_{lk}X_{lk} + \sum_{l\in\mathcal{L},j\in\mathcal{H}} \Psi_{lj}Y_{lj} + \sum_{j\in\mathcal{J},k\in\mathcal{K}} \xi_{jk}Z_{jk}$$

Subject to

$$\sum_{j \in \mathcal{J}_i} X_{ij} + \sum_{k \in \mathcal{K}_i} X_{ik} \leq s_i \qquad \forall i \in \mathcal{I} \tag{3.1}$$

$$\sum_{k \in \mathcal{K}} \sum_{j \in \mathcal{I}_k \bigcup \mathcal{J}_k} X_{jk} \geq d \tag{3.2}$$

$$\sum_{i \in \mathcal{I}_j} X_{ij} - \sum_{k \in \mathcal{K}_j} X_{jk} = 0 \qquad \forall j \in \mathcal{J} \tag{3.3}$$

$$\sum_{i \in \mathcal{I}_j} X_{ij} - \sum_{l \in \mathcal{L}} c_{lj}^{cap} Y_{lj} \leq 0 \qquad \forall j \in \mathcal{J} \tag{3.4}$$

$$\sum_{j \in \mathcal{I}_k \bigcup \mathcal{J}_k} X_{jk} - \sum_{l \in \mathcal{L}} c_{lk}^{cap} Y_{lk} \leq 0 \qquad \forall k \in \mathcal{K} \tag{3.5}$$

$$v_{jk}^{cap} Z_{jk} - X_{jk} \geq 0 \qquad \forall j \in \mathcal{J}, k \in \mathcal{K} \tag{3.6}$$

$$\sum_{l \in \mathcal{L}} Y_{lj} \leq 1 \qquad \forall j \in \mathcal{H} \tag{3.7}$$

$$X_{lk} \in \mathbb{R}^+ \qquad \forall (l,k) \in \mathcal{A} \tag{3.8}$$

$$Y_{lj} \in \mathbb{B} \qquad \forall j \in \mathcal{H} \tag{3.9}$$

$$Z_{jk} \in \mathbb{Z}^+ \qquad \forall j \in \mathcal{J}, k \in \mathcal{K} \tag{3.10}$$

The first term of the objective function is the total variable transportation cost, the second term is the total set-up cost of opening intermodal hubs and biorefineries and the third term is the fixed cost of sending cargo containers between the intermodal hubs and biorefineries. Constraints (4.1) indicate that the amount of biomass shipped from a harvesting site $i \in \mathcal{I}$ is limited by its availability. Constraints (4.2) set the minimum amount of biomass to be routed through the logistics network. Constraints (4.3) enforces flow-conservation at intermodal hubs $j \in \mathcal{J}$. Constraints (4.4) indicate that the total amount of biomass shipped through an intermodal hub $j \in \mathcal{J}$ is limited by the hub capacity c_{lj}^{cap}, $\forall l \in \mathcal{L}, j \in \mathcal{J}$. Similarly, Constraints (4.5) indicate that the total amount of biomass

shipped to a biorefinery is limited by the refinery capacity $c_{lk}^{cap}, \forall l \in \mathcal{L}, k \in \mathcal{K}$. Constraints (4.6) count the number of containers needed for shipping biomass on each arc. Constraints (3.7) indicate that at most one intermodal hub/biorefinery of capacity $l \in \mathcal{L}$ is operating in a given location $j \in \mathcal{H}$. Finally, constraints (4.7) are the standard non-negativity constraints, (4.8) are the binary constraints, and (4.9) are the integrality constraints.

To further incorporate intermodal hub disruptions observed in the real world, we will extend the basic model **[HUB-B]** to a reliable model **[HUB-R]** that hedges against disruption impacts by using back-up services. We assume that each hub in $j \in \mathcal{H}$ disrupts independently. The corresponding site-dependent probability is q_j. When either hub along route $((i,j),(j,k))$ disrupts, this route is no longer operating, and we assume the traffic is detoured to the highway arc $(i,k) \in \mathcal{A}_3$, which now serves as an emergency carrier. Since an emergency service usually costs much higher than a regularly scheduled service and may incur other risks to normal system operations, we consider that the unit emergency transportation cost is β times as much as the regularized cost c_{ik}, where the risk coefficient $\beta \geq 1$ and $\beta = 1$ denotes the risk neutral case. We further relax the minimum total biofuel production requirement and instead impose a penalty cost π per unit shortage of biomass. This penalty π can be also interpreted as a profit threshold such that if unit biomass transportation cost exceeds this threshold, producing biofuel will be no longer profitable and thus there is no point of shipping biomass at this transportation cost. To capture the hub disruption risks and biomass shortage penalty, we introduce additional decision variable as follows,

- $\mathbb{X} := \{X_{ijk}\}_{i\in\mathcal{I},j\in\mathcal{J},k\in\mathcal{K}}$ flow from i to k via intermodal hub j

- $\mathbb{U} := \{U\}$ total amount of unsatisfied demand

Then we adapt **[HUB-B]** to the following mixed integer linear programming (MILP) formulation for our reliable intermodal hub and spoke problem:

[HUB-R] Minimize $\sum_{l\in\mathcal{L},j\in\mathcal{H}} \Psi_{lj}Y_{lj} + \sum_{j\in\mathcal{J},k\in\mathcal{K}_j} \xi_{jk}Z_{jk} + \sum_{\forall i\in\mathcal{I},j\in\mathcal{J}_i,k\in\mathcal{K}_j} c_{ijk}(1-q_j)(1-q_k)X_{ijk} +$

$$\sum_{\forall i\in\mathcal{I},k\in\mathcal{K}_i} c_{ik}\left[X_{ik} + \beta \sum_{j\in\mathcal{J}_i\bigcap\mathcal{J}_k} (q_j + q_k - q_jq_k)X_{ijk}\right] + \pi U$$

Subject to

$$\sum_{j\in\mathcal{J}_i,k\in\mathcal{K}_j} X_{ijk} + \sum_{k\in\mathcal{K}_i} X_{ik} \leq s_i \qquad \forall i\in\mathcal{I} \tag{3.11}$$

$$\sum_{k\in\mathcal{K}}\left[\sum_{i\in\mathcal{I}_k} X_{ik} + \sum_{j\in\mathcal{J}_k,i\in\mathcal{I}_j} X_{ijk}\right] + U = d \tag{3.12}$$

$$\sum_{i\in\mathcal{I}_j,k\in\mathcal{K}_j} X_{ijk} \leq \sum_{l\in\mathcal{L}} c^{cap}_{lj}Y_{lj} \qquad \forall j\in\mathcal{J} \tag{3.13}$$

$$\sum_{i\in\mathcal{I}_k} X_{ik} + \sum_{i\in\mathcal{I}_j,j\in\mathcal{J}_k} X_{ijk} \leq \sum_{l\in\mathcal{L}} c^{cap}_{lk}Y_{lk} \qquad \forall k\in\mathcal{K} \tag{3.14}$$

$$v^{cap}_{jk}Z_{jk} - \sum_{i\in\mathcal{I}_j} X_{ijk} \geq 0 \qquad \forall j\in\mathcal{J},k\in\mathcal{K}_j \tag{3.15}$$

$$\sum_{l\in\mathcal{L}} Y_{lj} \leq 1 \qquad \forall j\in\mathcal{H} \tag{3.16}$$

$$X_{ijk} \in \mathbb{R}^+ \qquad \forall i\in\mathcal{I},j\in\mathcal{J}_i,k\in\mathcal{K}_j \tag{3.17}$$

$$X_{ik} \in \mathbb{R}^+ \qquad \forall i\in\mathcal{I},k\in\mathcal{K}_i \tag{3.18}$$

$$U \in \mathbb{R}^+ \tag{3.19}$$

$$Y_{lj} \in \mathbb{B} \qquad \forall l\in\mathcal{L},j\in\mathcal{H} \tag{3.20}$$

$$Z_{jk} \in \mathbb{Z}^+ \qquad \forall j\in\mathcal{J},k\in\mathcal{K}_j \tag{3.21}$$

In **[HUB-R]**, the objective function minimizes the total expected system cost, including the expected transportation cost across both normal and disruptive scenarios and the investment of opening hubs and using inter-hub arcs. More specifically, the first and second terms represent respectively the total set-up cost of establishing the intermodal hubs and biorefineries and the fixed cost of transporting cargo containers between the intermodal hubs. The third term is the regular transportation cost which is weighted by $(1-q_j)(1-q_k)$, the probability that both hubs operate normally along each route (i,j,k). When either or both the intermodal hub j and biorefinery k disrupt, which occurs at a probability of $(q_j+q_k-q_jq_k)$, flow X_{ijk} originally assigned to route (i,j,k) will be diverted to direct route (i,k) at a higher variable cost βc_{ik}, while route (i,k) in addition carries the planned regular flow X_{ik} at variable cost c_{ik}. This is reflected by the fourth and fifth terms of the objective function. The sixth term is the penalty cost for biomass supply shortage.

Again, constraints (4.10) indicate that the amount of biomass shipped from a harvesting site $i \in \mathcal{I}$ is limited by its availability. Constraints (4.11) indicate that the total demand for biomass will be fulfilled either through the hub-and-spoke distribution network or through emergency shipments. Constraints (4.12) indicate that the total amount of biomass shipped through intermodal hub $j \in \mathcal{J}$ is limited by the hub capacity c_{lj}^{cap}, $\forall l \in \mathcal{L}, j \in \mathcal{J}$. Similarly, constraints (4.13) indicate that the total amount of biomass shipped to a biorefinery is limited by the refinery capacity c_{lk}^{cap}, $\forall l \in \mathcal{L}, k \in \mathcal{K}$. Constraints (4.14) set a limit on the amount of biomass to be routed on the arcs $(j,k) \in \mathcal{A}_2$. Constraints (3.16) indicate that at most one intermodal hub/biorefinery of capacity $l \in \mathcal{L}$ is operating in a given location

$j \in \mathcal{H}$. Finally constraints (4.15) to (4.17) are the standard non-negativity constraints, (4.18) are the binary constraints, and (4.19) are the integrality constraints.

Method of Estimating Disruption Probability q_j: In order to better estimate the site dependent disruption probability q_j, our study proposes a model to calculate this probability using real-world data of disruption sources (e.g., natural disasters). We assume that an intermodal hub location can be disrupted by multiple types of disasters. The disruption probability at each location resulted from different types of disasters can be calculated by integrating the impact of each type of the disasters. In general, when we consider joint occurrence of different types of disasters, this resulting probability can be formulated in the following.

We denote the set of all disaster types by $\mathcal{C}$, and the joint occurrence of only a subset of $\mathcal{C}$ specifies a scenario. Define $\mathbb{C}_r = \{\mathcal{C}' \mid \mathcal{C}' \subseteq \mathcal{C}, \mid \mathcal{C}' \mid = r\}, \forall r = 0, 1, ..., \mid \mathcal{C} \mid$, which denotes the collection of all subsets of disasters (or scenarios) of size r. Note that $\bigcup_{r=0}^{|\mathcal{C}|} \mathbb{C}_r$ denotes all the disaster scenarios. Let $p_j(\mathcal{C}')$ denotes the frequency of occurring scenario $\mathcal{C}'$ at location j, and $g_j(\mathcal{C}')$ denotes the average disruption duration of hub j when scenario $\mathcal{C}'$ occurs. Then the disruption probability of hub j across all possible disaster scenarios can be analytically formulated by enumerating all the scenarios as follows:

$$q_j := \sum_{r=0}^{|\mathcal{C}|} \sum_{\mathcal{C}' \in \mathcal{C}_r} p_j(\mathcal{C}') g_j(\mathcal{C}') \qquad \forall j \in \mathcal{H} \tag{3.22}$$

In the special case when the occurrences of any two disasters are mutually exclusive, i.e., $p_j(\mathcal{C}') = 0, \forall \mathcal{C}' \in \mathcal{C}_r, r \geq 2, j \in \mathcal{H}$, then equation (3.22) can be simplified as

$$q_j := \sum_{c \in \mathcal{C}} p_{jc} g_{jc} \qquad \forall j \in \mathcal{H} \tag{3.23}$$

Where $p_{jc} := p_j(\{c\})$, $g_{jc} := g_j(\{c\})$ for the ease of notation.

Model **[HUB-R]** is an extension of the fixed charge, uncapacitated network design problem and is known to be an $\mathcal{NP}$-hard problem [79]. Therefore, the next section proposes a customized solution approach to efficiently solve this model.

3.4 Solution Methodology

Based on the structure of the model **[HUB-R]**, we develop an algorithm using the Benders decomposition method [9], which is a well-known partitioning method to solve mixed integer linear programs. This method separates the original problem into two simple problems: an integer *master problem* and a linear *subproblem*. In this section, we first describe the basic Benders decomposition to solve the **[HUB-R]**. Then we present problem specific valid inequalities and logic cuts for the master problem. Next, we present some stronger cuts such as pareto-optimal cuts, trust region and knapsack inequality for the master problem. Finally, we discuss a feasibility seeking Benders decomposition approach which is designed to produce a near optimal solution in a reasonable amount of time.

3.4.1 Benders Decomposition

The underlying Benders reformulation for model **[HUB-R]** is given below:

$$\text{Minimize} \sum_{l\in\mathcal{L},j\in\mathcal{H}} \Psi_{lj}Y_{lj} + \sum_{j\in\mathcal{J},k\in\mathcal{K}_j} \xi_{jk}Z_{jk} + \textbf{[HUB-SUB]}(X,U|\hat{Y},\hat{Z})$$

Subject to (4.10)-(4.19). **[HUB-SUB]**$(X,U|\hat{Y},\hat{Z})$ represents the Benders subproblem specified in the following.

For given values of the $\mathbb{Y} := \{Y_{lj}\}_{l\in\mathcal{L},j\in\mathcal{H}}$ and $\mathbb{Z} := \{Z_{jk}\}_{j\in\mathcal{J},k\in\mathcal{K}}$ variables that satisfy the integrality constraints (4.18) and (4.19), the model **[HUB-R]** reduces to the following *primal subproblem* involving only the continuous variables $\mathbb{X} := \{X_{ijk}\}_{i\in\mathcal{I},j\in\mathcal{J},k\in\mathcal{K}}$, $\mathbb{U} := \{U\}$ and $\mathbb{X}' := \{X_{ik}\}_{i\in\mathcal{I},k\in\mathcal{K}}$.

$$\textbf{[HUB-SUB]}(\hat{Y},\hat{Z}) \text{ Minimize} \sum_{\forall i\in\mathcal{I},j\in\mathcal{J}_i,k\in\mathcal{K}_j} c_{ijk}(1-q_j)(1-q_k)X_{ijk} +$$

$$\sum_{\forall i\in\mathcal{I},k\in\mathcal{K}_i} c_{ik}\left[X_{ik} + \beta \sum_{j\in\mathcal{J}_i\bigcap\mathcal{J}_k} (q_j+q_k-q_jq_k)X_{ijk}\right] + \pi U$$

Subject to

$$\sum_{j\in\mathcal{J}_i,k\in\mathcal{K}_j} X_{ijk} + \sum_{k\in\mathcal{K}_i} X_{ik} \leq s_i \qquad \forall i\in\mathcal{I} \qquad (3.24)$$

$$\sum_{k\in\mathcal{K}}\left[\sum_{i\in\mathcal{I}_k} X_{ik} + \sum_{j\in\mathcal{J}_k,i\in I_j} X_{ijk}\right] + U = d \qquad (3.25)$$

$$\sum_{i\in\mathcal{I}_j,k\in\mathcal{K}_j} X_{ijk} \leq \sum_{l\in\mathcal{L}} c_{lj}^{cap}\hat{Y}_{lj} \qquad \forall j\in\mathcal{J} \qquad (3.26)$$

$$\sum_{i\in\mathcal{I}_k} X_{ik} + \sum_{j\in\mathcal{J}_k,i\in\mathcal{I}_j} X_{ijk} \leq \sum_{l\in\mathcal{L}} c_{lk}^{cap}\hat{Y}_{lk} \qquad \forall k\in\mathcal{K} \qquad (3.27)$$

$$v_{jk}^{cap}\hat{Z}_{jk} - \sum_{i\in\mathcal{I}_j} X_{ijk} \geq 0 \qquad \forall j\in\mathcal{J},k\in\mathcal{K}_j \qquad (3.28)$$

$$X_{ijk} \in \mathbb{R}^+ \qquad \forall i \in \mathcal{I}, j \in \mathcal{J}_i, k \in \mathcal{K}_j \tag{3.29}$$

$$X_{ik} \in \mathbb{R}^+ \qquad \forall i \in \mathcal{I}, k \in \mathcal{K}_i \tag{3.30}$$

$$U \in \mathbb{R}^+ \tag{3.31}$$

Let $\delta = \{\delta_i \geq 0 \mid i \in \mathcal{I}\}$, $\gamma = \{\gamma\}$, $\chi = \{\chi_j \geq 0 \mid j \in \mathcal{J}\}$, $\eta = \{\eta_k \geq 0 \mid k \in \mathcal{K}\}$, and $\mu = \{\mu_{jk} \geq 0 \mid j \in \mathcal{J}; k \in \mathcal{K}\}$ be the dual variables associated with constraints (4.20)-(4.24), respectively. The dual of the primal subproblem, which we call the *dual subproblem* **[HUB-SUB(D)]**, can be written as:

[HUB-SUB(D)] Maximize $d\gamma - \sum_{\forall i \in \mathcal{I}} s_i \delta_i - \sum_{\forall l \in \mathcal{L}, j \in \mathcal{J}} c_{lj}^{cap} \hat{Y}_{lj} \chi_j - \sum_{\forall l \in \mathcal{L}, k \in \mathcal{K}} c_{lk}^{cap} \hat{Y}_{lk} \eta_k - \sum_{\forall j \in \mathcal{J}, k \in \mathcal{K}} v_{jk}^{cap} \hat{Z}_{jk} \mu_{jk}$

Subject to

$$-\delta_i + \gamma - \chi_j - \eta_k - \mu_{jk} \leq [c_{ijk}(1-q_j)(1-q_k) + \beta c_{ik}(q_j + q_k - q_j q_k)] \quad \forall i \in \mathcal{I}; j \in \mathcal{J}; k \in \mathcal{K} \tag{3.32}$$

$$-\delta_i + \gamma - \eta_k \leq c_{ik} \qquad \forall i \in \mathcal{I}, k \in \mathcal{K} \tag{3.33}$$

$$\gamma \leq \pi \tag{3.34}$$

$$\delta_i, \chi_j, \eta_k, \mu_{jk} \in \mathbb{R}^+ \tag{3.35}$$

$$\gamma \in \mathbb{R} \tag{3.36}$$

Introducing an extra variable θ, the underlying Benders reformulation can be equivalently written as the following Benders *master problem* **[HUB-MP]**:

[HUB-MP] Minimize $\sum_{l \in \mathcal{L}, j \in \mathcal{H}} \Psi_{lj} Y_{lj} + \sum_{j \in \mathcal{J}, k \in \mathcal{K}_j} \xi_{jk} Z_{jk} + \theta$

Subject to

$$\theta + \sum_{\forall l \in \mathcal{L}, j \in \mathcal{J}} c_{lj}^{cap} \chi_j Y_{lj} + \sum_{\forall l \in \mathcal{L}, k \in \mathcal{K}} c_{lk}^{cap} \eta_k Y_{lk} \geq d\gamma - \sum_{\forall i \in \mathcal{I}} s_i \delta_i - \sum_{\forall j \in \mathcal{J}, k \in \mathcal{K}} v_{jk}^{cap} \mu_{jk} Z_{jk} \quad \forall (\delta, \gamma, \chi, \eta, \mu) \in \mathcal{P}_D \tag{3.37}$$

$$\sum_{l \in \mathcal{L}} Y_{lj} \leq 1 \quad \forall j \in \mathcal{H} \tag{3.38}$$

$$Y_j \in \mathbb{B} \quad \forall j \in \mathcal{J} \bigcup \mathcal{K} \tag{3.39}$$

$$Z_{jk} \in \mathbb{Z}^+ \quad \forall j \in \mathcal{J}, k \in \mathcal{K}_j \tag{3.40}$$

Constraints (4.32) are referred to as *optimality cut* constraints where $\mathcal{P}_D$ is the set of the extreme points in the feasible region of **[HUB-SUB(D)]**. θ is bounded from above by the objective function value of **[HUB-SUB(D)]** i.e.,

$$\theta \geq d\gamma^n - \sum_{\forall i \in \mathcal{I}} s_i \delta_i^n - \sum_{\forall l \in \mathcal{L}, j \in \mathcal{J}} c_{lj}^{cap} \chi_j^n Y_{lj} - \sum_{\forall l \in \mathcal{L}, k \in \mathcal{K}} c_{lk}^{cap} \eta_k^n Y_{lk} - \sum_{\forall j \in \mathcal{J}, k \in \mathcal{K}} v_{jk}^{cap} \mu_{jk}^n Z_{jk} \quad \forall (\delta, \gamma, \chi, \eta, \mu) \in \mathcal{P}_D$$

Note that we did not add any feasibility cut in the master problem since for any feasible $\mathbb{Y}$, $\mathbb{Z}$ values, we can also find at least a set of feasible solution to $\mathbb{X}$, $\mathbb{X}'$ and $\mathbb{U}$ due to constraints (4.21). Master problem **[HUB-MP]** is actually equivalent to the original problem **[HUB-R]**. However, it is difficult to solve it directly due to the large number of optimality constraints (4.32). Instead, we can solve a *restricted master problem* **[HUB-RMP]** that replaces the full set $\mathcal{P}_D^n \subset \mathcal{P}_D$. Problem **[HUB-RMP]** is a relaxation of **[HUB-R]**, and thus an optimal solution to the **[HUB-RMP]** provides a lower bound to **[HUB-R]**. The general idea of the basic Benders Decomposition is to gradually increase the size of $\mathcal{P}_D$

by iteratively adding proper new extreme points until this lower bound gets very close (or identical) to a known upper bound, which is outlined below:

Let UB^n and LB^n denote an upper and lower bound of the original problem at iteration n. Let $\mathcal{P}_D^n$ denote the set of extreme points of D at iteration n. The algorithm starts by solving **[HUB-RMP]** which provides a valid lower bound to the original problem as well as set values for $\{\hat{Y}_{lj}^n\}_{l\in\mathcal{L},j\in\mathcal{H}}$, and $\{\hat{Z}_{jk}^n\}_{j\in\mathcal{J},k\in\mathcal{K}}$ that are then used to solve the dual subproblem **[HUB-SUB(D)]**. At each iteration, a solution to the master problem (z_{MP}^n) and its subproblem (z_{SUB}^n) provides an upper bound to the original problem. If the gap of the upper and lower bound falls below a specified threshold value ϵ then the algorithm terminates; otherwise, $\mathcal{P}_D^n$ is updated by adding an optimality cut (in the form (4.32)) that is violated. A pseudo-code of the basic Benders decomposition algorithm is provided in **Algorithm 1**.

3.4.2 Enhancements to Benders Decomposition

Contreras et al. [25] pointed out that the computational efficiency of the basic Benders decomposition algorithm (presented in **Algorithm 1**) depends mainly on: (i) the computational effort required to solve **[HUB-RMP]** (ii) the computational effort required to solve **[HUB-SUB(D)]**, and (iii) the number of iterations required to obtain an optimal solution. Initial computational experimentation of Benders decomposition with relatively large networks exposed its inability to converge within a reasonable amount of time. This motivated us to explore accelerated techniques used to improve the convergence and stability of the Benders decomposition algorithm. For our problem, it is observed that the subproblem is a

capacitated network flow problem which contains all the continuous variables. Therefore, this problem is relatively easy to solve. It implies that the convergence of the Benders decomposition algorithm depends mainly on its ability to solve the relaxed master problem repeatedly. With this finding, the following subsections will present some proper accelerated techniques to solve the relaxed master problem (**[HUB-RMP]**) efficiently.

3.4.2.1 Adding Valid Inequalities to [HUB-RMP]

Cordeau et al. [27] pointed out that adding valid inequalities in the master problem helps to find solutions that are close to the optimal. Therefore, in order to accelerate the solution of the master problem, we have added the following valid inequalities to the master problem.

$$Z_{jk} \leq \sum_{l \in \mathcal{L}} \lceil \frac{c_{lj}^{cap}}{v_{jk}^{cap}} \rceil Y_{lj} \qquad \forall j \in \mathcal{J}, k \in \mathcal{K} \tag{3.41}$$

$$Z_{jk} \leq \sum_{l \in \mathcal{L}} \lceil \frac{c_{lk}^{cap}}{v_{jk}^{cap}} \rceil Y_{lk} \qquad \forall j \in \mathcal{J}, k \in \mathcal{K} \tag{3.42}$$

Constraints (4.35) and (4.36) indicate that if no hub is established at location j and k then no containers will flow between the arc (j, k). The constraints also impose the maximum number of containers than can be transported among an active arc. Computational experiments showed that these valid inequalities significantly reduce the number of iterations of the Benders algorithm.

Additionally, to accelerate the solution of the Benders master problem **[HUB-RMP]**, we set proper branching priorities to decision variables of $\{Z_{jk}\}$ and $\{Y_{lj}\}_{l \in \mathcal{L}, j \in \mathcal{H}}$. That means we can set priorities to control the order in which CPLEX branches on variables.

Numerical analysis indicates that branching $\{Z_{jk}\}$ first followed by $\{Y_{lj}\}_{l\in\mathcal{L},j\in\mathcal{H}}$ saves some computational time in solving **[HUB-RMP]**.

3.4.2.2 Generating Pareto-Optimal Cuts

Pareto-optimal cuts, introduced by Magnanti and Wong [79], are cutting planes added to the master problem for the purpose of generating stronger cuts that are not dominated by any other optimality cuts. This is one way to improve the convergence of the Benders decomposition algorithm. Notice that the subproblem formed by constraints (4.20)-(4.27) has a network sub-structure. Typically such problems have multiple dual optimal solutions that may provide a number of alternatives for the optimality cut (shown in constraints (4.32)). While all these alternative cuts are valid, one cut may be dominated by another in the vicinity of the optimal solution [111]. The cut generated from an extreme point $(\delta^1, \gamma^1, \chi^1, \eta^1, \mu^1)$ dominates the cut generated from another extreme point $(\delta^2, \gamma^2, \chi^2, \eta^2, \mu^2)$ if and only if

$$\begin{aligned} d\gamma^1 - \sum_{\forall i\in\mathcal{I}} s_i\delta_i^1 - \sum_{\forall l\in\mathcal{L},j\in\mathcal{J}} c_{lj}^{cap} Y_{lj}\chi_j^1 - \sum_{\forall l\in\mathcal{L},k\in\mathcal{K}} c_{lk}^{cap} Y_{lk}\eta_k^1 - \sum_{\forall j\in\mathcal{J},k\in\mathcal{K}} v_{jk}^{cap} Z_{jk}\mu_{jk}^1 \quad \geq \\ d\gamma^2 - \sum_{\forall i\in\mathcal{I}} s_i\delta_i^2 - \sum_{\forall l\in\mathcal{L},j\in\mathcal{J}} c_{lj}^{cap} Y_{lj}\chi_j^2 - \sum_{\forall l\in\mathcal{L},k\in\mathcal{K}} c_{lk}^{cap} Y_{lk}\eta_k^2 - \sum_{\forall j\in\mathcal{J},k\in\mathcal{K}} v_{jk}^{cap} Z_{jk}\mu_{jk}^2 \end{aligned} \tag{3.43}$$

with strict inequality for at least one point $\{Y_{lj}\}_{l\in\mathcal{L},j\in\mathcal{H}} \in \mathbb{Y}$. Magnanti and Wong formulated a problem that generates a Pareto-optimal cut, using the notion of core points i.e., a point in the relative interior of the convex hull of feasible region, as a proxy for the optimal solution. Let $\mathbb{Y}^{LP}$ be the polyhedron defined by (3.38) and $0 \leq Y_{lj} \leq 1$,

$\forall l \in \mathcal{L}, j \in \mathcal{H}$. Let $ri(\mathbb{Y}^{LP})$ denote the relative interior point of $\mathbb{Y}^{LP}$. A Pareto-optimal cut can be obtained by solving the following subproblem, where $\{Y_{lj}^0\}_{l\in\mathcal{L},j\in\mathcal{H}} \in ri(\mathbb{Y}^{LP})$.

[HUB-SUB(MW)] Maximize $d\gamma - \sum_{\forall i\in\mathcal{I}} s_i\delta_i - \sum_{\forall l\in\mathcal{L},j\in\mathcal{J}} c_{lj}^{cap} Y_{lj}^0 \chi_j - \sum_{\forall l\in\mathcal{L},k\in\mathcal{K}} c_{lk}^{cap} Y_{lk}^0 \eta_k - \sum_{\forall j\in\mathcal{J},k\in\mathcal{K}} v_{jk}^{cap} Z_{jk}^0 \mu_{jk}$

Subject to

$$d\gamma - \sum_{\forall i\in\mathcal{I}} s_i\delta_i - \sum_{\forall l\in\mathcal{L},j\in\mathcal{J}} c_{lj}^{cap}\hat{Y}_{lj}\chi_j - \sum_{\forall l\in\mathcal{L},k\in\mathcal{K}} c_{lk}^{cap}\hat{Y}_{lk}\eta_k - \sum_{\forall j\in\mathcal{J},k\in\mathcal{K}} v_{jk}^{cap}\hat{Z}_{jk}\mu_{jk} = z(\hat{\delta}_i,\hat{\gamma},\hat{\chi}_j,\hat{\eta}_k,\hat{\mu}_{jk}) \quad (3.44)$$

$$-[c_{ijk}(1-q_j)(1-q_k) + \beta c_{ik}(q_j+q_k-q_jq_k)] \leq \delta_i - \gamma + \chi_j + \eta_k + \mu_{jk} \quad \forall i\in\mathcal{I}, j\in\mathcal{J}, k\in\mathcal{K} \quad (3.45)$$

$$-\delta_i + \gamma - \eta_k \leq c_{ik} \quad \forall i\in\mathcal{I}, k\in\mathcal{K} \quad (3.46)$$

$$\gamma \leq \pi \quad (3.47)$$

$$\delta_i, \chi_j, \eta_k, \mu_{jk} \in \mathbb{R}^+ \quad (3.48)$$

$$\gamma \in \mathbb{R} \quad (3.49)$$

Here, $z(\hat{\delta}_i,\hat{\gamma},\hat{\chi}_j,\hat{\eta}_k,\hat{\mu}_{jk})$ denotes the optimal solution to the dual subproblem and Y_{lj}^0, Y_{lk}^0 and Z_{jk}^0 is a core point of the master problem. The additional constraint (4.37) ensures that one will select an extreme point from the set of optimal solutions to the original dual subproblem. This method first solves the Benders master problem **[HUB-RMP]**, solves a dual subproblem **[HUB-SUB(D)]** with the decision variables obtained from the master problem. Then one needs to solve an auxiliary subproblem **[HUB-SUB(MW)]** with the

existing solution to **[HUB-SUB(D)]** embedded in order to produce a Pareto-optimal cut for the Benders master problem. The reliance on the solution from the dual subproblem **[HUB-SUB(D)]** to formulate the auxiliary subproblem to generate a Pareto-optimal cut can be a major computational drawback [98]. For instance, when the Benders subproblem is difficult, this algorithm will not generate suboptimal solutions $(\hat{\delta}_i, \hat{\gamma}, \hat{\chi}_j, \hat{\eta}_k, \hat{\mu}_{jk})$ quickly. Therefore, in this study we have used subproblem independent Pareto-optimal cuts proposed by Papadakos [98]. In this *Modified Magnanti-Wong (MMW)* method one needs to solve the following auxiliary sub-problem **[HUB-SUB(MMW)]**:

[HUB-SUB(MMW)] Maximize $d\gamma - \sum_{\forall i \in \mathcal{I}} s_i \delta_i - \sum_{\forall l \in \mathcal{L}, j \in \mathcal{J}} c_{lj}^{cap} Y_{lj}^0 \chi_j - \sum_{\forall l \in \mathcal{L}, k \in \mathcal{K}} c_{lk}^{cap} Y_{lk}^0 \eta_k - \sum_{\forall j \in \mathcal{J}, k \in \mathcal{K}} v_{jk}^{cap} Z_{jk}^0 \mu_{jk}$

subject to

$$-\left[c_{ijk}(1-q_j)(1-q_k) + \beta c_{ik}(q_j + q_k - q_j q_k)\right] \leq \delta_i - \gamma + \chi_j + \eta_k + \mu_{jk} \quad \forall i \in \mathcal{I}, j \in \mathcal{J}, k \in \mathcal{K} \quad (3.50)$$

$$-\delta_i + \gamma - \eta_k \leq c_{ik} \quad \forall i \in \mathcal{I}, k \in \mathcal{K} \quad (3.51)$$

$$\gamma \leq \pi \quad (3.52)$$

$$\delta_i, \chi_j, \eta_k, \mu_{jk} \in \mathbb{R}^+ \quad (3.53)$$

$$\gamma \in \mathbb{R} \quad (3.54)$$

It is clear from the above formulation that the auxiliary sub-problem is independent of the solutions to the original dual subproblem and the master problem. Generating Modified

Magnanti-Wong (MMW) method will assist the Benders master problem to be one step closer to the optimal solution from the very first iteration [98].

3.4.2.3 Trust Region

Ruszczynski [110] pointed out that, cutting plane based algorithms such as Benders decomposition exhibits unstable behavior in the initial iterations i.e., solutions tend to oscillate from one feasible region to another which leads to slow convergence. Therefore, Santoso et al. [111] suggested to use the following trust region that bounds the Hamming distance [55] of the master problem solution from the previous solution. Let, $\{\hat{Y}_{lj}^{(n)}\}_{l\in\mathcal{L},j\in\mathcal{H}}$ be the solution obtained from master problem at iteration n and let $\mathcal{Y}_1^n = \{(l,j)|\{\hat{Y}_{lj}^{(n)}\}_{l\in\mathcal{L},j\in\mathcal{J}} = 1\}$ and $\mathcal{Y}_2^n = \{(l,k)|\{\hat{Y}_{lk}^{(n)}\}_{l\in\mathcal{L},k\in\mathcal{K}} = 1\}$. Therefore, we impose the following constraint in the master problem in iteration $n+1$:

$$\sum_{(l,j)\in\mathcal{Y}_1^n}(1-Y_{lj}) + \sum_{(l,k)\in\mathcal{Y}_2^n}(1-Y_{lk}) + \sum_{(l,j)\notin\mathcal{Y}_1^n} Y_{lj} + \sum_{(l,k)\notin\mathcal{Y}_2^n} Y_{lk} \leq \Delta^n \quad (3.55)$$

where $\Delta^n < (|\mathcal{L}\times\mathcal{J}| + |\mathcal{L}\times\mathcal{K}|)$ represents the trust-region size in iteration n. Unfortunately, convergence cannot be guaranteed if a non-redundant trust region is maintained throughout the algorithm. Therefore, in the initial iterations when the algorithm tends to have the oscillating effect we impose constraint (3.55) in the restricted master problem **[HUB-RMP]** and dynamically adjust its size. When the algorithm reaches a sufficiently small optimality gap, we drop constraint (3.55) from the master problem in order to ensure convergence.

3.4.2.4 Knapsack Inequalities

Santoso et al [111] showed that if a good upper bound is available from the Benders decomposition algorithm, then adding a knapsack inequality (shown below) along with the optimality cut constraint (4.32) can have a significant impact to the solution quality from the Benders master problem. The authors also pointed out that a state-of-the-art solver such as CPLEX can derive a variety of valid inequalities from that knapsack inequality which expedite the convergence of the Benders decomposition algorithm. Let (4.32) be the optimality cut added to the master problem at the end of n^{th} iteration and let UB^n be the best known upper bound obtained so far. Since Benders decomposition ensures that: $UB^n \geq \sum_{l\in\mathcal{L},j\in\mathcal{H}} \Psi_{lj}Y_{lj} + \sum_{j\in\mathcal{J},k\in\mathcal{K}_j} \xi_{jk}Z_{jk} + \theta$, therefore, we derive the following valid inequalities which we added in **[HUB-RMP]** in iteration $n+1$:

$$UB^n - d\gamma^n + \sum_{\forall i\in\mathcal{I}} s_i\delta_i^n \geq \sum_{\forall l\in\mathcal{L},j\in\mathcal{J}} (\Psi_{lj} - c_{lj}^{cap}\chi_j^n)Y_{lj} + \sum_{\forall l\in\mathcal{L},k\in\mathcal{K}} (\Psi_{lk} - c_{lk}^{cap}\eta_k^n)Y_{lk} + \sum_{\forall j\in\mathcal{J},k\in\mathcal{K}} (\xi_{jk} - v_{jk}^{cap}\mu_{jk}^n)Z_{jk} \tag{3.56}$$

The outline of the overall accelerated Benders Decomposition algorithm is presented in **Algorithm 2**.

3.4.2.5 Feasibility seeking Benders cut

Geoffrion and Graves [49] presented a feasibility seeking Benders decomposition algorithm where the authors showed that the master problem can be stopped whenever a first feasible solution better than the best incumbent solution is obtained. The rationale behind this is the following: the master problem requires several Benders cuts in order to obtain

accurate information from the dual subproblem. Therefore, it is not worth to optimize the master problem until optimality is proved.

The master problem **[HUB-RMP]** is now a feasibility seeking problem and no longer provides a lower bound for the original problem **[HUB-R]**. This forces finding an alternative way to terminate the algorithm. Hence, an error margin ϵ_f^n is introduced and the algorithm terminates whenever the restricted master problem **[HUB-RMP]** does not find any feasible solution better than $UB^n - \epsilon_f^n$. At this moment the best incumbent solution is reported and is referred to as an ϵ-optimal solution of the original problem **[HUB-R]**.

To obtain an ϵ-optimal solution, the following feasibility cut is added to the Benders master problem:

$$UB^n - \epsilon_f^n \geq \sum_{l \in \mathcal{L}, j \in \mathcal{H}} \Psi_{lj} Y_{lj} + \sum_{j \in \mathcal{J}, k \in \mathcal{K}_j} \xi_{jk} Z_{jk} + \theta \qquad \forall n \in \mathcal{N}^P \text{ (3.57)}$$

Where UB^n is the best known upper bound obtained till $n-1$ iterations. Geoffrion and Graves [49] showed that when $\epsilon_f^n > 0$ the Benders cut which is represented by constraint (4.46) does not generate the same integer solution. Therefore, the restricted master problem **[HUB-RMP]** is now a feasibility seeking problem.

The outline of the feasibility seeking Benders Decomposition algorithm is presented in **Algorithm 3**.

3.5 Computational Study and Managerial Insights

This section conducts a computational study on model **[HUB-R]** to test our algorithm and to draw managerial insights. We use the southeast region of U.S. as the testing ground. The following subsections describe the data used, present the results from the experimental study, and compare the performance of the accelerated Benders decomposition algorithms and that of other solution alternatives.

3.5.1 Data Description

Biomass Supply: The region of interest in this case study consists of nine states which are Mississippi (MS), Alabama (AL), Louisiana (LA), Tennessee (TN), Arkansas (AR), Georgia (GA), Florida (FL), South Carolina (SC) and North Carolina (NC). Biomass availability data is obtained from Knowledge Discovery Framework (KDF) database provided by U.S. Department of Energy [11]. This data was further processed by Idaho National Lab (INL) to identify the amount of densified biomass available in this region. Table 3.5 provides the summary of the total biomass available in the southeast region of U.S. Every year this region produces 29.35 million tons of densified biomass from 491 different counties. We also set this amount as the total demand that we need to satisfy in a given time period.

Investment Costs: In this study we consider a total of 291 potential hubs; among them 271 are rail ramps and 20 are inland/sea ports. Figure 3.3 shows the location and distribution of potential hubs and biorefineries in the southeast region of U.S. We consider a total of 44 potential locations for biorefineries. The annualized fixed cost for a rail ramp

of capacity 1.05 million ton per year (MTY) that sends single railcar is set to $54,949/year [80, 107]. We consider 5 different rail ramp capacities (l = 0.6 MTY, 0.8 MTY, 0.9 MTY, 1.05 MTY, and 1.20 MTY). These costs are estimated based on a lifetime of 30 years, and a discount factor of 10% is assumed. The annualized fixed cost for inline port of capacity 2.35 MTY is set to $306,000/year which is derived from a study of Searcy et. al. [114]. We consider 5 different port capacities (l = 1.0 MTY, 1.5 MTY, 1.75 MTY, 2.00 MTY, and 2.25 MTY). Although the actual fixed cost would vary by location, we use a common fixed cost as a reasonable approximation. The annualized fixed cost for biorefinery of capacity 45 million gallon per year (MGY) is set to $159,400,000 [154]. This cost was estimated based on a project life of 20 years, and an interest rate of 15% was assumed. We consider 5 different biorefinery sizes (l = 20 MGY, 40 MGY, 60 MGY, 100 MGY, and 150 MGY).

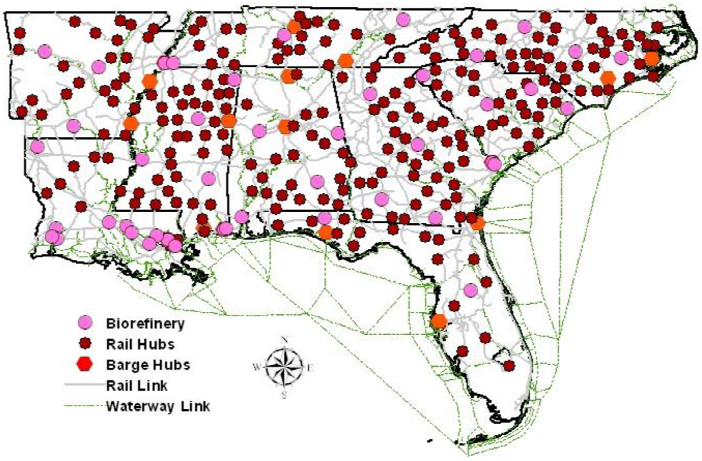

Figure 3.3

Network representation of intermodal supply chain

Transportation Costs: We consider that three different modes of transportation are available for transporting biomass from its source to destination: truck, single railcar and barge. Truck is used to transport biomass from a feedstock supply point $i \in \mathcal{I}$ to an intermodal hub facility $j \in \mathcal{J}$. Truck can further be used to transport biomass from its source $i \in \mathcal{I}$ to destination $k \in \mathcal{K}$ most likely under disrupted scenarios. The unit cost for truck transportation (c_{ij}) can be computed as follows [63]:

$$c_{ij} = \left[\frac{(t^d + \frac{t^t}{s_1})d_{ij}}{\delta_1^{cap}} + \Upsilon_1\right] \qquad \forall i \in \mathcal{I}, j \in \mathcal{J} \tag{3.58}$$

Where t^d represents distance dependent transportation cost ($/mile/truckload) such as expenses including fuel, insurance, maintenance and permitting costs. t^t represents time dependent transportation cost ($/hr/truckload) such as labor and capital costs. It is important to note that both t^d and t^t are distance dependent costs and varies with traveling distance d_{ij}. On the other hand, loading and unloading cost Υ_1 of biomass does not depend on traveling distance and is treated as fixed transportation cost. All the cost parameters are summarized in Table 4.5 [99]. These costs are estimated for a semi truck with a load capacity (δ_1^{cap}) of 25 tons, and average traveling speed (s_1) of 40 miles per hour. Note that we multiply a penalty term (i.e. 1.5) with c_{ij} in order to calculate the unit cost for truck transportation (c_{ik}) under disrupted scenarios.

Biomass can be transported in an intermodal hub by using barge or rail. Barge is the most cost-efficient mode of transportation as compared to rail and truck transportation for long-distance movement of grains. Barge rate is set as $0.017/mile/ton that is adopted from

a study of Gonzales et. al. [52]. This cost is estimated by assuming that a single tow can push up to 15 barges and each barge carries 1,500 tons of biomass. We further assume a trip length of 3 days.

Companies such as CSXT Corporation, Burlington Northern Santa Fe (BNSF) Corporation present on their websites the price charged per rail car for different origin destination pairs of rail ramps. These prices are a function of the capacity of the rail car, quantity shipped, shipment type, traveling distance and ownership of the equipment, rail car and rail line. Gonzales et. al. [52] perform a regression analysis in order to quantify the impact of distance (the independent variable) to rail transportation costs (the dependent variable) for the two companies defined above. The regression equations are based on the amount charged for a single railcar that carries 100 tons of grains:

$$Y_{CSXT} = 2,248 + 1.12x_1 \qquad R^2_{adj}(\%) = 29.0;\ p - Value(\%) = 2E^{-22} \quad (3.59)$$

$$Y_{BNSF} = 3,140 + 0.75x_1 \qquad R^2_{adj}(\%) = 50.0;\ p - Value(\%) = 0.01 \quad (3.60)$$

Where \$2,248 and \$3,140 are the fixed cost and \$1.12 and \$0.75 are charged per mile traveled (c_{jk}) by CSXT and BNSF companies for a single railcar. We assume that every week a train is shipped from its source to destination.

For all modes of transportation, we assume a shipment is moved from its source to destination using the corresponding shortest path. We used Arc GIS Desktop 10 to create a transportation network and used this network to identify shortest paths. The network includes actual railways and waterways as well as local, rural, urban roads and major high-

ways in the southeast region of U.S.

Identifying Disruption Probabilities: To apply equation (3.22) in model **[HUB-R]**, we index ports by $\mathcal{H}^p$ and rail ramps by $\mathcal{H}^r$, and then $\mathcal{H} = \mathcal{H}^p \bigcup \mathcal{H}^r$ for our study. We consider three types of major disasters in the Southeast U.S. i.e., hurricane, flooding and drought, indexed by h, f and d, respectively, i.e., $\mathcal{C} = \{h, f, d\}$[2]. Let q_{jh}, q_{jf} and q_{jd} denote the disruption probability of location j caused by flooding, draught and hurricane. Based on the nature of the disaster types, we know that drought does never jointly occur with hurricane or flood at the same place, and thus $q_j(\{f, d\}) = q_j(\{h, d\}) = 0, \forall j \in \mathcal{H}$. The data set we use seldom indicates simultaneous occurrences of hurricanes and floods at the same location, and thus we assume $q_j(\{f, h\}) = 0, \forall j \in \mathcal{H}$. We observe that all these disaster types are mutually exclusive; thus a special case of equation (3.23) is applied in the case study, and the disruption probability for ports can be written as:

$$q_j = p_{jf}g_{jf} + p_{jh}g_{jh} + p_{jd}g_{jd} \qquad \forall j \in \mathcal{H}^p \tag{3.61}$$

Where p_{jf} and g_{jf} are respectively the disaster frequency and the average disruption duration at location j due to flooding; p_{jh} and g_{jh} are respectively the disaster frequency and the average disruption duration at location j due to hurricane; finally, p_{jd} and g_{jd} represent the disaster frequency and the average disruption duration of location j due to

[2]We did not consider earthquakes since they rarely impacted port and rail operations in this region [141], [90]

drought. Since drought has little impact on rails, we set $p_{jd} = 0, \forall j \in \mathcal{H}^r$. Thus the disruption probability for rails from equation (3.23) becomes:

$$q_j = p_{jf}g_{jf} + p_{jh}g_{jh} \qquad \forall j \in \mathcal{H}^r \tag{3.62}$$

We predicted failure probabilities of intermodal hubs at 291 candidate locations, including 20 river ports and 271 rail ramps in the southeast region of U.S. in the target year of 2020. The failure probabilities are estimated based on historical records of these three prominent types of disasters in the study region. We have integrated data from multiple sources to forecast further disaster patterns. Table 3.7 summarizes the key input parameters that are used to estimate disruption probability in a given location j. Plugging the input data from Table 3.7 to equation (4.50) and (4.51), we can obtain estimated disruption probabilities of 291 candidate intermodal hubs in the target year of 2020, as illustrated in Figure 3.4, where the size of a circle is proportional to its disruption probability.

3.5.2 Experimental Results

We now discuss the results of our computational study. All the algorithms are coded in GAMS 22.7.1 [48] on a desktop with Intel Core i7 3.50 GHz processor and 32.0 GB RAM. The optimization solver used is ILOG CPLEX 11.0.

To understand the impact of intermodal hub disruption on biofuel supply chain network, we conduct three different experiments: (a) all intermodal hubs are robust and never fail (i.e., $\{q_j\}_{j\in\mathcal{H}} = 0.0$, and thus model **[HUB-B]** is applicable), (b) all intermodal hubs are subject to a disruption probability which are derived using the equations presented in

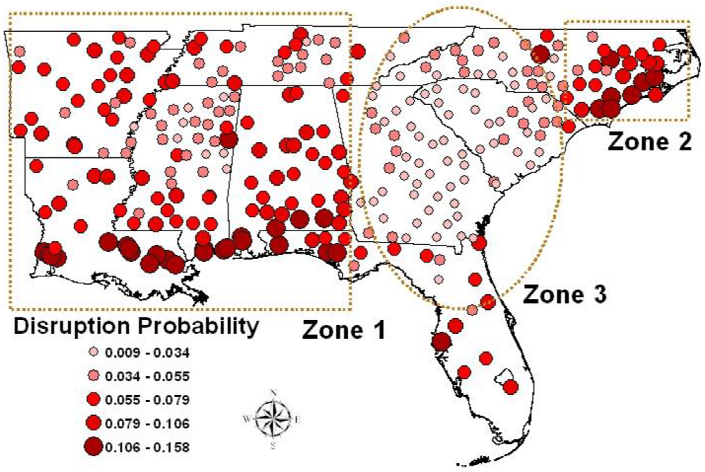

Figure 3.4

Disruption probability of intermodal hubs

(4.50) and (4.51), and (c) all intermodal hubs are subject to a disruption probability; however, this time the decision maker adopts a risk averse approach by setting high penalty coefficient ($\beta = 1.25$) on unit emergency transportation cost. Figure 3.5 shows the optimal hub deployment from these experiments. We divide each map into three zones, where zone 1 and zone 2 areas more vulnerable to disasters than zone 3. We see that the network design layout is significantly affected by hub disruption. For instance, we use 28 intermodal hubs in zone 1 if hub disruptions are ignored. When these disruption risks are properly considered, only 16 intermodal hubs are located in zone 1, and many intermodal hubs are moved to the relative reliable zone 3. The distribution of intermodal hubs for different zones under three experimental conditions (a), (b) and (c) are summarized in Table 3.8, where the columns under the heading $\mid \mathcal{J}^r \mid$ and $\mid \mathcal{J}^b \mid$ represent respectively the number of rail ramps and ports established in a particular zone.

Table 4.6 presents the impact of disruption on system performance. The column under the heading Z represents the total number of containers transporting between links $j \in \mathcal{J}$, $k \in \mathcal{K}$, i.e., $Z = \sum_{j\in\mathcal{J},k\in\mathcal{K}} Z_{jk}$. The columns $X^r_{ijk}(\%)$ and $X^b_{ijk}(\%)$ give the percentage of the total demand shipped via rail or barge transportation, i.e., $X^r_{ijk}(\%) = \sum_{i\in\mathcal{I},j\in\mathcal{J},k\in\mathcal{K}} X^r_{ijk}/d$ and $X^b_{ijk}(\%) = \sum_{i\in\mathcal{I},j\in\mathcal{J},k\in\mathcal{K}} X^b_{ijk}/d$. Similarly, the column $X_{ik}(\%)$ represents the percentage of the total demand shipped via trucks and $U(\%)$ represents the percentage of the total demand purchased from the outside market. The remaining column headings are self-explanatory. We observe that the unit shipping cost of biomass ($/ton) increases from $34.602/ton to $37.863/ton by considering disruption in the network designing process. We further observe that biomass shipped via intermodal hubs drops down to 35.27% from 65.85%. This is happening because intermodal hub disruptions force part of original intermodal shipments to be shifted to highways. The model may also finds it advantageous of purchasing biomass from the outside market by paying a penalty cost (π) of $80.00/ton. However, in this experiment we observe that the percentage of U does not change by considering disruption in the network designing process.

To understand the performance of the reliable model **[HUB-R]** solution over the minimum cost model **[HUB-B]** solution we create three different realistic hub disruption scenarios. In the first scenario, we assume that the Mississippi river floods. The Mississippi river and its tributaries have flooded on numerous occasions in the past. A list of major floods caused by Mississippi river can be found from the study of Trotter et al. [131]. In the second and third scenario we assume that the Tombigbee river flooded and a hurricane hits in North Carolina. State Climate Office of North Carolina reported that in total 39

different storms affected North Carolina between time period 2000-2008 [122]. The intermodal hubs which are impacted by these three disrupted scenarios are depicted in Figure **??**. Table 4.6 lists the unit cost of biomass under each disrupted scenarios where the reliable model solutions were obtained by solving model **[HUB-B]** with the fixed intermodal hub location decisions obtained from model **[HUB-R]**. Results indicate that the companies will have to pay an additional $0.47/ton (the difference between reliable cost and minimum cost solution) to hedge against unexpected intermodal hub disruptions. However, companies have the option to adopt the minimum cost solution strategy which results in higher system cost if any disaster happens. For instance, if Mississippi river floods and the two ports obtained from the minimum cost model become inactive (scenario 1 in Figure **??**), this scenario will increase the unit cost of biomass by 13.58% whereas adopting the reliable model solution will increase the unit cost of biomass by 1.94%. We further observe the similar trends from scenario 2 and 3 which highlights the need to consider intermodal hub disruption in the network design process.

Table 3.11 presents the impact of biomass supply changes on biofuel supply chain network. We observe that under different supply scenarios as the value of q_j increases ($q_j > 0.0$), the model finds it more economical to ship biomass through trucks or purchasing from outside market instead of using intermodal hubs in the network. This results in an increase of $X_{ik}(\%)$ and $U(\%)$ value and a decrease in $\mid \mathcal{J} \mid$ and Z_{jk} value as the value of q_j progressed. Furthermore, it is observed that the number of hubs and containers transported between the hubs is significantly impacted by biomass supply changes. For instance, a 10% increase in supply increases the number of containers transported between hubs by

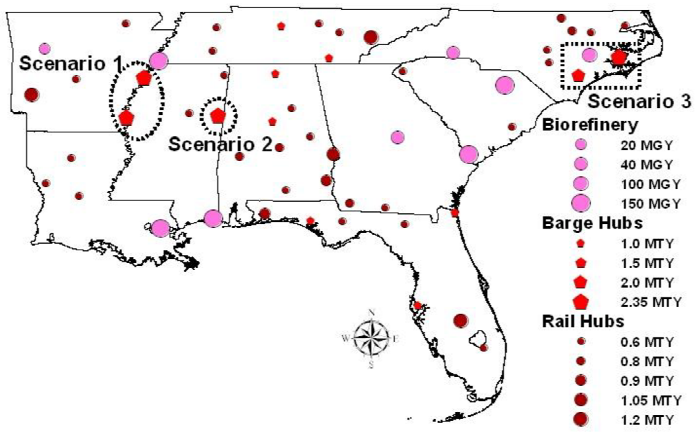

Figure 3.5

Identifying different hub disruption scenarios

9.32% in order to handle the increase of biomass shipped. This percentage is calculated when we assume that the intermodal hubs are robust and will never fail. On the other, when we assume that all intermodal hubs are subject to a disruption probability (i.e., $q_j = 0.10$), a 10% increase in supply increases the number of containers transported between the hubs by 11.10%. Additionally, under all supply scenarios it is observed that the percentage of biomass shipped via barge (X^b_{ijk}) is higher than the percentage shipped by railway (X^r_{ijk}). This is because barge is an inexpensive mode of transportation for shipping large quantity biomass over long distances as compared to other modes of transportation.

3.5.3 Analyzing the Performance of Solution Algorithms

This section presents our computational experience in solving model **[HUB-R]** using the algorithms proposed in Section 4.4. We first focus on analyzing the benefits of using different accelerated techniques over the standard Benders Decomposition algorithm.

Figure **??** shows the progression of lower and upper bound for different combination of Benders Decomposition as a function of iteration number. It is observed that the standard Benders Decomposition alone is unable to solve model **[HUB-R]** within 100 iterations and left with an optimality gap (i.e., $100 * (UB - LB)/UB\%$) of 16.65%. Adding valid inequalities (described in Section 3.4.2.1) in standard Benders Decomposition algorithm has a significant impact on reducing its optimality gap and solution time. This phenomenon is observed in Figure **??** where it is shown that the optimality gap now reduces down to 3.60%. We now add Modified Magnanti-Wong (MMW) cuts to the standard Benders Decomposition. Clearly, these stronger cuts have a significant impact on reducing the computational time and optimality gap over the standard Benders Decomposition algorithm. Finally, Figure 3.6 depicts how using all the cuts (Algorithm 2) effectively speeds up the convergence and improves the quality of the solution.

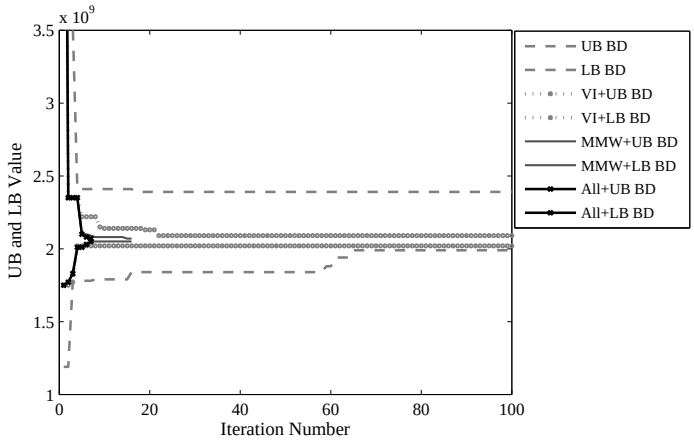

Figure 3.6

Benders' Decomposition with and without enhancements

Table 3.12 presents the computational results on solving model **[HUB-R]** under different hub sizes. We use the following terminating criteria for the algorithms: (a) $\epsilon = 0.01$ (b) $time_{max} = 36,000$ seconds and, (c) $iter_{max} = 1,000$. For the accelerated Benders decomposition algorithm, we solve the master problem initially with a large optimality gap and gradually reduce this gap as the algorithm progressed. We adopted this approach because it is observed that in the initial iterations the master problem does not receive enough information from the dual subproblem until several Benders cuts are added. This is why initially the optimality gap is set to 0.05, which we finally adjust to 0.01 when the gap between upper and lower bound of the algorithm reduces to 20%. For ϵ-optimal Benders decomposition, Geoffrion and Graves [49] used a fixed ϵ_f^n value throughout all iterations. Setting a ϵ_f^n value too large or small and maintaining the same value throughout all iterations would impact the performance of this algorithm [35]. Therefore, in this study we solved the master problem initially with a large ϵ_f^n value and gradually reduce this value as the algorithm progressed. For example, in every 20 iterations we reduce the initial ϵ_f^n value by 5%. Note that, in Table 3.12 we use the lower bound of CPLEX to present an optimality gap for ϵ-optimal Benders decomposition algorithm i.e., $100 * (UB_{\epsilon-Benders} - LB_{CPLEX})/UB_{\epsilon-Benders}\%$.

The results obtained from Table 3.12 confirm the efficiency of applying different accelerated techniques in the Benders Decomposition algorithm. It is observed that, CPLEX emerges as a good tool to solve **[HUB-R]** with a hub size up to $\mid \mathcal{H} \mid = 75$. However, as the number of potential hub increases ($\mid \mathcal{H} \mid > 75$) the benefit of using stronger cuts in the Benders Decomposition algorithm becomes evident. On average, our accelerated Benders Decomposition algorithm is 2.70 times faster than CPLEX. Both CPLEX and accelerated

Benders Decomposition algorithm are capable of solving all the problem instances within 1% optimality gap (shown in Table 3.12). On the other hand, the standard Benders Decomposition algorithm is able to solve only 15 out of the 40 instances.

ϵ-optimal Benders Decomposition algorithm is beneficial when the master problem is difficult to solve and there exists a small lower bound convergence rate [49]. Our computational experience shows that ϵ-optimal Benders Decomposition algorithm embedded with pareto optimality cuts is able to produce near optimal solution in a reasonable amount of time. On average, this algorithm is 5.01 times faster than CPLEX and 1.86 times faster than the accelerated Benders Decomposition algorithm. We conclude that, by controlling the ϵ_f^n value ϵ-optimal Benders Decomposition algorithm allows the operation research analyst to determine near optimal solutions faster than CPLEX.

Table 3.1

Summary of mathematical notations

Notation	Explanation
Sets	
$\mathcal{I}$	set of harvesting sites (farms)
$\mathcal{J}$	set of intermodal hubs
$\mathcal{K}$	set of biorefineries
$\mathcal{L}$	set of intermodal hub/biorefinery capacities
$\mathcal{J}_i$	set of intermodal hubs connected to harvesting sites i, $\forall i \in \mathcal{I}$
$\mathcal{I}_j$	set of harvesting sites connected to intermodal hubs j, $\forall j \in \mathcal{J}$
$\mathcal{K}_j$	set of biorefineries connected to intermodal hub j, $\forall j \in \mathcal{J}$
$\mathcal{J}_k$	set of intermodal hubs connected to biorefineries k, $\forall k \in \mathcal{K}$
$\mathcal{K}_i$	set of biorefineries directly connected to harvesting sites i via the emergency transportation service, $\forall i \in \mathcal{I}$
$\mathcal{I}_k$	set of harvesting sites directly connected to biorefineries k via the emergency transportation service, $\forall k \in \mathcal{K}$
Parameters	
s_i	amount of biomass available at site $i \in \mathcal{I}$
d	minimum total amount of biomass to be processed
v_{jk}^{cap}	maximum capacity of the cargo container transported along arc $(j,k) \in \mathcal{A}_2$
c_{lk}	unit flow cost along arc $(l,k) \in \mathcal{A}$
π	unit penalty cost for unsatisfied demand
Ψ_{lj}	fixed cost to open an intermodal hub of capacity $l \in \mathcal{L}$ at location j, $\forall j \in \mathcal{J}$
Ψ_{lk}	fixed cost to open a biorefinery of capacity $l \in \mathcal{L}$ at location k, $\forall k \in \mathcal{K}$
ξ_{jk}	fixed cost of a cargo container for transporting biomass along the arc $(j,k) \in \mathcal{A}_2$
c_{lj}^{cap}	acquirable capacity of a hub of capacity level l at location j, $\forall l \in \mathcal{L}, j \in \mathcal{H}$
q_j	failure probability of hub $j \in \mathcal{H}$
$\beta \geq 0$	penalty coefficient that reflects the risk aversion degree.

Table 3.2

Algorithm 1: Benders decomposition

$UB^n \leftarrow +\infty$, $LB^n \leftarrow -\infty$, $n \leftarrow 1$, ϵ, $\mathcal{P}_D \leftarrow 0$
terminate $\leftarrow$ **false**
while (*terminate* = **false**) **do**
    Solve **[HUB-RMP]** to obtain $\{Y_{lj}^n\}_{l\in\mathcal{L},j\in\mathcal{H}}$, $\{Z_{jk}^n\}_{j\in\mathcal{J},k\in\mathcal{K}}$ and z_{MP}^n
    if ($z_{MP}^n > LB^n$) **then**
        $LB^n \leftarrow z_{MP}^n$
    end if
    For fixed $\{\hat{Y}_{lj}^n\}_{l\in\mathcal{L},j\in\mathcal{H}}$, $\{\hat{Z}_{jk}^n\}_{j\in\mathcal{J},k\in\mathcal{K}}$ solve **[HUB-SUB(D)]** to obtain $(\delta_i, \gamma, \chi_j, \eta_k, \mu_{jk}) \in \mathcal{P}_D$ and z_{SUB}^n
    if ($z_{SUB}^n + \sum_{l\in\mathcal{L},j\in\mathcal{H}} \Psi_{lj}\hat{Y}_{lj}^n + \sum_{j\in\mathcal{J},k\in\mathcal{K}_j} \xi_{jk}\hat{Z}_{jk}^n < UB^n$) **then**
        $UB^n \leftarrow z_{SUB}^n + \sum_{l\in\mathcal{L},j\in\mathcal{H}} \Psi_{lj}\hat{Y}_{lj}^n + \sum_{j\in\mathcal{J},k\in\mathcal{K}_j} \xi_{jk}\hat{Z}_{jk}^n$
    end if
    if ($(UB^n - LB^n)/UB^n \leq \epsilon$) **then**
        terminate $\leftarrow$ **true**
    else
        $\mathcal{P}_D^{n+1} = \mathcal{P}_D^n \cup \{(\delta_i, \gamma, \chi_j, \eta_k, \mu_{jk})\}$
    end if
    $n \leftarrow n + 1$
end while

Table 3.3

Algorithm 2: Accelerated Benders Decomposition algorithm

Initialize, $UB^n \leftarrow +\infty$, $LB^n \leftarrow -\infty$, $n \leftarrow 1$, ϵ, ϵ', $\mathcal{P}_D \leftarrow 0$, $\{Y^0_{lj}\}_{l\in\mathcal{L},j\in\mathcal{H}}$, $\{Z^0_{jk}\}_{j\in\mathcal{J},k\in\mathcal{K}}$ and $\mathcal{Y}^n \leftarrow 0$.
terminate $\leftarrow$ **false**
while (*terminate* $=$ **false**) **do**
  Use $\{Y^0_{lj}\}_{l\in\mathcal{L},j\in\mathcal{H}}$ and $\{Z^0_{jk}\}_{j\in\mathcal{J},k\in\mathcal{K}}$ to solve **[HUB-SUB(MMW)]** and to obtain $(\delta_i, \gamma, \chi_j, \eta_k, \mu_{jk}) \in \mathcal{P}_D$
  $\mathcal{P}_D^{n+1} = \mathcal{P}_D^n \cup \{(\delta_i, \gamma, \chi_j, \eta_k, \mu_{jk})\}$
  Add (4.45) to **[HUB-MP]**. Solve **[HUB-MP]** to obtain $\{Y^n_{lj}\}_{l\in\mathcal{L},j\in\mathcal{H}}$, $\{Z^n_{jk}\}_{j\in\mathcal{J},k\in\mathcal{K}}$ and z^n_{MP}
  if ($z^n_{MP} > LB^n$) **then**
    $LB^n \leftarrow z^n_{MP}$
  end if
  For fixed $\{\hat{Y}^n\}_{l\in\mathcal{L},j\in\mathcal{H}}$, $\{\hat{Z}^n_{jk}\}_{j\in\mathcal{J},k\in\mathcal{K}}$ solve **[HUB-SUB(D)]** to obtain $(\delta_i, \gamma, \chi_j, \eta_k, \mu_{jk}) \in \mathcal{P}_D$ and z^n_{SUB}
  if ($z^n_{SUB} + \sum_{l\in\mathcal{L},j\in\mathcal{H}} \Psi_{lj}\hat{Y}_{lj} + \sum_{j\in\mathcal{J},k\in\mathcal{K}_j} \xi_{jk}\hat{Z}_{jk} < UB^n$) **then**
    $UB^n \leftarrow z^n_{SUB} + \sum_{l\in\mathcal{L},j\in\mathcal{H}} \Psi_{lj}\hat{Y}_{lj} + \sum_{j\in\mathcal{J},k\in\mathcal{K}_j} \xi_{jk}\hat{Z}_{jk}$
  end if
  if ($(UB^n - LB^n)/UB^n \leq \epsilon$) **then**
    terminate $\leftarrow$ **true**
  end if
  if ($(UB^n - LB^n)/UB^n \geq \epsilon'$) **then**
    Update $\mathcal{Y}^n$ and add (3.55) to **[HUB-MP]**
  end if
  $n \leftarrow n + 1$
end while

Table 3.4

Algorithm 3: Feasibility seeking Benders Decomposition algorithm

Initialize, $UB^n \leftarrow +\infty$, $n \leftarrow 1$, $\mathcal{P}_D \leftarrow 0$, $\{Y_{lj}^0\}_{l\in\mathcal{L},j\in\mathcal{H}}$, $\{Z_{jk}^0\}_{j\in\mathcal{J},k\in\mathcal{K}}$ and $\mathcal{Y}^n \leftarrow 0$.
terminate $\leftarrow$ **false**
while (*terminate* $=$ **false**) **do**
  Use $\{Y_{lj}^0\}_{l\in\mathcal{L},j\in\mathcal{H}}$ and $\{Z_{jk}^0\}_{j\in\mathcal{J},k\in\mathcal{K}}$ to solve **[HUB-SUB(MMW)]** and to obtain $(\delta_i, \gamma, \chi_j, \eta_k, \mu_{jk}) \in \mathcal{P}_D$
  $\mathcal{P}_D^{n+1} = \mathcal{P}_D^n \cup \{(\delta_i, \gamma, \chi_j, \eta_k, \mu_{jk})\}$
  Solve **[HUB-MP]** to obtain $\{Y_{lj}^n\}_{l\in\mathcal{L},j\in\mathcal{H}}$, $\{Z_{jk}^n\}_{j\in\mathcal{J},k\in\mathcal{K}}$ and z_{MP}^n
  if z_{MP}^n is *infeasible* **then**
    terminate $\leftarrow$ **true**
    Report: The best incumbent solution is a ϵ-optimal solution
  end if
  For fixed $\{\hat{Y}^n\}_{l\in\mathcal{L},j\in\mathcal{H}}$, $\{\hat{Z}_{jk}^n\}_{j\in\mathcal{J},k\in\mathcal{K}}$ solve **[HUB-SUB(D)]** to obtain $(\delta_i, \gamma, \chi_j, \eta_k, \mu_{jk}) \in \mathcal{P}_D$ and z_{SUB}^n
  if $(z_{SUB}^n + \sum_{l\in\mathcal{L},j\in\mathcal{H}} \Psi_{lj}\hat{Y}_{lj} + \sum_{j\in\mathcal{J},k\in\mathcal{K}_j} \xi_{jk}\hat{Z}_{jk} < UB^n)$ **then**
    $UB^n \leftarrow z_{SUB}^n + \sum_{l\in\mathcal{L},j\in\mathcal{H}} \Psi_{lj}\hat{Y}_{lj} + \sum_{j\in\mathcal{J},k\in\mathcal{K}_j} \xi_{jk}\hat{Z}_{jk}$
  end if
  $n \leftarrow n + 1$
end while

Table 3.5

Biomass supply data in Southeast region of U.S.

State	No. of Suppliers	Amount (tons/year)
Mississippi	56	6,246,500
Alabama	43	1,365,700
Louisiana	12	610,900
Tennessee	59	2,468,100
Arkansas	48	1,514,600
Georgia	99	2,681,900
Florida	37	698,400
South Carolina	39	3,875,700
North Carolina	98	9,892,000
Total	491	29,353,800

Table 3.6

Unit truck transportation cost

Costs	Parameters	Value	Unit
Loading/unloading	Υ_1	5.0	\$/wet ton
Time dependent	t^t	29.0	\$/hr/trucload
Distance dependent	t^d	1.20	\$/mile/trucload
Truck capacity	δ_1^{cap}	25	wet tons

Table 3.7

Parameters used to calculate $\{q_j\}_{j\in\mathcal{H}}$

Item	Disaster Types Flooding[a]	Hurricane[a]	Draught
Data period	1812-2012	1812-2012	2003-2012
Target year frequency	$p_{jf} = 1.726n_j$	$p_{jh} = 0.689n_j$	$p_{jd} = 0.10n_j^b$
Average disruption duration	0.822 year/occurence	2 year/occurence[c]	1 year/occurence
References	[1], [54], [45], [128]	[1], [93], [15]	[140], [129], [130], [91]

[a] n_j: average annual frequency at location $j \in \mathcal{H}$ over the data time period; it is multiplied by a trending factor obtained from regression analysis of historical data to extrapolate the annual frequency in the target year. For example, the city of Biloxi in Mississippi state has experienced 12 hurricanes in the past 160 years i.e., $n_j = 12/160 = 0.075$

[b] the probability of draught occurrence when SPI is less than or equal to -1.0

[c] we assume that the average disruption duration of an intermodal hub due to hurricane at each location $j \in \mathcal{J}$ is 2 years

Table 3.8

Impact of disruption on intermodal hubs

Scenario	β	Zone 1			Zone 2			Zone 3		
		$\mid \mathcal{J}^r \mid$	$\mid \mathcal{J}^b \mid$	$\mid \mathcal{J} \mid$	$\mid \mathcal{J}^r \mid$	$\mid \mathcal{J}^b \mid$	$\mid \mathcal{J} \mid$	$\mid \mathcal{J}^r \mid$	$\mid \mathcal{J}^b \mid$	$\mid \mathcal{J} \mid$
Minimum cost solution	1.00	20	8	28	6	2	8	6	1	7
Reliable solution	1.00	11	5	16	1	2	3	12	1	13
Reliable solution	1.25	9	4	13	1	2	3	10	1	11

Table 3.9

Impact of disruption on system performance

Scenario	β	Unit cost ($/ton)	$\mid \mathcal{J} \mid$	Z	X^r_{ijk} (%)	X^b_{ijk} (%)	X_{ijk} (%)	X_{ik} (%)	U (%)
Minimum cost solution	1.00	34.602	47	85,381	5.51	60.34	65.85	34.15	0.0
Reliable solution	1.00	37.863	37	58,365	7.57	27.70	35.27	64.73	0.0
Reliable solution	1.25	38.432	32	40,965	9.29	22.17	31.46	68.54	0.0

Table 3.10

Comparison of unit cost under different disrupted scenarios

Scenarios	Reliable ($/ton)	Min. Cost ($/ton)
No disruption	35.07	34.60
Scenario 1: Mississippi river flooded	35.75	39.30
Scenario 2: Tombigbee river flooded	35.76	36.96
Scenario 3: Hurricane in North Carolina	36.80	39.29

Table 3.11

Impact of supply changes on system performance

Supply changes (%)	q_j	Unit cost ($/ton)	$\mid \mathcal{J} \mid$	Z_{jk}	X^r_{ijk} (%)	X^b_{ijk} (%)	X_{ijk} (%)	X_{ik} (%)	U (%)
-10%	0.00	35.353	32	53,383	5.00	51.52	56.51	43.49	0.00
	0.05	38.329	19	41,487	1.97	36.14	38.12	61.88	0.00
	0.10	39.561	8	16,850	1.38	27.50	28.88	71.12	0.00
	0.15	39.843	6	12,116	0.84	18.86	19.70	80.30	0.00
	0.20	40.491	2	2,815	0.28	3.06	3.33	96.67	0.00
	0.25	40.669	1	1,115	0.00	0.93	0.93	99.06	0.00
	0.30	41.225	0	0	0.00	0.00	0.00	99.54	0.46
-5%	0.00	34.878	39	74,392	5.26	56.54	61.80	38.20	0.00
	0.05	37.698	21	56,247	2.18	41.35	43.53	56.47	0.00
	0.10	38.746	11	27,449	1.55	33.86	35.40	64.60	0.00
	0.15	39.180	9	24,218	1.06	23.22	24.28	75.72	0.00
	0.20	40.142	7	13,613	0.46	10.46	10.91	89.09	0.00
	0.25	40.346	5	6,158	0.28	8.29	8.57	91.43	0.00
	0.30	40.898	1	1,115	0.00	0.45	0.45	99.15	0.40
Base Case	0.00	34.602	47	85,381	5.51	60.34	65.85	34.15	0.00
(0%)	0.05	37.221	25	64,239	2.19	44.21	46.40	53.60	0.00
	0.10	38.588	21	51,478	1.61	35.27	36.88	63.12	0.00
	0.15	39.036	15	36,867	1.03	25.72	26.75	73.25	0.00
	0.20	39.911	12	23,933	0.54	17.55	18.09	81.91	0.00
	0.25	40.140	9	16,247	0.32	13.93	14.25	85.75	0.00
	0.30	40.360	3	1,660	0.22	0.34	0.57	99.40	0.04
$+5\%$	0.00	34.267	51	91,106	5.89	62.17	68.06	31.94	0.00
	0.05	36.896	27	67,452	5.43	47.45	52.88	47.12	0.00
	0.10	38.263	23	53,114	4.85	35.59	40.45	59.55	0.00
	0.15	39.004	16	38,741	4.28	25.91	30.19	69.81	0.00
	0.20	39.587	13	25,183	3.14	18.19	21.33	78.67	0.01
	0.25	40.107	10	17,129	0.97	16.49	17.46	82.51	0.03
	0.30	40.165	4	1,811	0.32	3.49	3.81	96.15	0.04
$+10\%$	0.00	34.117	56	93,340	9.30	62.17	71.47	28.53	0.00
	0.05	36.302	33	72,382	9.12	53.43	62.55	37.45	0.00
	0.10	37.557	27	57,191	6.61	40.01	46.61	53.36	0.03
	0.15	38.482	19	41,028	5.03	29.86	34.89	65.07	0.04
	0.20	39.187	14	25,357	3.66	22.99	26.65	73.20	0.15
	0.25	39.453	11	18,145	3.04	21.12	24.16	75.56	0.28
	0.30	39.949	6	2,766	0.35	8.39	8.74	90.77	0.49

Table 3.12

Comparison of different solution approaches

$\mid \mathcal{H} \mid$	q_j	CPLEX			Standard Benders				Accelerated Benders				ϵ-Benders			
		Obj. Val. ($ M)	Gap (%)	CPU (sec)	Obj. Val. ($ M)	Gap (%)	CPU (sec)	Iter	Obj. Val. ($ M)	Gap (%)	CPU (sec)	Iter	Obj. Val. ($ M)	Gap (%)	CPU (sec)	Iter
50	0.0	2,145.8	0.98	1.3	2,145.8	0.88	4.4	8	2,145.8	0.94	11.4	8	2,147.0	0.99	12.1	9
	0.1	2,152.8	0.35	1.2	2,152.8	0.78	4.4	8	2,152.8	0.87	11.2	8	2,154.2	1.00	12.1	9
	0.2	2,175.4	0.96	0.9	2,175.5	0.92	4.3	7	2,175.8	0.94	11.1	8	2,177.7	1.03	11.8	8
	0.3	2,176.5	0.73	0.9	2,176.5	0.96	4.3	7	2,176.4	0.97	10.3	7	2,177.1	0.95	11.2	8
75	0.0	2,137.1	0.61	6.9	2,137.1	0.97	8.3	11	2,137.1	0.99	24.2	9	2,139.2	1.04	31.2	10
	0.1	2,150.1	0.79	7.2	2,150.2	0.96	8.2	11	2,150.9	0.99	24.4	9	2,153.0	1.07	29.2	9
	0.2	2,161.2	0.94	7.1	2,161.9	0.99	8.1	9	2,161.7	0.98	23.9	8	2,165.0	1.10	28.7	9
	0.3	2,165.8	0.98	6.1	2,165.0	0.97	8.0	7	2,165.8	0.97	23.1	8	2,168.3	1.07	29.1	10
100	0.0	2,074.5	0.99	232.8	2,082.7	2.72	4,038.1	1,000	2,074.8	0.97	55.8	10	2,077.6	1.11	61.9	11
	0.1	2,104.7	0.98	144.2	2,114.9	1.21	3,543.2	1,000	2,105.1	0.99	54.9	10	2,108.3	1.12	63.8	12
	0.2	2,118.5	0.96	55.3	2,119.3	0.98	712.8	276	2,118.6	0.98	54.9	10	2,124.3	1.21	61.8	11
	0.3	2,119.5	0.98	54.1	2,119.7	0.99	582.2	222	2,119.7	0.99	52.2	9	2,125.1	1.20	61.8	11
125	0.0	2,074.5	0.74	433.9	2,087.8	3.21	5,379.8	1,000	2,076.8	0.98	84.2	11	2,077.8	1.12	84.8	13
	0.1	2,104.1	0.99	324.7	2,107.3	1.11	4,418.8	1,000	2,104.9	0.99	78.6	11	2,106.8	1.08	82.1	13
	0.2	2,117.7	0.98	127.9	2,118.1	0.99	1,123.1	323	2,118.1	0.99	64.2	10	2,121.8	1.14	73.8	12
	0.3	2,118.4	0.98	81.3	2,118.8	0.98	1,072.9	296	2,118.2	0.98	62.8	9	2,121.9	1.12	74.2	12
150	0.0	2,023.8	0.99	780.1	2,047.1	4.05	8,462.9	1,000	2,022.7	0.88	118.8	14	2,027.7	1.23	138.2	14
	0.1	2,054.4	0.98	751.1	2,068.2	3.28	7,790.6	1,000	2,054.7	0.97	111.7	14	2,062.2	1.35	134.3	14
	0.2	2,070.2	0.99	480.4	2,086.2	2.21	7,220.2	1,000	2,071.9	0.89	106.1	13	2,082.3	1.54	121.2	12
	0.3	2,071.5	0.98	396.1	2,072.1	0.98	2,347.8	482	2,071.2	0.98	94.6	11	2,076.8	1.23	114.8	12
175	0.0	2,023.4	0.99	1,140.5	2,061.7	4.21	9,799.1	1,000	2,023.9	0.98	207.1	19	2,026.6	1.14	317.9	18
	0.1	2,053.9	0.98	734.8	2,074.6	3.32	9,110.2	1,000	2,054.3	0.99	201.5	19	2,058.3	1.19	308.8	18
	0.2	2,074.3	0.98	732.8	2,096.2	2.28	8,128.7	1,000	2,074.0	0.88	193.2	19	2,083.5	1.41	249.4	14
	0.3	2,087.2	0.98	664.8	2,094.3	1.11	7,711.8	1,000	2,087.8	0.99	163.7	17	2,099.9	1.56	235.8	12
200	0.0	1,986.4	0.99	3,348.9	2,135.0	7.64	13,919.8	1,000	1,984.7	0.98	587.9	23	1,997.8	1.66	400.7	28
	0.1	2,013.2	0.99	3,115.8	2,189.2	8.87	12,558.2	1,000	2,014.8	0.96	551.7	22	2,014.3	1.05	381.2	27
	0.2	2,033.1	0.98	2,994.5	2,202.3	7.78	12,148.8	1,000	2,034.8	0.92	546.8	21	2,039.3	1.28	373.4	27
	0.3	2,038.2	0.99	2,888.7	2,227.6	7.28	11,958.5	1,000	2,038.1	0.99	505.2	19	2,044.5	1.29	354.2	24
225	0.0	1,922.4	0.99	6,877.9	2,009.5	8.91	25,148.1	1,000	1,919.3	0.99	1,364.6	29	1,935.9	1.84	476.2	30
	0.1	1,976.3	0.99	6,722.8	2,087.3	7.22	24,759.8	1,000	1,976.2	0.99	1,301.1	27	1,992.3	1.76	475.5	29
	0.2	1,988.2	0.96	5,752.9	2,105.5	7.29	21,147.8	1,000	1,988.0	0.98	1,225.2	25	2,006.4	1.87	462.8	28
	0.3	1,993.9	0.97	5,122.2	2,121.7	6.28	19,888.7	1,000	1,994.0	0.99	1,223.4	25	1,995.6	1.04	449.7	28
291	0.0	1,506.7	0.99	14,741.9	1,869.1	47.72	36,000.0	910	1,527.9	0.99	7,623.8	109	1,507.7	1.06	3,629.7	39
	0.1	1,619.6	0.96	13,784.5	1,889.3	42.47	36,000.0	989	1,620.3	0.99	7,424.2	104	1,624.1	1.27	3,476.8	37
	0.2	1,670.2	0.99	13,111.5	1,913.2	32.25	34,221.2	1,000	1,669.1	0.98	6,329.8	94	1,672.8	1.18	3,411.5	36
	0.3	1,688.0	0.99	12,258.7	1,922.8	24.47	33,182.8	1,000	1,688.2	0.99	5,712.7	86	1,697.8	1.52	3,285.4	33

3.6 Conclusion

This chapter studies the impact of intermodal disruption risk to the design and management of a biofuel supply chain network. A mixed integer linear programming model **[HUB-R]** is developed to determine the optimal intermodal hub locations and shipment routes for delivering biomass in order to optimize system's performance under normal conditions but also hedge against losses when intermodal hubs are disrupted because of natural disasters (e.g., flooding, hurricane, draught).

We have presented an enhanced Benders decomposition algorithm for solving our reliable intermodal hub location problem **[HUB-R]**. The enhanced Benders decomposition algorithm incorporates several algorithmic improvements such as the generation of pareto-optimality cuts, knapsack inequalities and the trust region cuts. Computational results showed that the enhanced Benders decomposition algorithm can be used to solve realistic instances of large size problems. Furthermore, we find that the ϵ-constrained Benders decomposition algorithm is capable of producing near optimal solution in a reasonable amount of time.

By using the southeast region of the U.S. as a testing ground, we conducted thorough computational experiments to test our model and to draw managerial insights. Our computational experiments reveal some insightful results about the impact of intermodal disruption risks on a biofuel supply chain network. Based on the results, the model selects to use intermodal hubs located in areas with low disruption probabilities. Moreover, when the disruption probability becomes high the model tends to locate only a few intermodal hubs and satisfy the remaining demand either by trucks or purchasing from outside mar-

kets. The sensitivity analysis further reveals how penalty coefficient β and supply changes affect the location and performance of the biofuel supply chain network.

In summary, the contributions of the chapter to the literature are manifold. First, we present a mathematical model to design a reliable, hub-and-spoke, biofuel supply chain network. We used a probabilistic model in order to estimate the disruption probability of the intermodal hubs. To the best of our knowledge, there is only one paper [4] that models reliable hub-and-spoke networks. There are no models to design reliable hub-and-spoke networks for biofuel supply chain networks. Second, we propose a customized solution approach to find high quality solutions to large instances of our problem in a time efficient manner. Finally, a real-world case study of the model is presented that reveals the impact of intermodal disruption risks on the biofuel supply chain network. The findings can be used by decision makers to design a reliable logistics network for biofuel supply chain networks.

This work can be extended in several directions. This study assumes that the intermodal hub fails independently. However, in order to represent a more realistic case, complex failure patterns such as correlated intermodal hub failures can be incorporated in the model. Furthermore, our work can be extended to consider congestions caused by intermodal hub disruption and incorporating additional arcs to deal with shipments during the emergency. These issues will be addressed in future studies.

CHAPTER 4

DESIGNING A RELIABLE AND DYNAMIC INTERMODAL HUB-AND-SPOKE SUPPLY CHAIN FOR BIOMASS

4.1 Introduction

Production of biofuels is expected to increase in the near future due to the requirements set by the Renewable Fuel Standards (RFS) [139]. Based on these requirements, 36 billion gallons a year (BGY) of biofuels should be produced by 2022. These standards cap corn-ethanol production to 15 BGY, and they require that at least 16 BGY of cellulosic biofuels be produced. In 2013, 1.3 billion gallons (BG) of biodiesel [137] and 13.3 BG of ethanol [104] were produced and production of cellulosic biofuels is expected to continue to increase. Investors will need tools to support their supply chain design and management decisions, so the goal of this paper is to build models of cellulosic biofuel supply chains that ensure efficient and reliable performance.

The efficiency and reliability of the supply chain are crucial aspects of the biofuel industry. Ensuring that these supply chains are cost-efficient is challenging due to the physical characteristics of the raw material used to produce these biomass fuels. Biomass is bulky and difficult to transport; its supply is seasonal and uncertain; and biomass is widely dispersed geographically. For these reasons, collection and transportation costs are high. Modes like rail and barge can be used to deliver biomass to reduce transportation

costs. These modes are typically used for long-haul and high-volume shipments of other bulk products, such as corn, soybeans, and other large harvest crops. When barge is used, the supply chain becomes vulnerable to unexpected natural disasters, such as floods, hurricanes, and droughts,- which interrupt the supply chain's regular operations. Therefore, designing reliable supply chains to hedge against risks from unexpected natural disasters is important. The model proposed here is an integer program that minimizes costs of supply chain activities and hedges against risks from unexpected natural disasters. This model will serve managers of biofuel plants who face supply chain design and management decisions.

One of the motivations for this work is the powerful impact that catastrophic events have on transportation infrastructure and logistics management. For example, natural disasters like Hurricane Katrina in 2005 [93], the earthquakes in China and Haiti in 2008 and 2009 respectively [144], and human-caused disasters, such as the 2003 U.S. Northeast blackout [97] and 2010 Gulf of Mexico Oil Spill [102], devastated transportation systems and consequently interrupted logistics and supply chain activities. Furthermore, the timing of potential disruptions due to hurricanes and floods corresponds with the harvest season for biomass. For example, the harvest season for corn stover - typically early September until late November - coincides with the hurricane season in the Southeast and is followed by droughts of agricultural waterways. Historical records indicate that the Southeast hurricane season starts in mid-August and continues until the end of October (see Figure 4.1) [122]. Hurricanes also impact agricultural waterways shipments of biomass to the Gulf of Mexico and shipments of stover to and from the North Carolina (NC) and South Carolina (SC) Atlantic coastlines. Droughts along the Mississippi River and other agricultural

waterways typically happen during the winter because of the impacts moisture and cold weather have in the Midwest [136]. Other disruptions, such as flooding of the Mississippi River and its tributaries (see Table 4.1), impacts biomass supply chain operations. Thus, biomass seasonality, coupled with transportation uncertainty due to disruptions, impacts supply chain performance. To handle these uncertainties efficiently, managers need to adjust their short-term and mid-term supply chain decisions dynamically.

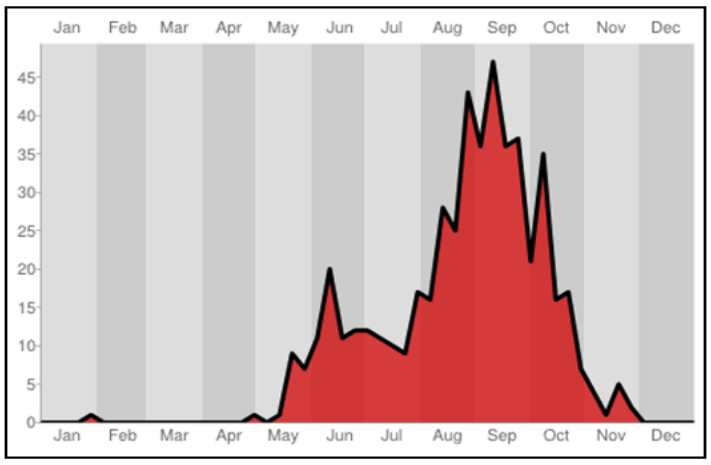

Figure 4.1

Stormy days in NC (1851-2012) [122]

To manage the supply chain and cope with facility disruptions, managers need decision-support tools. These tools should capture the seasonal nature of biomass supply, use the proper transportation modes for biomass transportation, and rely on existing practices used to manage agricultural products' supply chains. The model proposed in this chapter accounts for these important observations. We present a hub-and-spoke network model to design the inbound supply chain of biofuel facilities. Hub-and-spoke network models are

typically used to design supply chains for bulk products, such as corn and other agricultural products. The first hub in the network serves as a shipment consolidation point, and the second hub is a de-consolidation point. Rail and barge transport biomass between hubs since these modes are typically used for high-volume, long-haul transportation of bulk products. The model proposed is dynamic because it identifies when to open new biorefineries and in which season to use, or discontinue using, an intermodal hub. The model also determines a transportation schedule for shipments between facilities and identifies a production schedule and inventory levels.

Table 4.1

Mississippi river flooding history between 1900-2011 [131]

Name of the Flood	Year	Most Affected Months
Great Mississippi Flood of 1927	1927	May-December
Great Flood of 1937	1937	January-February
Flood of 1945	1945	March-May
Mississippi Flood of 1973	1973	March-May
Flood of 1975	1975	April
Flood of 1979	1979	April
Lower Mississippi Flood	1983	May-June
Great Mississippi and Missouri Rivers Flood	1993	April-October
Flood of 2002	2002	April
Flood of 2008	2008	April-May
Great Mississippi Flood of 2011	2011	April-May

To optimize costs in this supply chain, the model allows facilities the flexibility of using different modes of transportation - thus different hubs - in different seasons. This practice is followed by many companies that deliver corn and grains by barge from the Midwest to the Gulf of Mexico. For example, due to Mississippi river drought during winter, companies use rail or truck instead of barge. Another practice is to maintain inventories and

delay biomass delivery. While these practices reduce the impact that potential disruptions may have on the supply chain, transportation or inventory costs will increase because some modes of transportation are more expensive or because carrying inventory increases costs. Clearly, making these decisions is not easy since they are impacted by biomass availability, inventory holding costs, transportation costs, and other concerns. Models like the one proposed in this chapter are useful for decision-makers since they aid in making supply chain decisions that minimize the overall system costs. The model proposed here minimizes costs under normal and disruption scenarios.

The model proposed is an extension of the classical fixed charge network design problem which is known to be an $\mathcal{NP}$-hard problem [79]. Therefore, solving large instances of this supply chain problem is a challenging task. For this reason, we develop and implement two algorithms: a rolling horizon-based heuristic and an enhanced Benders decomposition algorithm. Numerical experiments confirm that both algorithms efficiently solve mid-sized problem instances. For large-scale problems, an algorithm that integrates the rolling horizon heuristic and the accelerated Benders decomposition algorithm provides near optimal solutions by avoiding the the stand alone algorithms prohibitively long running times. We implement these algorithms using data from a case study of the Southeast USA. The results from solving the case study provide detailed periodic production and transportation plans that capture feedstock seasonality and hedge against risk due to unexpected natural disasters.

4.2 Literature Review

In recent years, research in biofuel supply chains has focused on minimizing the total system costs. These studies develop integrated biofuel supply chain networks to deliver biomass at a competitive price to the end users. To achieve this goal, studies such as Zamboni et al. [156] and Eksioglu et al. [39] develop deterministic models optimizing the total plant location and transportation costs in biofuel supply chain networks. These works are extended by Eksioglu et al. [38], Kang et al. [68], Huang et al. [63], An et al. [3], Eksioglu et al. [41] and Xie et al. [153] to capture system dynamics better by considering multiple periods of optimization frameworks. Xie and Ouyang [147] develop a mixed-integer programming model for a dynamic, multi-type facility co-location problem which, during a fixed planning horizon, minimizes the total costs from facility construction, capacity expansion, and transportation. The authors use an accelerated Benders decomposition algorithm to solve large-sized problem instances. To capture system uncertainties, Kim et al. [71], Chen and Fan [22] and Huang et al. [64] develop stochastic models to aid with the design and management of biofuel supply chain networks. One of the key assumptions of the above mentioned literature is that facilities - some of which are intermodal hubs - are robust and never fail. However, unexpected disruptions at transportation hubs have been observed on multiple occasions [89], [29], [102]. These facts highlight the need to address the potential risk of facility failures in the process of designing and managing biofuel supply chain networks.

The practice with other agricultural products indicates that the inbound supply chain systems for biorefineries should have a hub-and-spoke structure. Research by Eksioglu et

al. [39] is one of the first analyzations of the impact of intermodal transportation systems on the biofuel supply chain network. Most recently, Xie et al. [153] extend that work by developing a fully integrated multi-modal transport system for the cellulosic biofuel supply chain network. Both these models consider biomass seasonality. The model proposed here is closely related to these studies. However, unlike these works which assume that the multi-modal transport system is reliable and never fails, the model proposed here considers the impact of intermodal hub disruptions in the biofuel supply chain performance.

Although many researchers have focused on hub location models, only two papers in the literature specifically study the dynamic hub location problem. Campbell [19] develops a continuous approximation model to help transportation terminals handle an increasing regional demand for their services. Contreras et al. [24] develops a dynamic, uncapacitated, hub location problem that minimizes the total system costs over a finite planning horizon. The model proposed in this paper is an extension of the paper by Contreras et al. [24]. Our work differs because it considers intermodal hub disruptions as part of a dynamic hub location problem. Additionally, we propose customized algorithms, extensions of the Benders decomposition algorithm and rolling horizon heuristic. The Benders decomposition algorithm has been studied and implemented by many researchers ([9]), and a number of papers discuss implementations of the rolling horizon algorithm ([72]).

Reliability issues in supply chain design are a topic of interest for many researchers. Peng et al. [100] state that even a carefully constructed supply chain network can be severely damaged if, during the design phase, managers fail to consider potential disruptions. Daskin [32, 33] first considers facility unavailability in a maximal covering loca-

tion problem. This work is extended by Drezner [36] by developing models for reliable p-median location problems. Snyder and Daskin [121] propose models for reliable uncapacitated fixed-charge location problems (UFLP) and the p-median problem where facility disruptions occur randomly with identical probability. Cui et al. [30], Li and Ouyang [77], Shen et al. [117], and Li et al. [76] extend existing models by relaxing the uniform disruption probability assumption introduced by Snyder and Daskin [121].

The reviewed literature focuses on reliable facility location models. To the best of our knowledge, the model by An et al. [4] is the only one that addresses reliability issues for the single- and multiple-allocation hub-and-spoke network design problems. Their work considers disruptions at transportation hubs where the risk of hubs becoming unavailable is mitigated by identifying backup hubs and alternative transportation routes. This work is closely related to the work presented here, but the model we propose mitigates risk by deciding, at the planning stage, what hub to use, or discontinue using, during different seasons of the year. Therefore, our model proposes a proactive, not a reactive approach to manage the supply chain.

Despite all these efforts, little work has been done to address the impact of disruptions to the biofuel supply chain network design and management. Li et al. [78] propose one discrete and one continuous model to design reliable bio-ethanol supply chain networks. They use numerical analysis to evaluate the impact of disruptions on optimal refinery deployment decisions. Wang and Ouyang [146] propose a game-theoretical-based, continuous approximation model to locate biorefineries under spatial competition and facility disruption risks. These studies only consider failure risks at biorefineries. These studies

do not focus on evaluating the impact that disruptions of intermediate transportation hubs have on the biofuel supply chain performance. The model we propose fills this gap that exists in the current literature.

4.3 Problem Description and Model Formulation

This section presents a mathematical model for a multiple period biofuel supply chain network design and management problem. The model considers potential facility disruptions and responds by dynamically identifying the intermodal hubs to use, or discontinue using, in each period in order to optimize system-wide costs. Section 4.3.1 provides a mixed-integer nonlinear programming (MINLP) formulation of the problem, referred to as **[DR]**. Section 4.3.2 provides a mixed-integer linear programming (MILP) formulation which is easier to solve with commercial software and the algorithms we propose in Section 4.4.

4.3.1 Nonlinear Problem Formulation

Let $\mathcal{G}(\mathcal{N}, \mathcal{A})$ denote the supply chain network for the problem presented in this chapter. Figure 4.2 gives an example of the network structure for a biofuel supply chain that consists of two suppliers, one intermodal hub, two biorefineries, and two markets. The set of nodes in $\mathcal{G}(\mathcal{N}, \mathcal{A})$, denoted by $\mathcal{N}$, consists of the set of suppliers $\mathcal{I}$, the set of candidate intermodal hub locations $\mathcal{J}$, the set of candidate biofuel plant locations $\mathcal{K}$, and the set of markets $\mathcal{G}$. Each supplier $i \in \mathcal{I}$ produces s_{it} units of biomass in time period $t \in \mathcal{T}$. Each market $g \in \mathcal{G}$ demands b_{gt} gallons of biofuel in period t. This formulation assumes that a substitute product in the market can be used to satisfy the demand for biofuel. The market

price for the substitute product is denoted by π_{gt}. This price, which is exogenously determined, represents the penalty per unit of unsatisfied demand. This penalty also serves as a threshold of the biofuel's unit delivery cost using the proposed system. That means, if the unit cost of delivering biofuel to markets through this supply chain exceeds the threshold, then, demand will be satisfied by the substitute product.

For nodes $j \in \mathcal{J}$, Ψ_{ljt} denotes the fixed cost of using this hub j of capacity $l \in \mathcal{L}^h$ at the beginning of time period t. These costs are used to establish the necessary infrastructure that will connect a biofuel plant to this hub. η_{ljt} denotes the recovery gain associated with discontinued use of the hub. Ψ_{lk} is the fixed cost of locating a biofuel plant of capacity $l \in \mathcal{L}^b$ in location $k \in \mathcal{K}$. Hubs serve as shipment consolidation/de-consolidation points. We assume that every biofuel plant is co-located with an intermodal hub of sufficiently large capacity, and the transportation costs between the refinery and the hub are negligible. This assumption is derived from the fact that many large-scale production facilities have direct access to shipping by rail and barge.

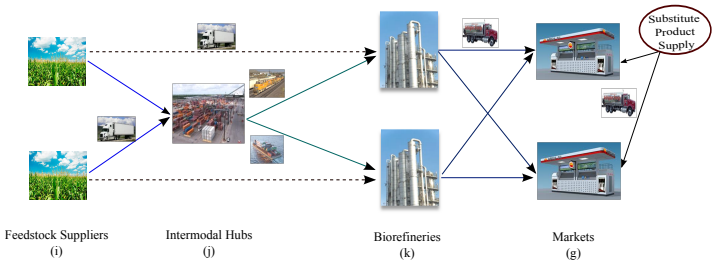

Figure 4.2

Network configuration of a biofuel supply chain

The set of arcs, denoted by $\mathcal{A}$, consists of four disjoint subsets, $\mathcal{A}^1, \ldots, \mathcal{A}^4$. Let c_{ijt} for $(i,j) \in \mathcal{A}$ denote the variable unit cost of moving products along these arcs in time period t. Set $\mathcal{A}^1$ consists of the arcs joining suppliers with intermodal hubs; set $\mathcal{A}^2$ consists of arcs connecting intermodal hubs. Set $\mathcal{A}^3$ consists of arcs that directly connect suppliers to biorefineries; and set $\mathcal{A}^4$ consists of arcs connecting biorefineries to markets. Travel distance along arcs in $\mathcal{A}^1$ is short. Thus biomass is shipped along these arcs by trucks. Transportation quantities along arcs in $\mathcal{A}^2$ are large, and transportation distances are typically long. Thus, transportation modes such as rail and barge are used to move biomass between hubs. We denote the unit cost along arcs $(i,j) \in \mathcal{A}^1$ and $(j,k) \in \mathcal{A}^2$ by c_{ijkt}. These costs are equal to $c_{ijkt} = c_{ijt} + c_{jkt}$. Arcs in $\mathcal{A}^3$ represent direct shipments of biomass from suppliers to biofuel plants. These arcs are used to consider the scenario when a supplier is located nearby a biofuel plant, and therefore, direct truck shipments are delivered. Biomass, when delivered by rail or barge, is transported using cargo containers. Therefore, for rail and barge transportation, in addition to the variable unit transportation cost, this study considers that a fixed cost ξ_{jkt}, represents the costs associated with the loading and unloading of containers, occurs in period t. Container capacity is denoted by v^{cap}. Biofuel is transported by truck from biofuel plants to the market. We assume that all the costing parameters, variable and fixed, will vary over the planning horizon. The sets and input parameters used in this section are described in Tables 4.2 and 4.3.

We assume that each hub is disrupted independently. While it may seem simplifying, there is a reasoning behind this assumption. Consider the location of the main hubs of Delta airlines in the USA: Detroit, Atlanta, New York, Minneapolis and Salt Lake City. Since

Table 4.2

Description of the sets

Symbol	Description
$\mathcal{I}$	set of harvesting sites (farms)
$\mathcal{J}$	set of intermodal hubs
$\mathcal{K}$	set of potential locations for biofuel plants
$\mathcal{G}$	set of markets
$\mathcal{L}^b$	set of production capacities for biofuel plants
$\mathcal{L}^h$	set of storage capacities for hubs
$\mathcal{T}$	set of time periods

hubs are shipment consolidation points, the chances are they are located further away - as it is the case with Delta airlines - and therefore will not be affected by the same disruptions. We denote by q_{jt} the disruption probability of hub $j \in \mathcal{J}$ in period t. Thus, $(1 - q_{jt})$ is the probability that this hub is operating during time t. A shipment can be delivered to a biofuel plant through the hub-and-spoke network if both, the consolidation (j) and de-consolidation (k) hubs are operating. This happens with a probability of $(1 - q_{jt})(1 - q_{kt})$. The probability that either, or both hubs fail is $(q_{jt} + q_{kt} - q_{jt}q_{kt})$. The coefficient βc_{ijkt} represents the unit emergency service costs in order to deliver the product in case of a disruption. This cost is β (for $\beta > 1$) units higher compared to the unit transportation costs c_{ijkt}. We assume that direct truck shipments are not affected by disruptions. Let X_{ijt} represent the amount shipped along $(i, j) \in \mathcal{A}$ in period t; and X_{ijkt} represent the amount of biomass delivered in period t from supplier i to biofuel plant k though hubs j and k. Then, the expected variable transportation cost along the hub-and-spoke network is:

$$\sum_{t\in\mathcal{T}}[\sum_{i\in\mathcal{I},j\in\mathcal{J},k\in\mathcal{K}}\left(c_{ijkt}(1-q_{jt})(1-q_{kt})+\beta c_{ijkt}(q_{jt}+q_{kt}-q_{jt}q_{kt})\right)X_{ijkt}+\sum_{(i,j)\in\mathcal{A}^3}c_{ijt}X_{ijt}]$$

Table 4.3

Input parameters

Symbol	Description
Ψ_{ljt}	fixed cost of using a hub of capacity $l \in \mathcal{L}^h$ at location $j \in \mathcal{J}$ in time period $t \in \mathcal{T}$
η_{ljt}	recovery gain associated with discontinued use of a hub of capacity l at$j$ in period t
Ψ_{lk}	fixed cost of opening a biofuel plant of capacity $l \in \mathcal{L}^b$ at location $k \in \mathcal{K}$
ξ_{jkt}	fixed cost of a cargo container for transporting biomass along arc $(j,k) \in \mathcal{A}^2$ in period t
c_{lkt}	unit flow cost along arc $(l,k) \in \mathcal{A}$ in period t
p_{lkt}	unit production cost at a biofuel plant of size l located at k in period t
h_{kt}	unit inventory cost at biofuel plant k in period t
π_{gt}	unit penalty cost of not satisfying demand of market g in period t
s_{it}	amount of biomass available at site $i \in \mathcal{I}$ in period t
b_{gt}	biofuel demand of market $g \in \mathcal{G}$ in period t
c_{lj}^{cap}	biomass storage/handling capacity of an intermodal hub of size $l \in \mathcal{L}^h$ at location j
h_{lk}^{cap}	biomass storage capacity of a biofuel plant of size $l \in \mathcal{L}^b$ at location k
v^{cap}	cargo container capacity
p_{lk}^{cap}	production capacity of a biofuel plant of size l at location k
ϕ	conversion rate from biomass to biofuel
q_{jt}	failure probability of intermodal hub $j \in \mathcal{J} \bigcup \mathcal{K}$ in time period t

We now introduce the remaining decision variables.

$$Y_{ljt} = \begin{cases} 1 & \text{if the intermodal hub } j \text{ of capacity } l \text{ is used in time period } t \\ 0 & \text{otherwise;} \end{cases}$$

$$Y_{lk} = \begin{cases} 1 & \text{if a biofuel plant of capacity } l \text{ is opened at location } k \\ 0 & \text{otherwise;} \end{cases}$$

Variables $\mathbb{Z}_{jkt}$ identify the number of containers used between hubs j and k in period t. Variables P_{lkt} represent the amount of biofuel produced at biofuel plant k of capacity l in period t. Variables H_{kt} represent the amount of biomass stored at biofuel plant k in period t, and U_{gt} represents the amount of unsatisfied demand in market g in period t.

The problem is to identify: where to locate biorefineries among the candidate locations $k \in \mathcal{K}$; what should be the production capacity of each biofuel plant; which transportation

hub to use or discontinue using in period t; how much biomass to deliver to a biofuel plant, how much biomass to keep in the inventory, and how much biofuel to deliver to the markets in each time period. The goal is to minimize the total system costs under normal and hub disruption scenarios. The following is an MINLP formulation of the problem referred to as model **[DR]**.

$$\begin{aligned}
\textbf{[DR]} Min. \quad & \sum_{l\in\mathcal{L}^b,k\in\mathcal{K}} \Psi_{lk}Y_{lk} + \sum_{t\in\mathcal{T}}\Bigg[\sum_{l\in\mathcal{L},j\in\mathcal{J}} (\Psi_{ljt}Y_{ljt}(1-Y_{lj,t-1}) - \eta_{ljt}Y_{lj,t-1}(1-Y_{ljt})) \\
& + \sum_{(i,j)\in\mathcal{A}^2} \xi_{ijt}Z_{ijt} + \sum_{(i,j)\in\mathcal{A}^3\bigcup\mathcal{A}^4} c_{ijt}X_{ijt} + \sum_{l\in\mathcal{L}^b,k\in\mathcal{K}} p_{lkt}P_{lkt} + \sum_{k\in\mathcal{K}} h_{kt}H_{kt} \\
& + \sum_{i\in\mathcal{I},j\in\mathcal{J},k\in\mathcal{K}} c_{ijkt}\left((1-q_{jt})(1-q_{kt})X_{ijkt} + \beta(q_{jt}+q_{kt}-q_{jt}q_{kt})X_{ijkt}\right) \\
& + \sum_{g\in\mathcal{G}} \pi_{gt}U_{gt}\Bigg]
\end{aligned}$$

Subject to

$$\sum_{k\in\mathcal{K}} X_{ikt} + \sum_{j\in\mathcal{J},k\in\mathcal{K}} X_{ijkt} \leq s_{it} \qquad \forall i\in\mathcal{I}, t\in\mathcal{T} \quad (4.1)$$

$$\phi\left[\sum_{i\in\mathcal{I}} X_{ikt} + \sum_{(i,j)\in\mathcal{A}^1} X_{ijkt} + H_{k,t-1} - H_{kt}\right] = \sum_{l\in\mathcal{L}^b} P_{lkt} \qquad \forall k\in\mathcal{K}, t\in\mathcal{T} \quad (4.2)$$

$$\sum_{g\in\mathcal{G}} X_{kgt} \leq \sum_{l\in\mathcal{L}^b} P_{lkt} \qquad \forall k\in\mathcal{K}, t\in\mathcal{T} \quad (4.3)$$

$$\sum_{k\in\mathcal{K}} X_{kgt} + U_{gt} = b_{gt} \qquad \forall g\in\mathcal{G}, t\in\mathcal{T} \quad (4.4)$$

$$\sum_{i\in\mathcal{I},k\in\mathcal{K}} X_{ijkt} \leq \sum_{l\in\mathcal{L}^h} c_{lj}^{cap}Y_{ljt} \qquad \forall j\in\mathcal{J}, t\in\mathcal{T} \quad (4.5)$$

$$\sum_{i\in\mathcal{I}} X_{ijkt} \leq v^{cap}Z_{jkt} \qquad \forall (j,k)\in\mathcal{A}^2, t\in\mathcal{T} \quad (4.6)$$

$$P_{lkt} \leq p_{lk}^{cap}Y_{lk} \qquad \forall l\in\mathcal{L}^b, k\in\mathcal{K}, t\in\mathcal{T} \quad (4.7)$$

$$H_{kt} \leq \sum_{l \in \mathcal{L}^b} h_{lk}^{cap} Y_{lk} \qquad \forall k \in \mathcal{K}, t \in \mathcal{T} \tag{4.8}$$

$$\sum_{l \in \mathcal{L}^b} Y_{lk} \leq 1 \qquad \forall k \in \mathcal{K} \tag{4.9}$$

$$Y_{lk} \in \{0,1\} \qquad \forall l \in \mathcal{L}^b, k \in \mathcal{K} \tag{4.10}$$

$$Y_{ljt} \in \{0,1\} \qquad \forall l \in \mathcal{L}^h, j \in \mathcal{J}, t \in \mathcal{T} \tag{4.11}$$

$$Z_{jkt} \in Z^+ \qquad \forall j \in \mathcal{J}, k \in \mathcal{K}, t \in \mathcal{T} \tag{4.12}$$

$$X_{ijkt}, X_{ikt}, X_{kgt}, P_{lkt}, H_{kt}, U_{gt} \geq 0 \qquad \forall i \in \mathcal{I}, j \in \mathcal{J}, k \in \mathcal{K}, g \in \mathcal{G}, t \in \mathcal{T} \tag{4.13}$$

The objective function minimizes the total expected system cost, including the expected transportation costs under normal conditions and disruption, costs of using and discontinued use of hubs, biofuel plant investment costs, biofuel production costs, biomass inventory holding costs and penalty costs of unsatisfied demand.

Constraints (4.1) indicate that the amount of biomass shipped from supplier i in period t is limited by biomass availability. Constraints (4.2) are the flow conservation constraints at biofuel plants. These constraints indicate that the amount of biofuel produced in period t is limited by the amount of biomass shipped in that period and the available inventories. If a biofuel plant only holds biomass inventories, capital investments for such plants will be extremely high. Therefore, in order to deal with biomass supply uncertainties, biomass inventory should be held to maximize utilization of the existing production capacity. Constraints (4.3) indicate that the amount of biofuel delivered to the market is limited by the amount of biofuel produced in period t. Constraints (4.4) indicate whether demand for biofuel will be fulfilled through the hub-and-spoke distribution network or through substitute products available in the market. Constraints (4.5) indicate that the total amount of

biomass shipped through an intermodal hub is limited by its capacity. Constraints (4.6) show that the amount of biomass shipped between hubs is limited by the number of available containers and container capacity. Constraints (4.7) are the biofuel production capacity limitations at a plant. Constraints (4.8) are the biomass storage limitations at a biofuel plant. Constraints (4.9) ensure that, at most, one biofuel plant is operating at a particular location in period t. Constraints (4.10) and (4.11) are the binary constraints, and (4.12) are the integer constraints. Constraints (4.13) are the non-negativity constraints.

4.3.2 A Linear Model Formulation

Model **[DR]** is nonlinear due to the $Y_{ljt}(1 - Y_{lj,t-1})$ and $Y_{lj,t-1}(1 - Y_{ljt})$ expressions in the objective function. The term $Y_{ljt}Y_{lj,t-1}$ in these expressions is the product of two binary decision variables, and therefore it takes values 0 and 1. We use the following technique to linearize model **[DR]** [50].

Let F_{ljt} be a new binary variable that is equal to $Y_{lj,t-1}Y_{ljt}$. Let $\overline{R}_{ljt}$ and $\hat{R}_{ljt}$ be two decision variables defined as follows:

$$\overline{R}_{ljt} = Y_{ljt}(1 - Y_{lj,t-1}) = Y_{ljt} - F_{ljt} \qquad \forall l \in \mathcal{L}^h, j \in \mathcal{J}, t \in \mathcal{T} \qquad (4.14)$$

$$\hat{R}_{ljt} = Y_{lj,t-1}(1 - Y_{ljt}) = Y_{lj,t-1} - F_{ljt} \qquad \forall l \in \mathcal{L}^h, j \in \mathcal{J}, t \in \mathcal{T} \qquad (4.15)$$

By simplifying constraints (4.14) and (4.15) we obtain the following:

$$Y_{lj,t-1} + \overline{R}_{ljt} = Y_{ljt} + \hat{R}_{ljt} \qquad \forall l \in \mathcal{L}^h, j \in \mathcal{J}, t \in \mathcal{T} \qquad (4.16)$$

$$\overline{R}_{ljt}, \hat{R}_{ljt} \in \{0, 1\} \qquad \forall l \in \mathcal{L}^h, j \in \mathcal{J}, t \in \mathcal{T} \qquad (4.17)$$

Since constraints (4.16) can be viewed as a network flow problem, for a given $j \in \mathcal{J}$ and $l \in \mathcal{L}$, the polytope $\{(Y_{ljt}, \overline{R}_{ljt}, \hat{R}_{ljt}) \in [0,1]^{3|T|} : Y_{lj,t-1} + \overline{R}_{ljt} = Y_{ljt} + \hat{R}_{ljt}, \forall t \in \mathcal{T}\}$ will have the integrality property. Therefore, the resulting mechanism will provide a tight linear programming formulation for model **[DR]**. The new linear formulation of model **[DR]** is denoted by **[LDR]** and it is presented below:

$$\begin{aligned}
\textbf{[LDR]}\ Minimize \quad & \sum_{l\in\mathcal{L}^b, k\in\mathcal{K}} \Psi_{lk} Y_{lk} + \sum_{t\in\mathcal{T}} \Bigg[\sum_{l\in\mathcal{L}^h, j\in\mathcal{J}} \left(\Psi_{ljt} \overline{R}_{ljt} - \eta_{ljt} \hat{R}_{ljt} \right) + \sum_{(i,j)\in\mathcal{A}^2} \xi_{ijt} Z_{ijt} \\
& + \sum_{i\in\mathcal{I}, j\in\mathcal{J}, k\in\mathcal{K}} c_{ijkt} \left((1-q_{jt})(1-q_{kt}) X_{ijkt} + \beta (q_{jt} + q_{kt} - q_{jt}q_{kt}) X_{ijkt} \right) \\
& + \sum_{(i,j)\in\mathcal{A}^3 \bigcup \mathcal{A}^4} c_{ijt} X_{ijt} + \sum_{l\in\mathcal{L}^b, k\in\mathcal{K}} p_{lkt} P_{lkt} + \sum_{k\in\mathcal{K}} h_{kt} H_{kt} + \sum_{g\in\mathcal{G}} \pi_{gt} U_{gt} \Bigg]
\end{aligned}$$

Subject to (4.1)-(4.13) and (4.16)-(4.17).

4.4 Solution Approaches

Problem **[LDR]** is $\mathcal{NP}$-hard since a special case of this problem is the capacitated facility location problem. Therefore, commercial solvers, such as CPLEX, cannot solve large-scale instances of this problem. In this section we propose the following approaches to solve **[LDR]**: a rolling horizon heuristic, a greedy rolling horizon heuristic, a Benders decomposition algorithm, and a Benders-based rolling horizon algorithm. The goal is to generate a near optimal solution for **[LDR]** in a reasonable amount of time.

4.4.1 A Rolling Horizon Heuristic

This algorithm is based on the rolling horizon scheme proposed by Balasubramanian and Grossman [72] and Kostina et al.[72]. The approach is suitable for large-scale prob-

lems where solving the overall problem exactly is computationally intractable. Based on this approach, the original problem is decomposed into a series of smaller subproblems. Each subproblem comprises a few consecutive periods during the planning horizon. These subproblems - which are of a smaller size - are solved sequentially. Figure 4.3 shows how we use the rolling horizon approach to solve a problem with three time periods.

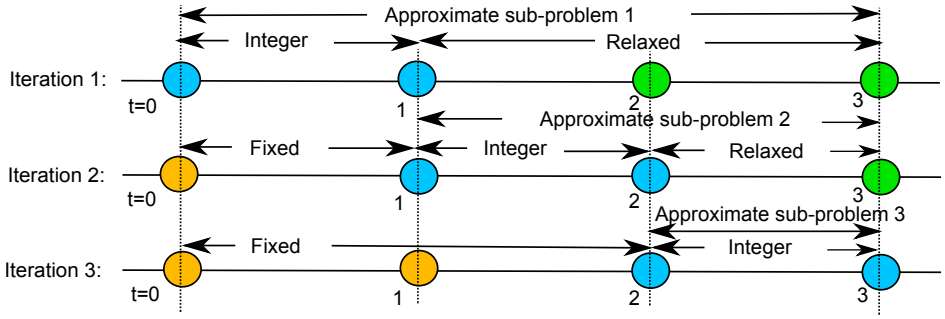

Figure 4.3

Application of a rolling horizon strategy for a three time period problem

Let t_0^s denote the starting time period of subproblem s. Let N^s denote the number of time periods comprised in subproblem s. Depending on the type of problem solved, N^s could be different or could be the same for all the subproblems created. The number of time periods within each subproblem stays fixed at N. We call *approximate subproblem* s the following approximation of problem **[LDR]**:

* Time horizon starts in period t_0^s and ends in period T.
* $Y_{ljt} \in \{0, 1\}$ and $Z_{jkt} \in Z^+$ for $t_0^s \leq t \leq t_0^s + N$.
* $0 \leq Y_{ljt} \leq 1$ and $Z_{jkt} \in R^+$ for $t > t_0^s + N$.
* The values of Y_{ljt} and Z_{jkt} for $t < t_0^s$ are fixed to the values found when solving approximate subproblem $s - 1$.

Let **[RH]** denote the rolling horizon algorithm described below. Let **[RH(s)]** denote the s-th approximate subproblem which is solved during the s-th iteration of the algorithm.

Step 1: Initialize; set starting time period to $t_0^s = 0$; set the length of time interval to N; set $s \leftarrow 1$.

Step 2: Solve the approximate sub-problem **[RH(s)]** using CPLEX.

Step 3: If $t_0 > |\mathcal{T}|$, then **Stop**; else, set $s \leftarrow s + 1$, go to **Step 2**.

4.4.2 A Greedy Rolling Horizon Heuristic

The most time-consuming step of the **[RH]** algorithm is solving the first approximate subproblem **[RH(1)]**, mainly because of its large size. Therefore, when solving **[RH(1)]** using CPLEX (Step 2 of **[RH]**), in order to optimize the running time of **[RH]**, the algorithm stops as soon as a feasible solution is found. Once subproblem **[RH(1)]** is solved, the corresponding integer variables are fixed. Typically, the remaining subproblems are easier to solve.

In order to tackle this challenge with **[RH]**, we adopt the following greedy approach, denoted by **[GRH]**. This approach solves the original problem **[LDR]** for $t = 1$ only. Next, the values of Y_{lj1} and Z_{jk1} are fixed, and the problem for the remaining time periods is solved by using **[RH]**. The steps of **[GRH]** are described below:

Step 1: Solve problem **[LDR]** for $t = 1$.

Step 2: Fix the Y_{lj1} and Z_{jk1} variables obtained from **Step 1**, and apply **[RH]** algorithm to solve the problem for the remaining time periods.

4.4.3 Benders Decomposition

The algorithm described in this section is an extension of Benders decomposition method proposed by Benders [9]. Benders decomposition is a well-known partitioning method used to solve mixed integer linear programs. The motivation for selecting this method is the structure of formulation **[LDR]**. The algorithm separates the original problem into two sub-problems: an integer *master problem* and a linear *subproblem*. The underlying Benders reformulation for **[LDR]** is the following:

$$Minimize \sum_{l\in\mathcal{L}^b,k\in\mathcal{K}} \Psi_{lk}Y_{lk} + \sum_{t\in\mathcal{T}}\{\sum_{l\in\mathcal{L}^h,j\in\mathcal{J}} \left(\Psi_{ljt}\overline{R}_{ljt} - \eta_{ljt}\hat{R}_{ljt}\right) + \sum_{(i,j)\in\mathcal{A}^2} \xi_{ijt}Z_{ijt}\}+$$

$$\textbf{[LDR-SUB]}(X,U,P,H|\hat{Y}^b,\hat{Y}^h,\hat{Z})$$

Subject to (4.1)-(4.13) and (4.16)-(4.17).

[LDR-SUB]$(X,U,P,H|\hat{Y}^b,\hat{Y}^h,\hat{Z})$ represents the Benders subproblem which is presented below. In this subproblem, the values of $Y^b := \{Y_{lk}|l \in \mathcal{L}^b, k \in \mathcal{K}\}$,$Y^h := \{Y_{ljt}|l \in \mathcal{L}^h, j \in \mathcal{J}, t \in \mathcal{T}\}$ and $Z := \{Z_{jkt}|j \in \mathcal{J}, k \in \mathcal{K}, t \in \mathcal{T}\}$ are given and satisfy constraints (4.10)-(4.13) and (4.16)-(4.17). Therefore, this subproblem has only continuous variables.

$$Min. \sum_{t\in\mathcal{T}}\{\sum_{i\in\mathcal{I},j\in\mathcal{J},k\in\mathcal{K}} c_{ijkt}\left((1-q_{jt})(1-q_{kt})X_{ijkt} + \beta(q_{jt}+q_{kt}-q_{jt}q_{kt})X_{ijkt}\right)$$

$$+ \sum_{(i,j)\in\mathcal{A}^3\bigcup\mathcal{A}^4} c_{ijt}X_{ijt} + \sum_{l\in\mathcal{L}^b,k\in\mathcal{K}} p_{lkt}P_{lkt} + \sum_{k\in\mathcal{K}} h_{kt}H_{kt} + \sum_{g\in\mathcal{G}} \pi_{gt}U_{gt}\}$$

Subject to

$$\sum_{k\in\mathcal{K}} X_{ikt} + \sum_{j\in\mathcal{J},k\in\mathcal{K}} X_{ijkt} \leq s_{it} \qquad \forall i \in \mathcal{I}, t \in \mathcal{T} \qquad (4.18)$$

$$\phi\left[\sum_{i\in\mathcal{I}} X_{ikt} + \sum_{(i,j)\in\mathcal{A}^1} X_{ijkt} + H_{k,t-1} - H_{kt}\right] = \sum_{l\in\mathcal{L}^b} P_{lkt} \qquad \forall k \in \mathcal{K}, t \in \mathcal{T} \qquad (4.19)$$

$$\sum_{g\in\mathcal{G}} X_{kgt} \leq \sum_{l\in\mathcal{L}} P_{lkt} \qquad \forall k \in \mathcal{K}, t \in \mathcal{T} \qquad (4.20)$$

$$\sum_{k\in\mathcal{K}} X_{kgt} + U_{gt} = b_{gt} \qquad \forall g \in \mathcal{G}, t \in \mathcal{T} \qquad (4.21)$$

$$\sum_{i\in\mathcal{I},k\in\mathcal{K}} X_{ijkt} \leq \sum_{l\in\mathcal{L}^h} c_{lj}^{cap}\hat{Y}_{ljt} \qquad \forall j \in \mathcal{J}, t \in \mathcal{T} \qquad (4.22)$$

$$\sum_{i\in\mathcal{I}} X_{ijkt} \leq v^{cap}\hat{Z}_{jkt} \qquad \forall (j,k) \in \mathcal{A}^2, t \in \mathcal{T} \qquad (4.23)$$

$$P_{lkt} \leq p_{lk}^{cap}\hat{Y}_{lk} \qquad \forall l \in \mathcal{L}^b, k \in \mathcal{K}, t \in \mathcal{T} \qquad (4.24)$$

$$H_{kt} \leq \sum_{l\in\mathcal{L}^b} h_{lk}^{cap}\hat{Y}_{lk} \qquad \forall k \in \mathcal{K}, t \in \mathcal{T} \qquad (4.25)$$

$$X_{ijkt}, X_{ikt}, X_{kgt}, P_{lkt}, H_{kt}, U_{gt} \geq 0 \qquad \forall i \in \mathcal{I}, j \in \mathcal{J}, k \in \mathcal{K}, g \in \mathcal{G}, t \in \mathcal{T} \qquad (4.26)$$

Note that, due to the presence of variables U_{gt} in constraints (4.21), formulation **[LDR]** will always generate a feasible solution which satisfies demand. This is because the model formulation allows substitute products - which are assumed to be available in the market - to satisfy demand if the supply chain cannot.

Let $\delta = \{\delta_{it} \geq 0 \mid i \in \mathcal{I}, t \in \mathcal{T}\}$, $\vartheta = \{\vartheta_{kt} \mid k \in \mathcal{K}, t \in \mathcal{T}\}$, $\Phi = \{\Phi_{kt} \geq 0 \mid k \in \mathcal{K}, t \in \mathcal{T}\}$, $\gamma = \{\gamma_{gt} \mid g \in \mathcal{G}, t \in \mathcal{T}\}$, $\chi = \{\chi_{jt} \geq 0 \mid j \in \mathcal{J}, t \in \mathcal{T}\}$, $\mu = \{\mu_{jkt} \geq 0 \mid j \in \mathcal{J}, k \in \mathcal{K}, t \in \mathcal{T}\}$, $\kappa = \{\kappa_{lkt} \geq 0 \mid l \in \mathcal{L}, k \in \mathcal{K}, t \in \mathcal{T}\}$ and $\varsigma = \{\varsigma_{kt} \geq 0 \mid k \in \mathcal{K}, t \in \mathcal{T}\}$ be the dual variables associated with constraints

(4.18)-(4.25), respectively. The dual of the primal subproblem, called the *dual subproblem* **[LRD-SUB(D)]**, can be written as:

$$\textbf{[LDR-SUB(D)]} Max. \sum_{t\in\mathcal{T}}\{\sum_{g\in\mathcal{G}} b_{gt}\gamma_{gt} - \sum_{i\in\mathcal{I}} s_{it}\delta_{it} - \sum_{l\in\mathcal{L}^h, j\in\mathcal{J}} c_{lj}^{cap}\hat{Y}_{ljt}\chi_{jt} -$$
$$\sum_{(i,j)\in\mathcal{A}^2} v^{cap}\hat{Z}_{ijt}\mu_{ijt} - \sum_{l\in\mathcal{L}^b, k\in\mathcal{K}} p_{lk}^{cap}\hat{Y}_{lk}\kappa_{lkt} - \sum_{l\in\mathcal{L}^b, k\in\mathcal{K}} h_{lk}^{cap}\hat{Y}_{lk}\varsigma_{kt}\}$$

Subject to

$$-\delta_{it} - \chi_{jt} - \mu_{jkt} + \phi\vartheta_{kt} \leq c_{ijkt}\left((1-q_{jt})(1-q_{kt}) + \beta(q_{jt}+q_{kt}-q_{jt}q_{kt})\right)$$
$$\forall i\in\mathcal{I}, j\in\mathcal{J}, k\in\mathcal{K}, t\in\mathcal{T} \quad (4.27)$$

$$-\delta_{it} + \phi\vartheta_{kt} \leq c_{ikt} \quad \forall (i,k)\in\mathcal{A}^3, t\in\mathcal{T} \quad (4.28)$$

$$\gamma_{gt} - \Phi_{kt} \leq c_{kgt} \quad \forall (k,g)\in\mathcal{A}^4, t\in\mathcal{T} \quad (4.29)$$

$$-\vartheta_{kt} + \Phi_{kt} - \kappa_{lkt} \leq p_{lkt} \quad \forall l\in\mathcal{L}^h, k\in\mathcal{K}, t\in\mathcal{T} \quad (4.30)$$

$$\phi\vartheta_{k,t+1} - \phi\vartheta_{kt} - \varsigma_{kt} \leq h_{kt} \quad \forall k\in\mathcal{K}, t\in\mathcal{T} \quad (4.31)$$

$$\gamma_{gt} \leq \pi_{gt} \quad \forall g\in\mathcal{G}, t\in\mathcal{T} \quad (4.32)$$

$$\delta, \chi, \mu, \Phi, \kappa, \varsigma \in \mathbb{R}^+ \quad (4.33)$$

$$\gamma, \vartheta \in \mathbb{R} \quad (4.34)$$

Let θ represent the objective function value of the sub-problem. Then, Benders *master problem* is represented as follows **[LDR-M]**:

$$Min. \sum_{l\in\mathcal{L}^b, k\in\mathcal{K}} \Psi_{lk}Y_{lk} + \sum_{t\in\mathcal{T}}\{\sum_{l\in\mathcal{L}^h, j\in\mathcal{J}}\left(\Psi_{ljt}\overline{R}_{ljt} - \eta_{ljt}\hat{R}_{ljt}\right) + \sum_{(i,j)\in\mathcal{A}^2}\xi_{ijt}Z_{ijt}\} + \theta$$

Subject to

$$\theta + \sum_{t\in\mathcal{T}}\{\sum_{i\in\mathcal{I}} s_{it}\delta_{it} + \sum_{l\in\mathcal{L}^h, j\in\mathcal{J}} c_{lj}^{cap}\chi_{jt}Y_{ljt}\} \geq \sum_{t\in\mathcal{T}}\{\sum_{g\in\mathcal{G}} b_{gt}\gamma_{gt} - \sum_{(i,j)\in\mathcal{A}^2} v^{cap}\mu_{ijt}Z_{ijt} - \sum_{l\in\mathcal{L}^b,k\in\mathcal{K}} p_{lk}^{cap}\kappa_{lkt}Y_{lk} - \sum_{l\in\mathcal{L}^b,k\in\mathcal{K}} h_{lk}^{cap}\varsigma_{kt}Y_{lk}\}$$
$$\forall(\gamma,\delta,\chi,\mu,\kappa,\varsigma)\in\mathcal{P}_D \quad (4.35)$$

$$Y_{lj,t-1} + \overline{R}_{ljt} = Y_{ljt} + \hat{R}_{ljt} \quad \forall l\in\mathcal{L}^h, j\in\mathcal{J}, t\in\mathcal{T} \quad (4.36)$$

$$\sum_{l\in\mathcal{L}^b} Y_{lk} \leq 1 \quad \forall k\in\mathcal{K} \quad (4.37)$$

$$Y_{lk} \in \{0,1\} \quad \forall l\in\mathcal{L}^b, k\in\mathcal{K} \quad (4.38)$$

$$Y_{ljt} \in \{0,1\} \quad \forall l\in\mathcal{L}^h, j\in\mathcal{J}, t\in\mathcal{T} \quad (4.39)$$

$$\overline{R}_{ljt}, \hat{R}_{ljt} \in \{0,1\} \quad \forall l\in\mathcal{L}^h, j\in\mathcal{J}, t\in\mathcal{T} \quad (4.40)$$

$$Z_{jkt} \in Z^+ \quad \forall j\in\mathcal{J}, k\in\mathcal{K}, t\in\mathcal{T} \quad (4.41)$$

In this formulation, constraints (4.35) are the *optimality cut* constraints, and $\mathcal{P}_D$ is the set of the extreme points of the feasible region of **[LDR-SUB(D)]**. Since θ is the optimal objective function value of **[LDR-SUB]**, its value is an upper bound to the objective function value of the solution from **[LDR-SUB(D)]** for fixed values of $\hat{Y}^b, \hat{Y}^h, \hat{Z}$. Therefore,

$$\theta \geq \sum_{t\in\mathcal{T}}\{\sum_{g\in\mathcal{G}} b_{gt}\gamma_{gt} - \sum_{i\in\mathcal{I}} s_{it}\delta_{it} - \sum_{l\in\mathcal{L}^h, j\in\mathcal{J}} c_{lj}^{cap}\chi_{jt}Y_{ljt} - \sum_{(i,j)\in\mathcal{A}^2} v^{cap}\mu_{ijt}Z_{ijt} - \sum_{l\in\mathcal{L}^b,k\in\mathcal{K}} p_{lk}^{cap}\kappa_{lkt}Y_{lk} - \sum_{l\in\mathcal{L}^b,k\in\mathcal{K}} h_{lk}^{cap}\varsigma_{kt}Y_{lkt}\} \quad \forall(\gamma,\delta,\chi,\mu,\kappa,\varsigma)\in\mathcal{P}_D \quad (4.42)$$

In order to accelerate the running time of the master problem, we add the following inequalities.

$$Z_{jkt} \leq \sum_{l \in \mathcal{L}^h} \lceil \frac{c_{lj}^{cap}}{v^{cap}} \rceil Y_{ljt} \qquad \forall (j,k) \in \mathcal{A}^2, t \in \mathcal{T} \tag{4.43}$$

$$Z_{jkt} \leq \sum_{l \in \mathcal{L}^b} \lceil \frac{c_{lk}^{cap}}{v^{cap}} \rceil Y_{lk} \qquad \forall (j,k) \in \mathcal{A}^2, t \in \mathcal{T} \tag{4.44}$$

Inequalities (4.43) and (4.44) are valid for **[LDR-M]** since they present the relationship that exists between the binary facility location variables and the integer, container flow variables. The ratio $\lceil \frac{c_{lj}^{cap}}{v^{cap}} \rceil$ represents the maximum number of containers initiated from hub j to deliver the available biomass. This amount is an upper bound on the total biomass delivered to biofuel plant k. The ratio $\lceil \frac{c_{lk}^{cap}}{v^{cap}} \rceil$ represents the maximum number of containers to be received at biofuel plant k in order to fully utilize its capacity. That number is clearly an upper bound on the total number of containers received from hub j. Additionally, these inequalities set the number of containers to zero if no facility is located in some of the potential facility location sites. Computational experiments indicate that these valid inequalities significantly reduce the number of iterations of the Benders algorithm.

The master problem **[LDR-M]** provides an equivalent formulation of the original problem **[LDR]**. The challenge faced when solving **[LDR-M]** is the problem size. Note that the number of inequalities (4.35) is equal to the number of extreme points of the feasible region of problem **[LDR-SUB(D)]**. This number could be very large. For this reason, we solve instead a *restricted master problem* **[LDR-RM]** that uses instead only a subset of $\mathcal{P}_D$ denoted by $\mathcal{P}_D^n \subset \mathcal{P}_D$. Therefore, problem **[LDR-RM]** is a relaxation of **[LDR]**, and the optimal solution to the restricted problem provides a lower bound for **[LDR]**.

The general idea of the standard Benders decomposition algorithm is to iteratively solve **[LDR-RM]**. In iteration n, subproblem **[LDR-SUB(D)]** is solved, and a new extreme point $p \in \mathcal{P}_D$ is identified and added to $\mathcal{P}_D^n = \mathcal{P}_D^{n-1} \bigcup p$. Next, the restricted master problem is solved. This procedure continue until the gap between the lower bound generated by solving the restricted master problem, and the upper bound generated by solving the subproblem is smaller than some predetermined value ϵ.

Let UB^n and LB^n denote the upper and the lower bound of **[LDR]** at iteration n. Let $\mathcal{P}_D^n$ denote the set of extreme points of **[LDR-SUB(D)]** at iteration n. The algorithm starts by solving **[LDR-RM]**, which provides a lower bound for this problem. We fix the values of the corresponding integer and binary variables to $\hat{Y}_{lk}^n$ for $l \in \mathcal{L}^b, k \in \mathcal{K}$, $\hat{Y}_{ljt}^n$ for $l \in \mathcal{L}^h, j \in \mathcal{J}, t \in \mathcal{T}$, and $\hat{Z}_{jkt}^n$ for $(j,k) \in \mathcal{A}_2, t \in \mathcal{T}$. We use these values to solve the dual subproblem **[LDR-SUB(D)]**. A pseudo-code of the basic Benders decomposition algorithm is provided below.

Let $z_{MAS}^n = \sum_{l \in \mathcal{L}^b, k \in \mathcal{K}} \Psi_{lk} Y_{lk}^n + \sum_{t \in \mathcal{T}} \{ \sum_{l \in \mathcal{L}_h, j \in \mathcal{J}} \left(\Psi_{ljt} \overline{R}_{ljt}^n - \eta_{ljt} \hat{R}_{ljt}^n \right) + \sum_{(i,j) \in \mathcal{A}^2} \xi_{ijt} Z_{ijt}^n \}$; let z_{MP}^n denote the solution to **[LDR-RM]** and z_{SUB}^n denote the solution to **[LDR-SUB(D)]** during the n-th iteration of the Benders decomposition algorithm.

4.4.4 Enhancements of Bender Decomposition Algorithm

In this section we present a few different cuts that we have identified and used to improve the performance of Benders decomposition algorithm.

4.4.4.1 Pareto-Optimal Cuts

Magnanti and Wong [79] introduce the *Pareto-optimal cuts*, which are added to the master problem. The motivation is to identify from a set of potential cuts which cut has the greatest impact on the quality of the master problem. Work by Van Roy [109], and Wentges [150] show that Pareto-optimal cuts contribute to improving the performance of Benders algorithm by strengthening the cut added to the master problem in each iteration of the algorithm.

With respect to our problem, recall that an optimality cut (4.35) for **[LDR-RM]** is generated using the information from an optimal solution to **[LDR-SUB(D)]**. Subproblem **[LDR-SUB(D)]** is a transportation problem, which are known to have multiple optimal solutions [143]. This inherent degeneracy property of transportation problems implies that multiple optimality cuts can be generated in an iteration of Benders algorithm, therefore, identifying the single cut that greatly impacts the quality of the solution to **[LDR-RM]** is critical. This study adopts an approach proposed by Papadakos [98] for implementing subproblem independent Pareto-optimal cuts. Papadakos [98] shows that when the solution of the auxiliary problem depends on the solution to the dual Benders subproblem, then generating a Pareto-optimal cut is computationally challenging. This challenge is greater especially when the Benders subproblem is a difficult problem to solve. To remedy this problem, Papadakos [98] proposes the *Modified Magnanti-Wong (MMW)* method that generates a Pareto-optimal cut using the concept of core points. A core point is located in the relative interior of the convex hull of feasible region and serves as a proxy for the optimal solution.

The following is the formulation of the *Modified Magnanti-Wong (MMW)* subproblem solved in each iteration of Benders algorithm instead of **[LDR-SUB(D)]**. We refer to this subproblem as **[LDR-SUB(MMW)]**. Let $\mathbb{Y}^{LP}$ be the polyhedron defined by (4.36), (4.37), $0 \leq Y_{ljt} \leq 1, \forall l \in \mathcal{L}, j \in \mathcal{J}, t \in \mathcal{T}$; $0 \leq Y_{lk} \leq 1, \forall l \in \mathcal{L}, k \in \mathcal{K}$; and $Z_{jkt} \geq 0 \; \forall j \in \mathcal{J}, k \in \mathcal{K}, t \in \mathcal{T}$. Let $ri(\mathbb{Y}^{LP})$ denote the relative interior of $\mathbb{Y}^{LP}$. A Pareto-optimal cut can be obtained by solving the following subproblem, for $Y^0_{ljt} \in ri(\mathbb{Y}^{LP}), \forall l \in \mathcal{L}^h, j \in \mathcal{J}, t \in \mathcal{T}$; and $Y^0_{lk} \in ri(\mathbb{Y}^{LP}), \forall l \in \mathcal{L}^b, k \in \mathcal{K}$.

[LDR-SUB(MMW)] $Max.$ $\sum_{t\in\mathcal{T}}\{\sum_{g\in\mathcal{G}} b_{gt}\gamma_{gt} - \sum_{i\in\mathcal{I}} s_{it}\delta_{it} - \sum_{l\in\mathcal{L},j\in\mathcal{J}} c^{cap}_{lj} Y^0_{ljt}\chi_{jt} -$

$$\sum_{(i,j)\in\mathcal{A}_2} v^{cap} Z^0_{ijt}\mu_{ijt} - \sum_{l\in\mathcal{L},k\in\mathcal{K}} p^{cap}_{lk} Y^0_{lk}\kappa_{lkt} - \sum_{l\in\mathcal{K},k\in\mathcal{K}} h^{cap}_{lk} Y^0_{lk}\varsigma_{kt}\}$$

Subject to

$$-\delta_{it} - \chi_{jt} - \mu_{jkt} + \phi\vartheta_{kt} \leq c_{ijkt}\left((1-q_{jt})(1-q_{kt}) + \beta(q_{jt}+q_{kt}-q_{jt}q_{kt})\right)$$

$$\forall i \in \mathcal{I}, j \in \mathcal{J}, k \in \mathcal{K}, t \in \mathcal{T} \quad (4.45)$$

$$-\delta_{it} + \phi\vartheta_{kt} \leq c_{ikt} \quad \forall (i,k) \in \mathcal{A}^3, t \in \mathcal{T} \quad (4.46)$$

$$\gamma_{gt} - \Phi_{kt} \leq c_{kgt} \quad \forall (k,g) \in \mathcal{A}^4, t \in \mathcal{T} \quad (4.47)$$

$$-\vartheta_{kt} + \Phi_{kt} - \kappa_{lkt} \leq p_{lkt} \quad \forall l \in \mathcal{L}^h, k \in \mathcal{K}, t \in \mathcal{T} \quad (4.48)$$

$$\phi\vartheta_{k,t+1} - \phi\vartheta_{kt} - \varsigma_{kt} \leq h_{kt} \quad \forall k \in \mathcal{K}, t \in \mathcal{T} \quad (4.49)$$

$$\gamma_{gt} \leq \pi_{gt} \quad \forall g \in \mathcal{G}, t \in \mathcal{T} \quad (4.50)$$

$$\delta, \chi, \mu, \Phi, \kappa, \varsigma \in \mathbb{R}^+ \quad (4.51)$$

$$\gamma, \vartheta \in \mathbb{R} \quad (4.52)$$

In this formulation, Y^0_{ljt}, Y^0_{lk}, and Z^0_{jkt} are core points. These points are updated as follows:

$$Y^0_{ljt} = \tau Y^0_{ljt} + (1-\tau)\overline{Y}_{ljt}, \qquad \forall\ l \in \mathcal{L}^h, j \in \mathcal{J}, t \in \mathcal{T}$$

$$Y^0_{lk} = \tau Y^0_{lk} + (1-\tau)\overline{Y}_{lk}, \qquad \forall\ l \in \mathcal{L}^b, k \in \mathcal{K}$$

$$Z^0_{jkt} = \tau Z^0_{jkt} + (1-\tau)\overline{Z}_{jkt}, \qquad \forall\ j \in \mathcal{J}, k \in \mathcal{K}, t \in \mathcal{T}$$

$\overline{Y}_{ljt}$, $\overline{Y}_{lk}$, and $\overline{Z}_{jkt}$ are the solutions obtained from the current master problem. Experimental results indicate that setting $\tau = 0.5$ provides the best empirical results. Note that, the auxiliary subproblem **[LDR-SUB(MMW)]** is independent of the solutions obtained from the original dual subproblem (**[LDR-SUB(D)]**) and will assist the Benders master problem to be one step closer to the optimal solution from the very first iteration [98].

4.4.4.2 Knapsack Inequalities

Santoso et al. [111] show that when a good upper bound is available from the Benders decomposition algorithm, then adding a knapsack inequality - presented below - along with the optimality cut constraint (4.35) will improve the quality of solutions derived from the Benders master problem. The authors also point out that state-of-the-art solvers such as CPLEX can derive a variety of valid inequalities from the knapsack inequality, which expedites the convergence of the Benders decomposition algorithm. Let UB^n be the best known upper bound obtained so far. The following valid inequality is added to the master problem **[LDR-RM]** in iteration $n+1$:

$$UB^n \geq \sum_{t\in\mathcal{T}}\{\sum_{l\in\mathcal{L}^h,j\in\mathcal{J}}\left(\Psi_{ljt}\overline{R}_{ljt}-\eta_{ljt}\hat{R}_{ljt}\right)+\sum_{l\in\mathcal{L}^b,k\in\mathcal{K}}\left(\Psi_{lkt}-p_{lk}^{cap}\kappa_{lkt}-h_{lk}^{cap}\varsigma_{kt}\right)Y_{lk}+$$
$$\sum_{(i,j)\in\mathcal{A}_2}\left(\xi_{ijt}-v^{cap}\mu_{ijt}\right)Z_{ijt}+\sum_{g\in\mathcal{G}}b_{gt}\gamma_{gt}-\sum_{i\in\mathcal{I}}s_{it}\delta_{it}-\sum_{l\in\mathcal{L},j\in\mathcal{J}}c_{lj}^{cap}Y_{ljt}\chi_{jt}\} \tag{4.53}$$

Similarly, we add the following valid inequalities to the master problem **[LDR-RM]** to speed up the branch-and-bound procedure of the solver. LB^n denotes the best known lower bound obtained so far.

$$LB^n \leq \sum_{l\in\mathcal{L}^b,k\in\mathcal{K}}\Psi_{lk}Y_{lk}+\sum_{t\in\mathcal{T}}\{\sum_{l\in\mathcal{L}^h,j\in\mathcal{J}}\left(\Psi_{ljt}\overline{R}_{ljt}-\eta_{ljt}\hat{R}_{ljt}\right)+\sum_{(i,j)\in\mathcal{A}_2}\xi_{ijt}Z_{ijt}\}+\theta \tag{4.54}$$

4.4.4.3 Logistics Constraints

In the initial stages of the Benders decomposition algorithm, the master problem produces very few first-stage decision variables. This is the case until sufficient information is gathered from solving the subproblem. In order to overcome this issue with the master problem, we add the following logistics constraints. The rationale is to bring to the master problem some information from the subproblem. Doing this will improve the running time of the Benders decomposition algorithm.

Recall the demand satisfying constraints described in equation (4.4). Since this is a minimization problem, these constraints can be expressed as follows:

$$\sum_{k\in\mathcal{K}}X_{kgt}+U_{gt} \geq b_{gt} \qquad \forall g\in\mathcal{G},t\in\mathcal{T} \tag{4.55}$$

Furthermore, constraints (4.3) and (4.7) can be rewritten as follows:

$$\sum_{g \in \mathcal{G}} X_{kgt} \leq \sum_{l \in \mathcal{L}^b} p_{lk}^{cap} Y_{lk} \qquad \forall k \in \mathcal{K}, t \in \mathcal{T} \tag{4.56}$$

Combining constraints (4.55) and (4.56) and dropping the penalty term U_{gt} obtains the following inequalities that are added to the master problem:

$$\sum_{l \in \mathcal{L}^b, k \in \mathcal{K}} p_{lk}^{cap} Y_{lk} \geq \sum_{g \in \mathcal{G}} \bar{b}_{gt} \qquad \forall t \in \mathcal{T} \tag{4.57}$$

Here $\bar{b}_{gt}$ represents the amount of biofuel demand expected to be met through the supply chain network. Thus, $\bar{b}_{gt} = \alpha * b_{gt}, \forall g \in \mathcal{G}, t \in \mathcal{T}$. We can initialize the value of α between 0.0 to 1.0; and when $\alpha = 1.0$, constraints (4.57) require that all the demand is satisfied by this supply chain.

4.4.4.4 Integer Cuts

To expedite the running time of the master problem we add the following inequalities generated using a local branching technique [46]. These inequalities when added to the master problem during iteration $n+1$, force the problem to generate a solution different from the solution generated during iteration n. In other words, adding these cuts to the mater problem excludes from the feasible region the solutions identified in the previous iteration. Let $\hat{Y}_{ljt}^n$ for $l \in \mathcal{L}^h, j \in \mathcal{J}, t \in \mathcal{T}$ and $\hat{Y}_{lk}^n$ for $l \in \mathcal{L}^b, k \in \mathcal{K}$ be the solutions obtained from solving the master problem in iteration n. Let $\mathcal{Y}_1^n = \{(l,j,t) | \hat{Y}_{ljt}^n = 1, \forall l \in$

$\mathcal{L}^h, j \in \mathcal{J}, t \in \mathcal{T}\}$ and $\mathcal{Y}_2^n = \{(l,k)|\hat{Y}_{lk}^n = 1, \forall l \in \mathcal{L}^b, k \in \mathcal{K}\}$. We add the following constraint to the master problem in iteration $n+1$:

$$\sum_{(l,j,t)\in\mathcal{Y}_1^n}(1-Y_{ljt}) + \sum_{(l,k)\in\mathcal{Y}_2^n}(1-Y_{lk}) + \sum_{(l,j,t)\notin\mathcal{Y}_1^n} Y_{ljt} + \sum_{(l,k)\notin\mathcal{Y}_2^n} Y_{lk} \geq 1 \quad (4.58)$$

This inequality forces the values of the binary facility location variables in iteration $n+1$ to be different from iteration n. The two consecutive solutions will differ by at least one variable.

Similarly, in order to reduce the search space and the number of iterations of the Benders decomposition algorithm, we add to the master problem the following superset and subset cuts. These cuts help reduce the solution space of the master problem by limiting the number of feasible network configurations. Consequently, adding these constraints reduces the search space for the binary variables [67].

$$\sum_{(l,j,t)\in\mathcal{Y}_1^n} Y_{ljt} + Y_{ljt} \leq |\ \mathcal{Y}_1^n\ | \qquad \forall l \in \mathcal{L}^h, j \in \mathcal{J}, t \in \mathcal{T} \quad (4.59)$$

$$\sum_{(l,j,t)\notin\mathcal{Y}_1^n} Y_{ljt} + Y_{ljt} \geq 1 \qquad \forall l \in \mathcal{L}^h, j \in \mathcal{J}, t \in \mathcal{T} \quad (4.60)$$

4.4.4.5 Heuristics Improvement

Obtaining Good Solutions before Convergence: The master problem is a mixed integer linear program. This problem is difficult to solve; thus, obtaining an optimal solution for moderate sized networks is a challenging problem. The solutions obtained from solving the master problem in the initial iterations of the Benders algorithm are of low quality. This is mainly because initially, the master problem has not received much information about the subproblem. The quality of the solutions found improves as the algorithm progresses.

Therefore, in order to reduce the running time of the algorithm, one can stop solving the master problem as soon as a feasible solution is found in the initial iterations of the Benders algorithm. As the algorithm progresses, we search for better solutions to the master problem.

In order to implement this, we initially set a large optimality gap when solving the master problem. This gap is gradually reduced as the algorithm progresses. The initial optimality gap is 5% and is reduced gradually to 1%.

Setting Branching Priorities: In order to accelerate the solution of the master problem, we set proper branching priorities for the decision variables of Z_{jkt}, Y_{lk} and Y_{ljt}. Setting branching priorities provides CPLEX with the order in which the solver branches these variables. Numerical analysis indicates that branching on Z_{jkt} variables first followed by Y_{lk} and Y_{ljt} saves some computational time when solving the master problem.

4.4.5 A Hybrid Benders based Rolling Horizon Algorithm

This approach combines the rolling horizon and accelerated Benders decomposition algorithms. The Benders decomposition algorithm is used to solve the subproblems created during the implementation of the rolling horizon algorithm.

When problems with sufficiently large sized networks are solved using **[RH]**, solving the first few subproblems created using CPLEX is difficult. However, as soon as the first few subproblems are solved, then the remaining subproblems can easily be solved by CPLEX. For this reason, when implementing the **[RH]** algorithm, we solve the first few subproblems using an accelerated Benders decomposition algorithm, and solve the remain-

ing subproblems using CPLEX. The overall procedure, named **[BRH]** is described below:

Step 1: Initialize; set starting time period to $t_0^s = 0$; set the length of time interval to N; set $s \leftarrow 1$.

Step 2: Solve the approximate sub-problem **[RH(s)]** using Accelerated Benders decomposition algorithm.

Step 3: If $t_0 > |\mathcal{T}|$, then **Stop**; else, set $s \leftarrow s + 1$, go to **Step 2**.

4.5 Computational Study and Managerial Insights

This section summarizes and interprets the results from the numerical study. The goal of this section is to test the performance of the algorithms proposed and drawing important managerial insights about the supply chain. The case study is developed using data from the Southeast region of the USA.

4.5.1 Data Description

Biomass Supply: We have collected data about biomass availability from the following nine States: Mississippi, Alabama, Louisiana, Tennessee, Arkansas, Georgia, Florida, South Carolina and North Carolina. The two main biomass feedstocks in this region are corn stover and forest residues. The biomass availability data is provided by the Knowledge Discovery Framework (KDF) database of United States Department of Energy [11]. This data was further processed by Idaho National Lab (INL) to identify the amount of densified biomass available in this region. Altogether, 491 counties contributed to the col-

lected data. The total amount of densified biomass available in the region is 29.35 million tons (MT) per year.

Biofuel Demand: The total fuel consumption in 2012 for the nine states listed above is 44.4 BGY [138]. Based on the amount of biomass available in the region and considering a conversion rate of 72.6 gallons per MT, the total biofuel production in this region could be as high as 2.1 BGY. This amount corresponds to about 5% of the total fuel consumption in 2012. We consider this to be the total demand for cellulosic biofuel in the region. Recall that based on the proposed model, substitute products can be used to meet demand. The model allows this substitution to happen if the cost of producing biofuel exceeds the market price for substitute products. Therefore, setting the demand level high will not force the system to meet demand at any cost.

Counties with a population greater than 30,000 are considered as demand points in this study. Based on this criteria, we selected a total of 381 counties from the region. We assume that the distribution of the population in a particular region is a good indicator of the distribution of demand for biofuel. We use the centroid of the county as the point where demand occurs, and thus, where biofuel is to be delivered. In a year, the demand for gasoline typically rises in May and continues until September [137], so the seasonality of demand in the biofuel demand data is incorporated in these formulations.

Investment Costs: We consider a total of 259 potential hub locations: 242 are rail ramps and 17 are inland/sea ports. Figure 4.4 presents the exact potential locations of these hubs and biorefineries. We consider a total of 44 potential biofuel plant locations. The annualized fixed cost for plants with a capacity 45 million gallon per year (MGY) is

set to $159.4 million [154]. This cost was estimated based on a project life of 20 years and an interest rate of 15%. We consider five different plant sizes: 20 MGY, 40 MGY, 60 MGY, 100 MGY, and 150 MGY. Wallace et al. [145] estimates that doubling the size of the plant increases the investment cost by a factor of 1.6. We used this factor to calculate investment costs for the other biofuel plant sizes considered. The annualized fixed cost for a rail ramp of capacity 1.05 million ton per year (MTY) is equal to $54,949/year [80]. We consider five different rail ramp capacities, where $l = 0.6$ MTY, 0.8 MTY, 0.9 MTY, 1.05 MTY, and 1.20 MTY. These costs are estimated based on a lifetime of 30 years and a discount factor of 10%. The annualized fixed cost for an inland port of capacity 2.35 MTY is equal to $306,000/year which is derived from a study of Searcy et. al. [114]. We consider five different port capacities, where $l = 1.0$ MTY, 1.5 MTY, 1.75 MTY, 2.00 MTY, and 2.25 MTY. Although the actual fixed cost would vary by location, a common fixed cost is used as a reasonable approximation.

Transportation Costs: This study assumes that trucks are used to transport biomass from farms to intermodal hubs and biofuel plants. Trucks are also used to deliver biofuel to the market. Major cost components for truck transportation are obtained from a study by Parker et al. [99], and these costs are summarized in Table 4.5.

Barge or rail can be used to deliver biomass at an intermodal hub. The unit transportation cost for barge shipments is estimated to be $0.017/mile/ton [52]. This cost is calculated assuming that a single tow boat pushes up to 15 barges, and each barge carries 1,500 tons of biomass.

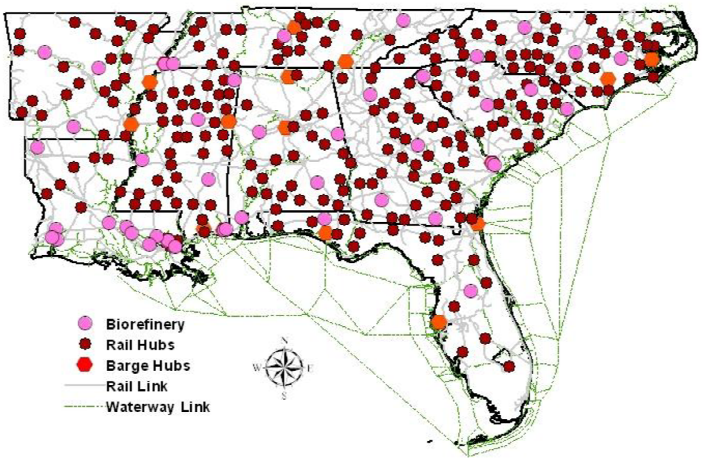

Figure 4.4

Hub locations

Transportation costs by rail using CSXT and Burlington Northern Santa Fe (BNSF) Corporations are calculated using the following equations developed by Gonzales et al. [52]. These equations represent the total transportation cost for a single rail car of capacity 100 tons. This cost is a function of the distance traveled (x_1).

$$Y_{CSXT} = 2,248 + 1.12x_1 \qquad R^2_{adj}(\%) = 29.0; p - Value(\%) = 2E^{-22} \quad (4.61)$$

$$Y_{BNSF} = 3,140 + 0.75x_1 \qquad R^2_{adj}(\%) = 50.0; p - Value(\%) = 0.01 \quad (4.62)$$

The values \$2,248 and \$3,140 represent the fixed shipment cost per rail car, ξ_{jk}. The values \$1.12 and \$0.75 represent the unit transportation cost per mile. We multiply these costs with the travel distance between $j \in \mathcal{J}$ and $k \in \mathcal{J}$ to calculate c_{jk}.

We assume that a shipment is delivered from its source to its destination using the shortest path. Arc GIS Desktop 10 is used to create a transportation network, and then, this

network identifies the shortest paths. The network includes existing railways; waterways; local, rural, urban roads; and major highways in Southeast.

Estimating Disruption Probabilities: Failure probabilities at intermodal hubs are obtained from a study by Marufuzzaman et al. [84]. In developing these estimates, the authors consider the three major types of disasters that affect the Southeast: hurricanes, floods and droughts. Based on National Hurricane Center data, the hurricane season starts late August and ends in late September [92]. Historically, the largest number of hurricanes were observed during the month of September. The U.S. Drought Monitor Center provides historical data and weekly forecasts about the nationwide drought severity [135]. The data for the period 2009 to 2013 indicates that the drought season starts in August and continues to January. The severity of droughts is greatest in September and October. We incorporated this information in the data set by assigning higher disruptions probabilities during these months compared to other months of the season.

4.5.2 Experimental Results

We now discuss the results of our computational study. All the algorithms are coded in GAMS 24.2.1 [48] and executed on a desktop computer with Intel Core i7 3.50 GHz processor and 32.0 GB RAM. The optimization solver used is ILOG CPLEX 12.6.

4.5.2.1 Analyzing the impact of disruptions on the supply chain performance

The goal of these numerical experiments is to evaluate the impact that disruptions have on the performance of the supply chain. In order to demonstrate the benefits of using the model proposed in this research, we compare its performance with the following two

models: (a) minimum cost model, and (b) reliable and static model. We refer to **[LDR]** as the reliable and dynamic model. The reliable and static model is a special case of **[LDR]** which considers that once an intermodal hub opens, it will continue to be available for use. Therefore, the fixed intermodal hub cost is paid from the period the facility is open, and thereafter. The minimum cost model does not consider disruptions; the model considers that hubs will be dynamically used throughout the year.

Figure 4.5 presents the amount of biomass and biofuel produced, transported, and inventoried during each month of the planning horizon. This figure also presents the number of hubs operating each month and the number of containers shipped. This information is essential to supporting strategic decisions and to guiding the planning of manpower and equipment during the year.

In the numerical experimentation, time $t = 1$ corresponds to the month of July. Corn stover is typically harvested from September until November, which corresponds to periods $t = 3$ to 5. Forest residues are harvested all year round except during the winter months of December to February (t = 6, 7, 8) due to the heavy rains which make harvesting/collection challenging. To support the delivery of biomass to biofuel plants from September to November, additional hubs and containers are used. During this period, the amount shipped by trucks via highways also increases. The increase of truck transportation also occurs because weather conditions during the months of September and October correspond with the Southeast's hurricane season. This pick biomass production results in increased biofuel production and accumulation of biofuel inventory during periods 5 and 6 (November and December). Biomass transportation equals zero during the winter

months. To satisfy demand for biofuels during these months, the inventories built up during September to November are depleted.

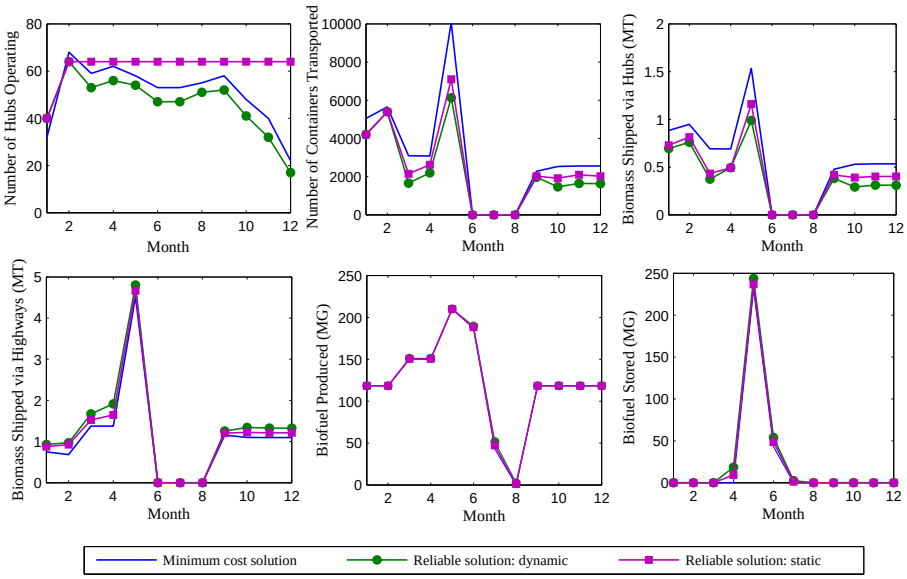

Figure 4.5

Impact of disruption on system performance

The three models compared above result from the same amount of biofuel produced and inventoried. The major difference between these models is the number of hubs operating. Almost the same number of hubs is open under each model in periods 1 and 2; however, the reliable and static model does not close these hubs during the months of low supply or during the hurricane season. Therefore, the annual costs related to hub operation are higher for the reliable and static model. This is one of the reasons why the unit delivery cost for such a system is so high -$4.05 per gallon - compared to the $3.86 and $3.96 per gallon provided by the other two models (see Table 4.6). The minimum cost solution uses more

hubs compared to reliable and dynamic solution because rail and barge transportation are more cost efficient than truck transportation. The reliable solution delivers less by barge during the hurricane season. The static and dynamic reliable solutions open three more biorefineries than the minimum cost solution. Building redundancies into the supply chain in order to hedge against disruptions is a common practice.

To quantify the benefits of designing reliable and dynamic supply chain systems, three different disruption scenarios are created. Table 4.6 summarizes the unit delivery cost of biofuel under each scenario. The first scenario assumes flooding of the Mississippi River. The second assumes flooding of the Tombigbee River, and the third scenario assumes a hurricane making landfall in North Carolina. The results indicate that in normal conditions, the minimum cost solution provides the minimum delivery cost for this supply chain. The minimum cost model provides a solution which is 2.59% cheaper than the reliable and dynamic model and 4.92% cheaper than the reliable and static model. However, under disaster scenarios, the reliable and dynamic supply chain model outperforms both the minimum cost and reliable and static models. The minimum cost model is 2.65% to 9.20% more expensive than the reliable and static model and 6.28% to 17.73% more expensive than the reliable and dynamic model.

Figure 4.6 presents the impacts of disruptions on the supply chain network. Note that the number of facilities located in Zone 3 (high supply and high risk Zone) changes from one model to the next. The three models open a biofuel plant in this Zone to take advantage of the available biomass in the area. The minimum cost model relies heavily in using intermodal transportation to deliver the excess biomass to other plants. The reliable models

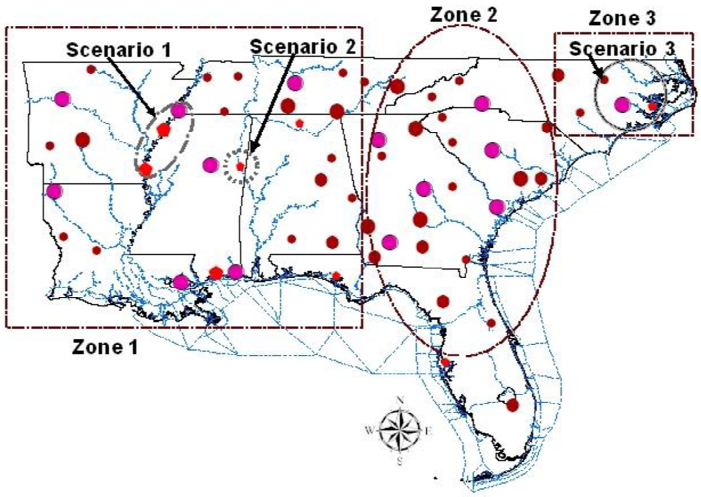

Figure 4.6

Impacts of disruption scenarios on network configuration

open a smaller capacity port to deliver biomass and, in general, use fewer intermodal hubs. Fewer hubs are used for the dynamic than the static model.

4.5.2.2 Analyzing the impact of the biomass supply chain on highway transportation

One of the challenges that the biofuel industry faces is delivering biomass to biofuel plants. Due to the high volume and low energy density of biomass, the volume of biomass required at a biofuel plant is large. Truck transportation - although more expensive as compared to other transportation modes - has been used extensively due to its availability and flexibility. Additionally, as the numerical analysis indicates, reliable supply chains use highways as a means of hedging against the risk of disruptions from natural disasters. Therefore, we think it important to evaluate the increased shipment volumes in highways due to biomass transportation. Figure 4.7 summarizes some of the numerical results.

The results presented compare the minimum cost model with the reliable and dynamic model, as well as reliable and static model, as the amount of biomass available for delivery changes. The base for these comparisons uses the minimum cost solution to determine the amount of biomass to be shipped along highways.

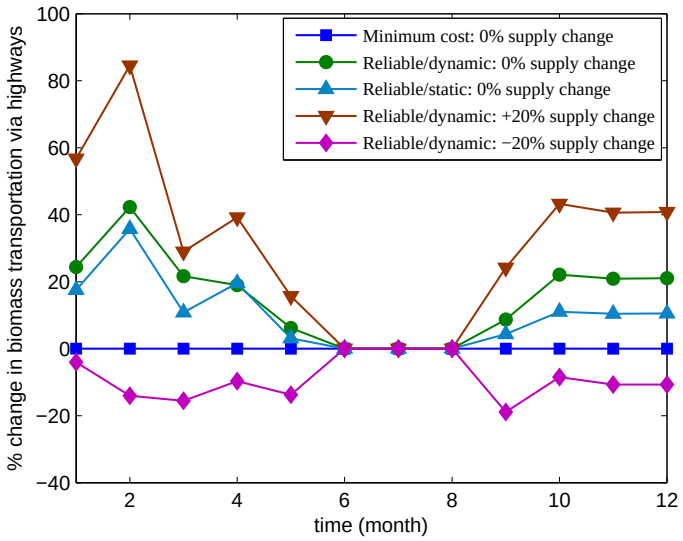

Figure 4.7

Biomass transported via highways

The results indicate that more biomass is shipped on highways under the reliable solutions than the minimum cost solutions; more biomass is shipped under the dynamic rather than static solutions. The amount shipped increases with the amount of biomass available. To deliver biomass available using minimum cost solution, on average, a total of 1,329 truck deliveries (trips) are required daily. Each truck on average travels 258 miles daily. This number increases to 1,543 truck deliveries daily for the reliable and dynamic model.

Then, each truck on average travels 287 miles daily. This number further increases to 1,763 truck deliveries daily when biomass supply increases by 20% and the average number of miles traveled per truck is 304. The increase of truck transportation impacts the traffic on highways. Traffic congestion increases the noise around the communities where biofuel plants are located and impacts highway safety.

4.5.3 Analyzing the Performance of Solution Algorithms

This section presents our computational experience in solving the **[LDR]** model using the algorithms proposed in Section 4.4. We initially assess the performance of different accelerated techniques compared to the standard Benders decomposition algorithm (Table 4.7). Next, the performance of the rolling horizon algorithm assessed and compared with CPLEX (Table 4.8). Finally, we compare the performance of all the algorithms proposed with CPLEX (Table 4.9). The algorithms presented are terminated when at least one of the following conditions is met: (a) the optimality gap falls below a threshold value $\epsilon = 0.01$. The optimality gap is calculated as $\epsilon = \mid UB - LB \mid /UB$; or (b) the maximum time limit $t_{max} = 36,000$ (in CPU seconds) is reached. In order to terminate the Benders decomposition algorithm we use an additional criterion: the maximum number of iteration $n = 1,000$ is reached. The columns of the tables presented in this section provide the optimality gap (ϵ), the running time of the algorithm (t_{max}) and the corresponding number of iterations (n). The best result is identified for each problem solved and is presented using boldface. Since a stopping criteria for the algorithm is $\epsilon \leq 1\%$, the algorithms are stopped when such a solution is found within the maximum time limit. The algorithm

which gave the smallest running time is then highlighted. Otherwise, if such a quality solution is not found within the maximum time limit or number of iterations, the algorithm with the smallest optimality gap is highlighted.

Table 4.7 summarizes the results from enhancements of Benders decomposition algorithm. These enhancements are due to implementing the cuts described in Section 4.4.4. All the algorithms presented in this table are further enhanced through the improvement techniques presented in Section 4.4.4.5. The total number of potential hubs for all the problems presented in this table is 100. We do not present results from implementing the standard Benders decomposition algorithm, since when using this algorithm to solve the problems presented here, the solutions found within 1,000 iterations had an optimality gap of at least 20%. The results indicate that implementing the cuts presented in section 4.4.4 substantially improves the performance of the Benders algorithm. The results from *All cuts* Benders decomposition algorithm - which in addition to Pareto optimal, knapsack, and logistics cuts uses the integer cuts - indicate a running time improved 1.68 times compared to the accelerated Benders decomposition algorithm without these integer cuts. Results indicate that incorporating the integer cuts significantly reduces the average number of iterations required by the accelerated Benders decomposition algorithm compared to implementations of the accelerated Benders decomposition algorithm without the integer cuts.

Table 4.8 compares the computational results of solving the **[LDR]** model using the rolling horizon algorithm and CPLEX. The number of potential hubs and time periods differ from one problem to another. The performance of the algorithm is investigated as

the values of these two problem parameters change because they greatly impact problem size, and consequently, the running time of the algorithm. Each subproblem created during the implementation of the rolling horizon algorithm is solved using CPLEX. We experiment with the stopping criteria used to stop CPLEX when solving these subproblems. We investigate the performance of the **[RH]** algorithm when the optimality gap used for subproblems equals 1% and 2%. Increasing the gap from 1% to 2% reduces the overall running time of the **[LDR]** algorithm. Another criterion used to stop CPLEX is a maximum running time of 10,800 CPU seconds.

Results indicate that the benefits of the **[RH]** algorithm over CPLEX are evident as the problem size increases, either due to increasing the number of potential hubs or the number of time periods considered in this problem. Our experience with **[RH]** algorithm indicates that solving the first subproblem is difficult, and therefore time consuming. Stopping CPLEX when ϵ =1% or 2% - while it helped some - did not have a great impact on reducing the time it took to solve this subproblem. Because the first subproblem is challenging, CPLEX fails to solve it as the number of potential hubs increases. Note the results for $\mid \mathcal{H} \mid = 140$, $\mid \mathcal{T} \mid = 10$ and 12 in Table 4.8. Once the first subproblem is solved, the rest can be solved quickly.

Table 4.9 presents the results from solving the **[LDR]** model using the algorithms proposed in this paper. The problems solved differ by the number of potential hub locations considered, the length of planning horizon, and thus, the problem size. We do not present results for problems with $\mid \mathcal{H} \mid < 100$. For those problems, CPLEX provided the best results and outperformed the algorithms presented here. The benefits of using the algo-

rithms we develop becomes evident as the problem size increases, which is the case when $| \mathcal{H} | \geq 100$.

Results indicate that, in 33 out of 36 problem instances solved, the Accelerated Benders decomposition algorithm provides solutions with an optimality gap less than 1.0% within the specified time limit. The benefits of using the greedy **[RH]** and the hybrid Benders based **[RH]** algorithms can clearly be seen as the problem size increases. Both algorithms are able to find high quality solutions within relatively small computational time. The overall average optimality gap for the greedy **[RH]** algorithm is 1.82%, with only 1 out of 36 problem instances exceeding 5.0% gap. The overall average optimality gap for the hybrid Benders based **[RH]** algorithm is 1.41%. The largest three problem instances presented in Table 4.9 show a noticeable improvements of both algorithms in terms of solution quality and running time as compared to other solution approaches. Overall, both the greedy **[RH]** and the hybrid Benders based **[RH]** algorithms seem to offer high quality solutions consistently within the experimental range.

4.6 Conclusion

This chapter presents an MIP model which helps supply chain managers to design cost-efficient and reliable supply chain networks for biomass delivery to biofuel plants, and biofuel delivery to markets. The proposed inbound supply chain of biofuel plants has a hub-and-spoke structure. Hub-and-spoke networks are typically used for high-volume, long-haul transportation of bulk products. Such a network design facilitates the transportation of biomass in a cost-efficient manner. This system relies on using in-land ports, sea

ports, and rail stations for the delivery of biomass by rail and barge between intermodal hubs. Activities at ports could be disrupted by natural disasters, such as floods, hurricanes, and droughts. Therefore, considering the risks associated with these disruptions when designing biofuel supply chains makes sense.

The model we propose captures supply chain uncertainties due to natural disruptions and biomass seasonality since these factors impact the performance of biofuel supply chain. To handle these uncertainties efficiently, the model proposes to adjust short-term and mid-term supply chain decisions dynamically under disaster scenarios. Numerical results indicate that such an approach results in cost savings in the supply chain.

The MIP model proposed is an extension of the capacitated facility location problem, and therefore, it is an *NP*-hard problem. In order to solve this problem, we propose the following solution approaches: a rolling horizon algorithm; a greedy rolling horizon algorithm; an accelerated Benders decomposition algorithm; and a hybrid Benders-based rolling horizon algorithm. We test the performance of these algorithms in a case study we build using data from the Southeast USA. Numerical results indicate that the Accelerated Benders and the hybrid algorithms outperform the rest. While the Accelerated Benders provides solutions of high quality, the hybrid algorithm provides good quality solutions in a reasonable amount of time. For very large problem instances, the hybrid algorithm outperforms the Accelerated Benders decomposition algorithm. For these large problem instances CPLEX runs out of memory, and the rolling horizon algorithm fails to find an integer-feasible solution within the time limit.

We conducted extensive numerical analyses in order to provide insights about the advantages of using the model proposed to optimize the performance of the supply chain. We compare our model to a minimum cost model, with the goal of minimizing total costs, to with a reliable but static model, with the goal minimizing expected costs under normal and disruption scenarios. Under normal conditions, the minimum cost model outperforms the rest. However, under disaster scenarios, the reliable and dynamic supply chain model proposed in this paper outperforms the minimum cost and reliable and static models. The minimum cost model is 2.65% to 9.20% more expensive than the reliable and static model and 6.28% to 17.73% more expensive than the reliable and dynamic model.

Table 4.4

Algorithm: Benders decomposition

$UB^n \leftarrow +\infty$, $LB^n \leftarrow -\infty$, $n \leftarrow 1$, ϵ, $\mathcal{P}_D \leftarrow 0$
terminate $\leftarrow$ **false**
while (*terminate* = **false**) **do**
  Solve **[LDR-RM]** to obtain $\{Y^n_{lk}\}_{l\in\mathcal{L}^b,k\in\mathcal{K}}$, $\{Y^n_{ljt}\}_{l\in\mathcal{L}^h,j\in\mathcal{J},t\in\mathcal{T}}$, $\{Z^n_{ijt}\}_{(i,j)\in\mathcal{A}^2,t\in\mathcal{T}}$, z^n_{MP}, z^n_{MAS}
  if ($z^n_{MP} > LB^n$) **then**
    $LB^n \leftarrow z^n_{MP}$
  end if
  Set:
    $\hat{Y}^n_{lk} = Y^n_{lk}$ for $l \in \mathcal{L}^b, k \in \mathcal{K}$
    $\hat{Y}^n_{ljt} = Y^n_{ljt}$ for $l \in \mathcal{L}^h, j \in \mathcal{J}, t \in \mathcal{T}$
    $\hat{Z}^n_{jkt} = Z^n_{jkt}$ for $(j,k) \in \mathcal{A}^2, t \in \mathcal{T}$
  Solve **[LDR-SUB(D)]** to obtain $(\gamma_{gt}, \delta_{it}, \chi_{gt}, \mu_{jkt}, \kappa_{lkt}, \varsigma_{kt}) \in \mathcal{P}_D$ and z^n_{SUB}
  if ($z^n_{SUB} + z^n_{MAS} < UB^n$) **then**
    $UB^n \leftarrow z^n_{SUB} + z^n_{MAS}$
  end if
  if ($(UB^n - LB^n)/UB^n \leq \epsilon$) **then**
    terminate $\leftarrow$ **true**
  else
    $\mathcal{P}^{n+1}_D = \mathcal{P}^n_D \cup \{(\gamma_{gt}, \delta_{it}, \chi_{gt}, \mu_{jkt}, \kappa_{lkt}, \varsigma_{kt})\}$
  end if
  $n \leftarrow n + 1$
end while

Table 4.5

Data about truck transportation

	Feedstock		Biofuel	
Item	Value	Unit	Value	Unit
Loading/unloading	5.0	$/wet ton	0.02	$/gallon
Time dependent	29.0	$/hr/truckload	32.0	$/hr/truckload
Distance dependent	1.20	$/mile/truckload	1.3	$/mile/truckload
Truck capacity	25	wet tons/truckload	8,000	gallons/truckload
Average travel speed	40	miles/hour	40	miles/hour

Table 4.6

Comparison of unit cost under different disrupted scenarios

Scenarios	Min. Cost ($/gallon)	Reliable & Static Hubs ($/gallon)	Reliable & Dynamic ($/gallon)
1: Flooding of Mississippi River	4.91	4.78	4.48
2: Flooding of Tombigbee River	4.62	4.49	4.33
3: Hurricane in North Carolina	5.98	5.43	4.92
No disruption	3.86	4.05	3.96

Table 4.7

Results of the enhancement of Benders decomposition algorithm

$\mid \mathcal{T} \mid$	q_j^t	Benders+PO			Benders+PO+KI			Benders+PO+KI+LC			All cuts		
		ϵ	t_{max}	n	ϵ	t_{max}	n	ϵ	t_{max}	n	ϵ	t_{max}	n
4	0.0	0.81	383.6	28	0.81	348.7	25	0.92	335.1	24	0.75	**73.2**	6
	0.1	0.77	322.8	24	0.94	301.4	22	0.77	287.1	21	0.76	**73.7**	6
	0.2	0.74	266.9	20	0.68	244.6	18	0.85	273.7	20	0.76	**73.8**	6
5	0.0	0.95	513.4	29	0.92	470.3	26	0.97	429.4	24	0.91	**90.7**	6
	0.1	0.52	461.1	26	0.91	451.5	26	0.78	431.5	24	0.92	**91.5**	6
	0.2	0.94	297.6	18	0.95	342.7	20	0.85	344.5	20	0.91	**91.8**	6
6	0.0	0.91	704.7	34	0.97	566.4	26	0.82	565.2	26	0.05	**104.5**	5
	0.1	0.77	532.5	26	0.87	524.8	24	0.91	487.2	23	0.62	**105.9**	5
	0.2	0.61	394.1	21	0.94	385.9	18	0.98	364.2	17	0.52	**106.1**	5
7	0.0	0.97	731.4	30	0.74	740.7	29	0.29	723.1	28	0.92	**169.2**	7
	0.1	0.91	688.2	26	0.89	711.8	28	0.48	687.5	26	0.89	**170.2**	7
	0.2	0.99	486.2	20	0.84	614.1	27	0.38	520.4	20	0.87	**169.9**	7
8	0.0	0.78	816.6	29	0.60	894.9	30	0.89	916.5	31	0.27	**204.1**	8
	0.1	0.87	998.1	37	0.88	989.4	35	0.91	929.1	32	0.21	**223.0**	8
	0.2	0.99	701.4	25	0.78	616.0	21	0.77	523.0	18	0.22	**226.6**	8
9	0.0	0.97	1,085.5	34	0.36	1,118.2	33	0.97	1,073.1	30	0.91	**219.1**	7
	0.1	0.94	1,178.4	37	0.89	1,194.1	35	0.91	1,101.4	31	0.93	**222.4**	7
	0.2	0.87	761.5	24	0.78	724.8	22	0.79	660.7	20	0.89	**228.0**	7
10	0.0	0.98	1,400.4	39	0.99	1,400.6	38	0.94	1,164.7	31	0.84	**320.1**	9
	0.1	0.96	1,480.6	37	0.94	1,311.8	34	0.97	1,308.1	35	0.78	**321.8**	9
	0.2	0.97	1,105.8	31	0.86	882.0	24	0.91	779.2	21	0.92	**324.8**	9
11	0.0	0.97	2,337.6	56	0.97	2,340.1	51	0.96	1,837.6	39	0.98	**727.1**	18
	0.1	0.94	1,752.8	38	0.94	1,344.5	32	0.94	1,322.3	31	0.94	**743.2**	18
	0.2	0.89	1,218.4	32	0.97	1,175.1	29	0.96	1,167.4	28	0.97	**717.7**	16
12	0.0	0.97	2,427.9	56	0.95	2,354.0	49	0.98	2,527.6	54	0.95	**1,216.9**	26
	0.1	0.98	1,778.8	39	0.97	1,545.9	33	0.87	1,524.1	33	0.89	**1,028.6**	23
	0.2	0.97	1,268.8	29	0.96	1,180.3	27	0.95	1,368.1	29	0.94	**756.2**	16
Avg.		0.89	966.5	31.3	0.86	917.6	29.0	0.84	876.0	27.3	0.76	**325.9**	9.7

Table 4.8

Summary of results from implementing the RH algorithm and CPLEX

$\mid \mathcal{H} \mid$	$\mid \mathcal{T} \mid$	q_j^t	CPLEX		RH-1.0%		RH-2.0%	
			ϵ	t_{max}	ϵ	t_{max}	ϵ	t_{max}
100	10	0.0	**0.99**	686.5	1.17	190.8	1.30	120.8
		0.1	**0.99**	454.4	1.04	256.4	1.41	143.1
	12	0.0	**0.99**	1,626.2	1.17	480.8	1.45	249.0
		0.1	0.95	1,865.7	0.91	**658.6**	1.44	288.7
120	10	0.0	0.75	9,648.8	0.30	**1,477.6**	1.59	722.2
		0.1	0.21	10,110.4	0.29	**1,913.3**	1.23	889.5
	12	0.0	0.72	11,748.1	0.91	**3,161.6**	1.71	1,121.5
		0.1	0.82	12,723.7	0.86	**4,123.2**	1.62	1,485.5
140	10	0.0	5.65	36,000.0	**2.08***	10,847.8	2.18	1,247.8
		0.1	5.15	36,000.0	**2.09***	11,623.3	2.12	2,023.3
	12	0.0	12.69	36,000.0	**3.04***	12,427.3	**3.04***	12,427.3
		0.1	12.86	36,000.0	**3.29***	12,716.8	**3.29***	12,716.8
		Average	3.56	16,072.0	**1.43**	4,989.8	1.86	2,786.3

*Unable to solve the first subproblem within the specified optimality gap within 10,800 CPU seconds

Table 4.9

Comparison of different solution approaches

$\mid \mathcal{H} \mid$	$\mid \mathcal{T} \mid$	q_j^t	CPLEX		RH-algorithm		Greedy RH		Accelerated Benders			RH-Benders	
			ϵ	t_{max}	ϵ	t_{max}	ϵ	t_{max}	ϵ	t_{max}	n	ϵ	t_{max}
100	4	0.0	0.72	64.8	0.72	47.9	0.77	**30.8**	0.75	73.2	6	0.88	106.7
		0.1	0.51	120.7	1.01	107.8	1.17	40.9	0.76	**73.7**	6	0.58	109.1
		0.2	0.46	127.4	1.60	119.9	1.14	37.2	0.76	**73.8**	6	0.81	120.1
	8	0.0	0.66	**109.8**	1.22	96.6	1.14	90.2	0.27	204.1	8	1.05	174.0
		0.1	0.75	195.9	0.97	**166.6**	1.17	104.7	0.21	223.0	8	0.92	169.1
		0.2	0.74	195.8	1.18	223.3	1.15	95.8	0.22	226.6	8	0.92	**173.1**
	12	0.0	0.99	1,626.2	1.17	480.8	1.26	299.2	0.95	**1,216.9**	26	1.10	449.6
		0.1	0.95	1,865.7	0.91	**658.6**	1.34	219.1	0.89	1,028.6	23	1.07	423.8
		0.2	0.98	1,368.1	1.09	547.7	1.65	236.5	0.94	756.2	16	0.61	**406.1**
150	4	0.0	5.40	36,000	0.52	1015.6	0.66	**378.3**	0.91	559.5	8	0.55	442.2
		0.1	5.30	36,000	1.12	2066.1	1.17	712.2	0.94	**563.8**	8	1.22	747.5
		0.2	4.98	36,000	1.55	2436.2	1.41	615.8	0.93	**561.3**	8	0.82	698.7
	8	0.0	7.47	36,000	2.59	11,203	0.61	1,091.1	0.97	2,393.4	14	0.74	**1,017.2**
		0.1	4.16	36,000	2.39	7,234.5	1.31	1,798.5	0.88	**2,428.3**	15	1.12	1,121.2
		0.2	4.58	36,000	1.53	6,940.0	1.69	2,308.5	0.79	**2,210.2**	13	1.67	1,160.3
	12	0.0	16.70	36,000	3.35	12,830	0.55	2,830.9	0.87	9,758.8	37	0.85	**2,814.5**
		0.1	17.02	36,000	3.13	12,210	0.55	**2,449.8**	0.96	9,112.5	36	1.18	2,842.1
		0.2	15.70	36,000	5.97	11,035	0.63	**2,367.4**	0.86	9,142.6	36	1.22	2,902.8
200	4	0.0	6.74	36,000	2.19	1,862.0	2.23	726.2	0.39	**799.0**	6	1.10	1132.6
		0.1	6.82	36,000	2.35	3,247.6	2.22	1,125.8	0.76	**822.1**	6	1.65	1215.6
		0.2	9.09	36,000	2.23	3,349.4	1.99	1,014.9	0.49	**963.8**	7	1.70	1255.5
	8	0.0	10.67	36,000	3.48	12,733	2.89	1,974.3	0.97	**2,640.3**	9	1.83	1805.3
		0.1	10.75	36,000	3.02	8,477.9	2.75	2,122.5	0.84	**2,998.6**	10	2.04	1600.2
		0.2	10.39	36,000	4.60	8,847.6	2.69	2,899.4	0.69	**2627.8**	9	1.72	1578.8
	12	0.0	19.89	36,000	5.51	13,581	5.03	4,294.4	0.11	**14,357**	27	2.57	4693.0
		0.1	17.57	36,000	5.67	13,612	4.49	4,688.7	0.23	**14,412**	27	2.00	4585.5
		0.2	13.96	36,000	5.19	13,771	3.92	4,442.9	0.49	**14,222**	27	1.99	4492.2
259	4	0.0	11.75	36,000	1.75	12,094	1.10	3,531.1	0.94	**10,413**	23	2.00	3,780.3
		0.1	15.04	36,000	2.37	12,174	1.65	3,811.5	0.89	**11,254**	24	1.85	3,752.1
		0.2	13.04	36,000	2.53	12,221	1.63	4,289.4	0.84	**11,294**	24	1.58	3,698.5
	8	0.0	12.39	36,000	2.33	15,121	0.97	**7,214.5**	0.86	30,180	28	1.75	6,592.6
		0.1	15.80	36,000	3.13	15,249	2.22	7,415.8	0.97	**28,322**	27	1.91	6,789.4
		0.2	13.89	36,000	4.59	15,987	2.66	7,445.9	0.94	**28,111**	27	2.12	6,994.2
	12	0.0	mem^a	mem	$n.a.^b$	$n.a.$	1.58	15,988	17.22	36,000	18	0.99	**14,155**
		0.1	mem	mem	$n.a.$	$n.a.$	2.37	16,289	14.61	36,000	19	**1.95**	14,478
		0.2	mem	mem	$n.a.$	$n.a.$	3.82	16,672	13.89	36,000	19	**2.75**	14,214
		Avg.	8.36	26,354	2.51	7,025.8	1.82	3,379.3	1.94	8,945.2	17	**1.41**	**3,130.4**

[a] runs out of memory

[b] unable to find an integer feasible solution within the time limit

REFERENCES

[1] Advameg Inc., ," Available from: http://www.city-data.com/, 2013.

[2] S. Ahmed, M. Tawarmalani, and N. V. Sahinidis, "A finite branch-and-bound algorithm for two-stage stochastic integer programs.," *Mathematical Programming*, vol. 100, 2004, pp. 355–377.

[3] H. An, W. E. Wilhelm, and S. W. Searcy, "A mathematical model to design a lignocellulosic biofuel supply chain system with a case study based on a region in central Texas," *Bioresource Technology*, vol. 102, 2011, pp. 7860–7870.

[4] Y. An, Y. Zhang, and B. Zeng, "The reliable hub-and-spoe design problem: Models and algorithms.," *Available from:* `http://www.optimization-online.org/DB_HTML/2011/05/3043.html`, 2011.

[5] I. Awudu and J. Zhang, "Uncertainty and sustainability concepts in biofuel supply chain management: A review.," *Renewable and Sustainable Energy Reviews*, vol. 16, 2012, pp. 1359–1368.

[6] T. Aykin, "Networking policies for hub-and-spoke with applications to the air transportation system.," *Transportation Science*, vol. 29, no. 3, 1995, pp. 201–221.

[7] Y. Bai, T. Hwang, S. Kang, and Y. Ouyang, "Biofuel refinery location and supply chain planning under traffic congestion.," *Transportation Research Part B: Methodological*, vol. 45, no. 1, 2011, pp. 162–175.

[8] J. Bauer, T. Bektas, and T. G. Crainic, "Minimizing greenhouse gas emissions in intermodal freight transport: an application to rail service design.," *Journal of the Operational Research Society*, vol. 61, no. 3, 2010, pp. 531–542.

[9] J. F. Benders, "Partitioning procedures for solving mixed-variables programming problems.," *Numerische Mathematik*, vol. 4, 1962, pp. 238–252.

[10] S. Benjaafar, Y. Li, and M. Daskin, "Carbon footprint and the management of supply chains: Insights from simple models," $doi : 10.1109/TASE.2012.2203304$, 2010.

[11] Bioenergy Knowledge Discovery Framework (KDF), "Available from: https://bioenergykdf.net/taxonomy/term/1036,", 2013.

[12] J. R. Birge and F. V. Louveaux, "A multicut algorithm for two-stage stochastic linear programs.," *European Journal of Operational Research*, vol. 34, no. 3, 1988, pp. 384–392.

[13] J. R. Birge and F. V. Louveaux, *Introduction to stochastic programming.*, Springer, New York, 1997.

[14] M. Bonney and M. Y. Jaber, "Environmentally responsible inventory models: Non-classical models for a non-classical era.," *International Journal of Production Economics*, vol. 133, 2011, pp. 43–53.

[15] M. J. Brennan, R. D. Knabb, M. Mainelli, and T. B. Kimberlain, "Atlantic Hurricane Season of 2007.," *Monthly Weather Review*, vol. 137, 2009, pp. 4061–4088.

[16] M. Brower, "Woody biomass Economics.," Available from: http://www.mosaicllc.com/documents/34.pdf, 2010.

[17] D. Burtraw, K. Palmer, and D. Kahn, "A symmetric safety valve," *Energy Policy*, vol. 38, no. 9, 2010, pp. 4921–4932.

[18] R. S. Camargo, J. G. Miranda, R. Ferreira, and H. P. Luna, "Multiple allocation hub and spoke network design under hub congestion.," *Computers & Operations Research*, vol. 36, no. 12, 2009, pp. 3097–3106.

[19] J. F. Campbell, "Locating transportation terminals to serve an expanding demand.," *Transportation Research Part B*, vol. 3, 1990, pp. 173–192.

[20] C. C. Caroe and R. Schultz, "Dual decomposition in stochastic integer programming.," *Operations Research Letters*, vol. 24, 1999, pp. 37–45.

[21] C. C. Caroe and J. Tind, "L-shaped decomposition of two-stage stochastic programs with integer recourse.," *Mathematical Programming*, vol. 83, 1998, pp. 451–464.

[22] C.-W. Chen and Y. Fan, "Bioethanol supply chain system planning under supply and demand uncertainities," *Transportation Research Part E*, vol. 48, 2012, pp. 150–164.

[23] S. Cholette and K. Venkat, "The energy and carbon intensity of wine distribution: a study of logistical options for delivering wine to customers.," *Journal of Cleaner Production*, vol. 17, no. 16, 2009, pp. 1401–1413.

[24] I. Contreras, J. Cordeau, and G. Laporte, "The dynamic uncapacitated hub location problem.," *Transportation Science*, vol. 45, no. 1, 2011, pp. 18–32.

[25] I. Contreras, J. F. Cordeau, and G. Laporte, "Benders Decomposition for Large-Scale Uncapacitated Hub Location.," *Operations Research*, vol. 59, no. 6, 2011, pp. 1477–1490.

[26] I. Contreras, J. A. Diaz, and E. Fernandez, "Branch and price for large scale capacited hub location problems with single assignment.," *INFORMS Journal of Computing*, vol. 23, no. 1, 2011, pp. 41–55.

[27] J. F. Cordeau, F. Pasin, and M. M. Solomon, "An integrated model for logistics network design.," *Annals of Operations Research*, vol. 144, no. 1, 2006, pp. 59–82.

[28] G. Cornuejols, G. L. Nemhauser, and L. A. Wolsey, *Discrete Location Theory*, chapter The uncapacitated facility location problem, John Wiley and Sons, New York, 1990, pp. 119–171.

[29] M. J. Credeur, "FedEx in Paris disrupted as workers walk out," Available from: http://www.bloomberg.com/news/2011-05-13/fedex-s-paris-hub-disrupted-as-union-workers-walk-off-job-1-.html, 2011.

[30] T. Cui, Y. Ouyang, and Z. M. Shen, "Reliable facility location under the risk of disruptions.," *Operations Research*, vol. 58, no. 4, 2010, pp. 998–1011.

[31] J. S. Cundiff, N. Dias, and H. D. Sherali, "A linear programming approach for designing a herbaceous biomass delivery system.," *Bioresource Technology*, vol. 59, 1997, pp. 47–55.

[32] M. S. Daskin, "Application of an expected covering model to emergency medical service system design.," *Decision Sciences*, vol. 13, no. 3, 1982, pp. 416–439.

[33] M. S. Daskin, "A maximum expected covering location model: formulation, properties and heuristic solution.," *Transportation Science*, vol. 17, no. 1, 1983, pp. 48–70.

[34] S. C. Davis, S. W. Diegel, and R. G. Boundy, "Transportation energy data book : Edition 30,", 2011, <http://cta.ornl.gov/data/tedb30/Edition30_Full_Doc.pdf>.

[35] R. S. de Camargo, J. G. Miranda, and H. P. Luna, "Benders decomposition for the uncapacited multiple allocation hub location problem.," *Computers & Operations Research*, vol. 35, 2008, p. 10471064.

[36] Z. Drezner, "Heuristic solution methods for two location problems with unreliable facilities.," *Journal of the Operational Research Society*, vol. 38, no. 6, 1987, pp. 509–514.

[37] S. Dufreche, R. Hernandez, and T. French, "Extraction of Lipids from Municipal Wastewater Plant Microorganisms for Production of Biodiesel," *Journal of American Oil Chemistry Society*, vol. 84, 2007, pp. 181–187.

[38] S. D. Ekşioğlu, A. Acharya, L. E. Leightley, and S. Arora, "Analyzind the design and management of biomass-to-biorefinery supply chain," *Computers & Industrial Engineering*, vol. 57, 2009, pp. 1342–1352.

[39] S. D. Eksioglu, S. Li, S. Zhang, S. Sokhansanj, and D. Petrolia, "Analyzing impact of intermodal facilities on design and management of biofuel supply chain.," *Transportation Research Record*, vol. 2191, 2010, pp. 144–151.

[40] S. D. Eksioglu, G. Palak, A. Mondala, and A. Greenwood, "Supply chain designs and management for biocrude production via wastewater treatment.," *Environmental Progress & Sustainable Energy*, 2011, doi: 10.1002ep.10605.

[41] S. D. Eksioglu, G. Palak, A. Mondala, and A. Greenwood, "Supply chain designs and management for biocrude production via wastewater treatment.," *Environmental Progress & Sustainable Energy*, vol. 32, no. 1, 2013, pp. 139–147.

[42] J. A. Elia, R. C. Baliban, X. Xiao, and C. A. Floudas, "Optimal energy supply network determination and life cycle analysis for hybrid coal, biomass, and natural gas to liquid (CBGTL) plants using carbon-based hydrogen production," *Computers & Chemical Engineering*, vol. 35, no. 8, 2011, pp. 1399–1430.

[43] L. F. Escudero, A. Garin, M. Merino, and G. Perez, "A general algorithm for solving two-stage stochastic mixed-integer programs.," *Computers and Operations Research*, vol. 36, 2009, pp. 2590–2600.

[44] EU ETS, "Emissions Trading System," Available from: $http : //ec.europa.eu/clima/policies/ets/index_en.htm$, 2009.

[45] Federal Highway Administration (FHWA)., "Corrosion costs and preventive strategies in the United States.," Available from: http://www.nace.org/uploadedFiles/Publications/ccsupp.pdf, 2002.

[46] M. Fischetti and A. Lodi, "Local branching.," *Mathematical Programming*, vol. 98, 2003, pp. 23–47.

[47] B. Gebreslassie, Y. Yao, and F. You, "Design under uncertainty of hydrocarbon biorefinery supply chains: Multiobjective stochastic programming models, decomposition algorithm, and a comparison between CVaR and downside risk.," *AIChE Journal*, vol. 58, no. 7, 2012, p. 21552179.

[48] General Algebraic Modeling System, "GAMS,", Available from: http://www.gams.com/, 2011.

[49] A. M. Geoffrion and G. W. Graves, "Multicommodity distributed system design by Benders decomposition.," *Management Science*, vol. 20, 1974, pp. 822–844.

[50] A. Ghaderi, N. Boland, and M. S. JabalAmeli, "Exact and heuristic approaches to the budget-constrained dynamic uncapacitated facility location-network design problem.," Available from: `http://www.optimization-online.org/DB-FILE/2012/02/3336.pdf`, 2012.

[51] S. Giarola, A. Zamboni, and F. Bezzo, "Spatially explicit multi-objective optimization for designing and planning of hybrid fast and second generation biorefineries," *Computers & Chemical Engineering*, vol. 35, 2011, pp. 1782–1797.

[52] D. Gonzales, E. M. Searcy, and S. D. Eksioglu, "Cost analysis for high-volume and long-haul transportation of densified biomass feedstock.," *Transportation Research Part A*, vol. 49, 2013, pp. 48–61.

[53] M. Grubb and L. Neuhoff, "Allocation and competitiveness in the EU emissions trading scheme: Policy overview," *Climate Policy*, vol. 6, no. 1, 2006, pp. 7–30.

[54] S. Hallegatte, "An adaptive regional input-output model and its application to the assessment of the economic cost of Katrina.," *Risk Analysis*, vol. 28, no. 3, 2008, pp. 779–799.

[55] R. W. Hamming, "Error detecting and error correcting codes.," *Bell System Tech Journal*, vol. 9, 1950, pp. 147–160.

[56] N. C. Healey, A. Irmak, K. G. Hubbard, and J. D. Lenters, "Environmental variables controlling site suitability for corn-based ethanol production in Nebraska.," *Biomass and Bioenergy*, vol. 35, no. 7, 2011, pp. 2852–2860.

[57] R. Hemmecke and R. Schultz, "Decomposition methods for two-stage stochastic integer programs.," *Online Optimization of Large Scale Systems.*, M. Groetschel, S. O. Krumke, and J. Rambau, eds., Springer, 2011, pp. 601–622.

[58] J. R. Hess, T. C. Wright, L. K. Kenney, and M. E. Searcy, "Uniform-format solid feedstock supply system: A commodity-scale design to produce an infrastructure-compatible bulk solid from lignocellulosic biomass.," INL/EXT-09-15423. Available from: http://www.inl.gov/technicalpublications/Documents/4408280.pdf, 2009.

[59] K. M. R. Hoen, T. Tan, J. C. Fransoo, and G. J. v. Houtum, "Effect of carbon emission regulations on transport mode selection in supply chains," Available from: $http://cms.ieis.tue.nl/Beta/Files/WorkingPapers/Beta_wp308.pdf$, 2010.

[60] K. M. R. Hoen, T. Tan, J. C. Fransoo, and G. J. J. A. N. van Houtum, "Effect of carbon emission regulations on transport mode selection under stochastic demand," *Flexible Services and Manufacturing Journal*, vol. 26, no. 1-2, 2014, pp. 170–195.

[61] W. Hoffman, "Who's carbon free?: Wal-mart takes on supply chains of products as expansive carbon measuring plan eyes distribution.," 2007.

[62] G. Hua, T. C. E. Cheng, and S. Wang, "Managing carbon footprints in inventory management," *International Journal of Production Economics*, vol. 132, 2011, pp. 178–185.

[63] Y. Huang, C. W. Chen, and Y. Fan, "Multistage optimization of the supply chains of biofuels," *Transportation Research Part E*, vol. 46, no. 6, 2010, pp. 820–830.

[64] Y. Huang and W. Pang, "Optimization of resilient biofuel infrastructure systems under natural hazards.," *Journal of Energy Engineering*, vol. doi : $10.1061/(ASCE)EY.1943-7897.0000138$, 2013.

[65] "Transport, Energy and CO2: Moving toward sustainability,", 2009, <http://www.iea.org/textbase/nppdf/free/2009/transport2009.pdf>.

[66] P. Ioannou, A. Chassiakos, A. Abadi, H. Chang, H. Jula, M. Lestas, L. Saggam, D. Thomas, and Y. Wang, "Reconfiguration strategies for mitigating the impacts of port disruptions.," Final Report. METRANS Project 07-14, 2011.

[67] R. R. Iyer and I. E. Grossmann, "A bilevel decomposition algorithm for long-range planning of process networks.," *Industrial & Engineering Chemistry Research*, vol. 37, no. 2, 1998, p. 47417481.

[68] S. Kang, H. Onal, Y. Ouyang, J. Scheffran, and D. Tursun, *Optimizing the biofuels infrastructure: Transportation networks and biorefinery locations in illinois.*, vol. 33 of *Natural Resource Management and Policy.*, chapter In: Handbook of Bioenergy Economics and Policy, Springer, 2010, pp. 151–173.

[69] D. M. Kargbo, "Biodiesel Production from Municipal Sewage Sludges," *Energy & Fuels*, vol. 24, 2010, pp. 2791–2794.

[70] H. Kim and M. E. O'Kelly, "Reliable p-hub location problems in telecommunication networks.," *Geographical Analysis*, vol. 41, no. 3, 2009, pp. 283–306.

[71] J. Kim, M. J. Realff, and J. H. Lee, "Optimal design and global sensitivity analysis of biomass supply chain networks for biofuels under uncertainty.," *Computers & Chemical Engineering*, vol. 35, 2011, pp. 1738–1751.

[72] A. M. Kostina, G. Guillen-Gosalbeza, F. D. Meleb, M. J. Bagajewiczc, and L. Jimeneza, "A novel rolling horizon strategy for the strategic planning of supply chains. Application to the sugar cane industry of Argentina.," *Computers & Chemical Engineering*, vol. 35, 2011, pp. 2540–2563.

[73] A. Kumar, J. B. Cameron, and P. C. Flynn, "Pipeline Transport and Simultaneously Saccharification of Corn Stover," *Bioresource Technology*, vol. 96, no. 7, 2005, pp. 819–829.

[74] G. Laporte and F. V. Louveaux, "The integer L-shaped method for stochastic integer programs with complete recourse.," *Operations Research Letters*, vol. 13, no. 3, 1993, pp. 133–142.

[75] S. Leduc, F. Starfelt, E. Dotzauer, G. kindermann, I. McCallum, M. Obersteiner, and J. Lundgren, "Optimal location of lignocellulosic ethanol refineries with polygeneration in Sweden.," *Energy*, vol. 35, no. 6, 2010, pp. 2709–2716.

[76] Q. Li, B. Zeng, and A. Savachkin, "Reliable facility location design under disruptions.," *Computers & Operations Research*, vol. 40, 2013, pp. 901–909.

[77] X. Li and Y. Ouyang, "A continuous approximation approach to reliable facility location design under correlated probabilistic disruptions.," *Transportation Research Part B*, vol. 44, 2010, pp. 535–548.

[78] X. Li, F. Peng, Y. Bai, and Y. Ouyang, "Effects of Disruption Risks on Biorefinery Location Design: Discrete and Continuous Models.," *proceeding of the* 90^{th} *TRB Annual Meeting, Washington D.C.*, January 2011.

[79] T. L. Magnanti and R. T. Wong, "Acclerating Benders Decomposition: Algorithmic enhancement and model selection criteria.," *Operations Research*, vol. 29, 1981, pp. 464–484.

[80] H. Mahmudi and P. Flynn, "Rail vs. truck transport of biomass," *Applied Biochemistry & Biotechnology.*, vol. 129, no. 1, 2006, pp. 88–103.

[81] M. Marufuzzaman, S. D. Eksioglu, and R. Hernandez, "Optimization models to design and manage environmentally friendly biofuel supply chains.," Proceedings of the Industrial & Systems Engineering Research Conference (ISERC), May 19-23, Orlando, Fl, USA, 2012.

[82] M. Marufuzzaman, S. D. Eksioglu, and R. Hernandez, "Environmentally friendly supply chain planning and design for biodiesel production via wastewater sludge.," Transportation Science. In press., 2014.

[83] M. Marufuzzaman, S. D. Eksioglu, and Y. Huang, "Two-stagestochastic programming supply chain model for biodiesel production via wastewater treatment.," *Computers & Operations Research*, vol. 49, 2014, pp. 1–17.

[84] M. Marufuzzaman, S. D. Eksioglu, X. Li, and J. Wang, "Analyzing the impact of intermodal-related risk to the design and management of biofuel supply chain.," *Transportation Research Part E*, vol. 69, 2014, pp. 122–145.

[85] M. Marufuzzaman, S. D. Eksioglu, and A. Mondala, "A techno economic analysis of pipelining wastewater sludge transportation.," Proceedings of the Industrial & Systems Engineering Research Conference (ISERC), May 19-23, Orlando, Fl, USA, 2012.

[86] G. E. Metcalf and D. Weisbach, "The design of a carbon tax,", Available from: http://www.law.harvard.edu/students/orgs/elr/vol33(underscore) 2/Metcalf(percent)20Weisbach.pdf, 2009.

[87] Mississippi Institute for Forest Inventory, "MIFI," (http://www.mifi.ms.gov/), 2009.

[88] A. Mondala, K. Liang, H. Toghiani, R. Hernandez, and T. French, "Biodiesel production by in situ transesterification of municipal primary and secondary sludges.," *Bioresource Technology*, vol. 100, 2009, pp. 1203–1210.

[89] J. Mouawad, "Katrinas shock to the system," Available from: http://www.nytimes.com/2005/09/04/business/04oil.html?pagewanted=all&-r=0, 2005.

[90] National Centers for Environmental Prediction., "A Special Spring Extremes Report.," Available from: http://www.ncdc.noaa.gov/special-reports/2011-spring-extremes/, 2013.

[91] National Drought Mitigation Center., "Current Climate Summary Maps-Powered by ACIS.," Available from: http://www.hprcc.unl.edu/maps/current/index.php?action=update-product&product=SPIData, 2013.

[92] National Hurricane Center, "Hurricane season summaries and reports.," Available from: http://www.nhc.noaa.gov, 2013.

[93] National Oceanic and Atmospheric Administration., "Hurricane Katrina.," Available from: http://www1.ncdc.noaa.gov/pub/data/extremeevents/specialreports/Hurricane-Katrina.pdf, 2005.

[94] G. L. Nemhauser and L. A. Wolsey, *Integer and combinatorial optimization*, John Wiley & Sons, Inc., 1988.

[95] L. Ntaimo and S. Sen, "The million variable 'march' for stochastic combinatorial optimization.," *Journal of Global Optimization*, vol. 32, 2005, pp. 385–400.

[96] Official Nebraska Government Website., "Ethanol facilities capacity by state and plant," Available from: $http://www.neo.ne.gov/statshtml/122.htm$, 2012.

[97] Pacific Northwest National Laboratory., "Looking back at the August 2003 blackout.," Available from: http:http://eioc.pnnl.gov/research/2003blackout.stm, 2013.

[98] N. Papadakos, "Practical enhancements to the Magnanti-Wong method.," *Operations Research Letters*, vol. 36, 2008, pp. 444–449.

[99] N. Parker, P. Tittmann, Q. Hart, M. Lay, J. Cunningham, and B. Jenkins, "Strategic assessment of bioenergy development in the west: Spatial analysis and supply curve development.," *Western Governors' Association*, 2008.

[100] P. Peng, L. V. Snyder, A. Lim, and Z. Lio, "Reliable logistics networks design with facility disruptions.," *Transportation Research Part B*, vol. 45, 2011, p. 1190171211.

[101] A. Perimenis, H. Walimwipi, S. Zinoviev, F. Muller-Langer, and S. Miertus, "Development of a decision support tool for the assessment of biofuels.," *Energy policy*, vol. 39, no. 3, 2011, pp. 1782–1793.

[102] J. Polson, "BP oil still ashore one year after end of Gulf spill," Available from: $http://www.bloomberg.com/news/2011-07-15/bp-oil-still-washing-ashore-one-year-after-end-of-gulf-spill.html$, 2011.

[103] C. G. Rawls and M. A. Turnquist, "Pre-positioning of emergency suppliers for disaster response," *Transportation Research Part B*, vol. 44, 2010, pp. 521–534.

[104] Renewable Fuels Association, "Monthly U.S. Fuel Ethanol Production/Demand," http://ethanolrfa.org/pages/monthly-fuel-ethanol-production-demand, 2013.

[105] R. T. Rockafellar and R. J.-B. Wets, "Scenario and policy aggregation in optimisation under uncertainty.," *Mathematics of Operations Research*, vol. 16, 1991, pp. 119–147.

[106] H. Rogner, D. Zhou, R. Bradley, P. Crabbé, O. Edenhofer, B. Hare(Australia), L. Kuijpers, and M. Yamaguchi, "Introduction," *Climate Change 2007: Mitigation. Contribution of Working Group III to the Fourth Assessment Report of the Intergovernmental Panel on Climate Change*, B. Metz, O. Davidson, P. Bosch, R. Dave, and L. Meyer, eds., Cambridge University Press, Cambridge, United Kingdom and New York, NY, USA, 2007, pp. 95–116.

[107] M. S. Roni, S. D. Eksioglu, E. Searcy, and J. J. Jacobson, "Estimating the variable cost for high-volume and long-haul transportation of densified biomass and biofuel.," *Transportation Research Part D: Transport and Environment*, vol. 29, 2014, pp. 40–55.

[108] M. S. Roni, S. D. Eksioglu, E. Searcy, and K. Jha, "A supply chain network design model for biomass co-firing in coal-fired power plants.," *Transportation Research Part E: Logistics and Transportation Review*, vol. 61, 2014, pp. 115–134.

[109] T. J. V. Roy, "A cross decomposition algorithm for capacitated facility location.," *Operations Research*, vol. 34, 1986, pp. 145–163.

[110] A. Ruszczynski, "Decomposition methods in stochastic programming.," *Mathematical programming*, vol. 79, no. 1, 1997, pp. 333–353.

[111] T. Santoso, S. Ahmed, M. Goetschalckx, and A. Shapiro, "A stochastic programming approach for supply chain network design under uncertainty.," *European Journal of Operational Research*, vol. 167, 2005, pp. 96–115.

[112] K. Sato and N. Fukumura, "Real-time freight locomotive rescheduling and uncovered train detection during disruption.," *European Journal of Operational Research*, vol. 221, 2012, pp. 636–648.

[113] S. R. Schill, "Flooding impacts Iowa ethanol.," Available from: http://www.ethanolproducer.com/articles/4333/flooding-impacts-iowa-ethanol, 2010.

[114] E. Searcy, P. Flynn, E. Ghafoori, and A. Kumar, "The Relative Cost of Biomass Energy Transport.," *Applied Biochemistry and Biotechnology*, vol. 136140, 2007, pp. 639–652.

[115] S. Sen and J. L. Higle, "c3 theorem and the d2 algorithm for large scale stochastic mixed-integer programming: set convexification.," *Mathematical Programming*, vol. 104, 2005, pp. 1–20.

[116] S. sen and H. Sherali, "Decomposition with branch-and-cut approaches for two-stage stochastic mixed-integer programming.," *Mathematical Programming Series A*, vol. 105, 2006, pp. 203–223.

[117] J. M. Shen, R. L. Zhan, and J. Zhang, "The reliable facility location problem: Formulations, heuristics, and approximation algorithms.," *INFORMS Journal on Computing*, vol. 23, no. 3, 2011, pp. 470–482.

[118] H. Sherali and X. Zhu, "On solving discrete two-stage stochastic programs having mixed-integer first- and second-stage variables.," *Mathematical Programming Series B*, vol. 108, 2006, pp. 597–611.

[119] H. D. Sherali and B. M. P. Fraticelli, "A modification of Benders' decomposition algorithm for discrete subproblems: An approach for stochastic programs with integer recourse.," *Journal of Global Optimization*, vol. 22, 2002, pp. 319–342.

[120] T. Sim, T. J. Lowe, and B. W. Thomas, "The stochastic p-hub center problem with service-level constraints.," *Computers & Operations Research*, vol. 36, 2009, pp. 3166–3177.

[121] L. V. Snyder and M. S. Daskin, "Reliability models for facility location: The expected failure cost case.," *Transportation Science*, vol. 39, no. 3, 2005, pp. 400–416.

[122] State Climate Office at North Carolina, "Total storms affecting NC by decades within 150 miles (1851-2012).," Available from: http://www.nc-climate.ncsu.edu/climate/hurricanes/statistics.php, 2012.

[123] M. SteadieSeifi, N. P. Dellaert, W. Nuijten, T. V. Woensel, and R. Raoufi, "Multimodal freight transportation planning: A literature review.," *European Journal of Operational Research*, vol. 233, 2014, pp. 1–15.

[124] R. Subramanian, S. Gupta, and B. Talbot, "Compliance strategies under permits for emissions," *Production and Operations Management*, vol. 16, no. 6, 2007, pp. 763–779.

[125] T. French and R. Hernandez, "BioCrude LLC,", Available from: http://www.tcee.msstate.edu/funded/biocrude.htm, 2012.

[126] T. French and R. Hernandez, "BioCrude LLC,", Available from: http://www.bio-energyllc.com/, 2012.

[127] S. Takriti and J. Birge, "Lagrangean solution techniques and bounds for loosely coupled mixed-integer stochastic programs.," *Operations Research*, vol. 48, 2000, pp. 91–98.

[128] Tennessee State Library and Archives., "Flooding in Tennessee.," Available from: http://www.tennessee.gov/tsla/exhibits/disasters/floods2.htm, 2013.

[129] Texas Water Development Board., "Drought Information Summary.," Available from: http://www.twdb.state.tx.us/apps/droughtinfo/default.aspx, 2013.

[130] The Ojos Negros Research Group., "Drought facts.," Available from: http://ponce.sdsu.edu/three-issues-droughtfacts03.html, 2013.

[131] P. S. Trotter, G. A. Johnson, R. Ricks, and D. R. Smith, "Floods on the lower Mississippi: An historical economic overview.," Available from: http://www.srh.noaa.gov/topics/attach/html/ssd98-9.htm, 2011.

[132] U. S. Census Bureau, "States & County QuickFacts Mississippi," Available from: http://quickfacts.census.gov/qfd/states/28000.html, 2012.

[133] U. S. Energy Information Administration., "State Energy Data System ," Available from: $http://www.eia.gov/state/seds/hf.jsp?incfile=sep_use/total/use_tot_MSa.html\&mstate=Mississippi$, 2010.

[134] UNFCCC, "Kyoto Protocol," Available from: $http://unfccc.int/kyoto_protocol/items/2830.php/$, 1997.

[135] United States Drought Monitor, "Percent area in U.S. drought monitor categories.," Available from: `http://www.droughtmonitor.unl.edu/DataArchive/Tables.aspx`, 2013.

[136] United States Drought Monitor, "U.S. drought monitor data archive.," Available from: http://www.droughtmonitor.unl.edu/DataArchive.aspx, 2013.

[137] United States Energy Information Administration, "Monthly Biodiesel Production Report," http://www.eia.gov/biofuels/biodiesel/production/, 2013.

[138] United States Energy Information Administration, "State Energy Data System (SEDS): 2012 (Updates)," http://www.eia.gov/state/seds/seds-data-fuel.cfm?sid=US, 2014.

[139] United States Environmental Protection Agencie, "Renewable Fuels: Regulations & Standards," http://www.epa.gov/otaq/fuels/renewablefuels/regulations.htm, 2007.

[140] University of Nebraska Lincoln., "How do I Measure Drought?.," Available from: http://drought.unl.edu/ranchplan/DroughtBasics/WeatherDrought/ MeasuringDrought.aspx, 2013.

[141] U.S. Department of the Interior., "Mississippi Earthquake History.," U.S. Geological Survey. Available from: http://earthquake.usgs.gov/earthquakes/states/mississippi/history.php, 2013.

[142] U.S. Energy Information Administration., "International energy statistics.," Available from: http://www.eia.gov/cfapps/ipdbproject/iedindex3.cfm?tid=79\&pid=80\&aid=1\&cid=regions\&syid=2000\&eyid=2011\&unit=TBPD, 2013.

[143] H. Uster and H. Agrahari, "A Benders decomposition approach for a distribution network design problem with consolidation and capacity considerations.," *Operations Research Letters*, vol. 39, 2011, pp. 138–143.

[144] G. Victoria, "Lessons to be learned from Haiti's tsunami.," Available from: http://news.bbc.co.uk/2/hi/science/nature/8536561.stm, 2010.

[145] R. Wallace, K. Ibsen, A. McAloon, and W. Yee, "Feasibility study for co-locating and integrating ethanol production plants from corn starch and lignocellulose feedstocks.," NREL/TP-510-37092. USDA/USDOE/NREL, Revised Edition. Golden, Colorado., 2005.

[146] X. Wang and Y. Ouyang, "A continuous approximation approach to competitive facility location design under facility disruption risks.," *Transportation Research Part B*, vol. 50, 2013, pp. 90–103.

[147] X. Wang, Y. Ouyang, H. Yang, and Y. Bai, "Optimal biofuel supply chain design under consumption mandates with renewable identification numbers.," *Transportation Research Part B: Methodological*, vol. 57, 2013, pp. 158–171.

[148] Water-Environment-Federation., "Activated sludge MOP OM-9.," Second ed. Water Environment federation, Virginia., 2002.

[149] M. Webster, I. S. Wing, and L. Jakobovits, "Second-best instruments for near-term climate policy: Intensity targets vs. the safety valve," *Journal of Environmental Economics and Management*, vol. 59, 2010, pp. 250–259.

[150] P. Wentges, "Accelerating Benders decomposition for the capacitated facility location problem.," *Mathematical Methods of Operations Research*, vol. 44, no. 2, 1996, pp. 267–290.

[151] R. B. Williams, B. M. Jenkins, and M. C. Gildart, "California biofuel goals and production potential," 15^{th} European Biomass Conference & Exhibition. May 7-11, Berlin, Germany., 2007.

[152] World Recourse Institutes, *Corporate Value Chain (Scope 3) Accounting and Reporting Standard*, Tech. Rep., 2012.

[153] F. Xie, Y. Huang, and S. D. Eksioglu, "Integrating multimodal transport into cellulosic biofuel supply chain design under feedstock seasonality with a case study based on California.," *Bioresource Technology*, vol. 152, 2014, pp. 15–23.

[154] F. You, L. Tao, D. J. Graziano, and S. W. Snyder, "Optimal design of sustainable cellulosic biofuel supply chains: Multiobjective optimization coupled with life cycle assessment and input-output analysis.," *AIChE Journal*, vol. 58, no. 4, 2012, p. 11571180.

[155] A. Zamboni, F. Bezzo, and N. Shah, "Spatially explicit static model for the strategic design of future bioethanol production systems. 2. Multi-objective environmental optimization," *Energy & Fuels*, vol. 23, no. 10, 2009, pp. 5134–5143.

[156] A. Zamboni, N. Shah, and F. Bezzo, "Spatially explicit static model for the strategic design of future bioethanol production systems. 1. Cost Minimization," *Energy & Fuels*, vol. 23, no. 10, 2009, pp. 5121–5133.